GENERAL METHOD FOR PRODUCING BIODEGRADABLE NANOPARTICLES AND NANOFIBERS BASED ON NANOPOROUS MEMBRANES

By

PENG GUO

A DISSERTATION PRESENTED TO THE GRADUATE SCHOOL
OF THE UNIVERSITY OF FLORIDA IN PARTIAL FULFILLMENT
OF THE REQUIREMENTS FOR THE DEGREE OF
DOCTOR OF PHILOSOPHY

UNIVERSITY OF FLORIDA

2011

To my family, for their continued support and love

ACKNOWLEDGEMENTS

The work presented in this dissertation was conducted between August 2006 and May 2011 in graduate school at the University of Florida. I would like to acknowledge every individual who gives me help, advice, and encouragement.

I would like to sincerely thank my advisor, Prof. Charles Martin, who supports and guides me in both my research and life. Prof. Martin is always helpful and prepared to give me guidance. Besides research, I also matured as an individual in many areas; in relationships, such as trusting coworkers, self-confidence, and desire of exploration. My future career and life have and will continue to significantly benefit from working with Prof. Charles Martin.

I am very grateful to have had the opportunity to work in the Martin lab, where I met and collaborated with many fantastic students and postdoctoral fellows. Dr. Pu Jin and Dr. Jillian Perry helped me begin my thesis research. Both taught me many experiments and how to use instruments during my early graduate years. Dr. Jiahai (Jay) Wang also worked with me in the first three years and provided many valuable suggestions. Dr. Hitomi Mukaibo, Dr. Lloyd Horne, Dr. Lindsay Sexton, Dr. Kaan Kececi, Dr. Dooho Park, Dr. Fan Xu, Gregory Bishop, Funda Mira, William Hardy and Li Zhao are group members who worked with me and provided valuable support and suggestions during my research.

I also would like to sincerely thank Prof. Richard Zare at Stanford University. During my visiting study in the Zare lab between April 2009 and May 2011, Prof. Zare took me in as one of his own graduate students, generously helping and training me to pursue my research. I also thank all the Zare lab group members for their support in my visiting research at Stanford University.

I also acknowledge our collaborators in Stanford Univeristy: Prof. Gerald Fuller and Dr. Michael Maas in Dept. of Chemical Engineering; Prof. Fan Yu and Dr. Michael Keeney in Dept. of Bioengineering; Prof. Ramin Beygui and Dr. Evgenios Neofytou in Medical Center Line: Cardiothoracic Surgery; Prof. A.C. Matin and Matthew Sylvester in Dept. of Microbiology and Immunology; and Prof. Christopher Contag and Dr. Tobi Schmidt in Dept. of Pediatrics. Without these great minds I could not accomplish close to as much.

My family has provided the most important support during my research. I am very fortunate to have such a loving and supportive family. I want to thank my lovely wife Jing Huang. During the long and sometimes challenging graduate study, Jing has always stood beside me, providing encouragement and support, through both the highs and lows. Her delicate care and tenderness sustained me through every step of my research. I owe much to her. I want to thank my mother Shuying Wang for taking care of me, her kindness and support never wavered.

TABLE OF CONTENTS

page

LIST OF TABLES

LIST OF FIGURES

Abstract of Dissertation Presented to the Graduate School
of the University of Florida in Partial Fulfillment of the
Requirements for the Degree of Doctor of Philosophy

GENERAL METHOD FOR PRODUCING BIODEGRADABLE NANOPARTICLES AND NANOFIBERS BASED ON NANOPOROUS MEMBRANES

By

Peng Guo

May 2011

Chair: Charles R. Martin
Major: Chemistry

Biocompatible and biodegradable nanostructured materials have attracted more and more attention since they offer numerous exciting possibilities in medical sciences, such as drug delivery and tissue engineering. The increasing need for novel drug delivery systems with enhanced specificity/activity and reduced side toxicity has led to the development of nano-sized drug vehicles, which provide the advantage of delivering small molecular drugs, as well as macromolecules, via both targeted delivery and controlled release. For tissue engineering, considerable effort has been made to develop three dimensional artificial nanofibrous scaffolds, which closely resemble the natural protein nanofiber network in the extracellular matrix (ECM).

The goal of this thesis is to develop a simple and efficient method to produce nanostructured biomaterials for drug delivery or tissue engineering applications. We present here a novel strategy, referred to as nanopore-injection (N-I) method, based on the use of a nanoporous membrane that separates the feed and receiver solutions. By pumping one solution into the other, through the membrane, one can generate nanostructured materials at the exits of the membrane nanopores. The first part of the dissertation (Chapters 2, 3, 4) involves the fabrication of biodegradable nanoparticles,

including hydrophobic drugs and drug-encapsulated polymeric nanoparticles, as well as exploring their applications in drug delivery. The N-I approach was designed by either anti-solvent or pH-sensitive features, and the particle size was found to be affected by the flow rate and viscosity of the feed solution and the pore size of the membrane. These nanoparticles exhibit excellent biocompatibility and sustained release capabilities. The second part of the dissertation (Chapters 5, 6) focuses on the fabrication of biodegradable nanofibrous scaffolding and their applications in tissue engineering. By using a modified N-I setup, polymers and organic/inorganic hybrid nanofibers were generated with a controlled morphology and size. The obtained nanofibrous scaffolds could support stem cell proliferation and differentiation.

CHAPTER 1
INTRODUCTION AND BACKGROUND

Introduction

The application of nanotechnology in medical sciences is changing the landscape of drug delivery and tissue engineering industry as a whole.[1-14] Nanostructured biomaterials, featuring a nanoscale morphology and size, exhibit a wide range of advantages over the conventional biomaterials, such as high bioavailability, improved cellular interaction, and specific designed functions.[1] It offers a promising solution to many difficulties in drug delivery and tissue engineering.[2,6] For example, a nano-sized drug vehicle has made significant progress in the delivery of conventionally undeliverable molecules, such as compounds with low water solubility and genetic biomolecules.[3-5] In tissue engineering, nanofibrous scaffolds ideally imitate the natural extracellular matrix (ECM) with cell behavior modulation functions.[7-14]

In this thesis, we present a simple and efficient nanopore-injection (N-I) method to produce biodegradable nanoparticles and nanofibers based on the use of nanoporous membranes, the function of which is to separate two liquids.[15] By pumping one liquid into the other, through the membrane, we can generate nanoparticles or fibers at the exit of the nanopore. We illustrated this technique for the preparation of a series of nanostructured biomaterials (e.g. chitosan, PLGA-PEG, and collagen) and also explored their applications in drug delivery and tissue engineering.

Current Progress in Biodegradable Nanostructures

Biodegradable Nanoparticles in Drug Delivery

Drug delivery is the science that administers the drug compounds to improve their pharmaceutical and therapeutic properties. Many drug delivery systems have been

developed to improve drug release, dissolution, biodistribution and elimination; the delivery efficiency, convenience and safety could also be enhanced.[16] The developed drug delivery systems include polymeric nanoparticles,[17] lipid particulate carriers,[18] drug loaded microspheres,[19] drug-polymer conjugates,[20] etc. Due to the advantages offered by sustained release and targeted delivery, biodegradable polymeric nanoparticle are currently under intense investigation.[17]

Polymeric nanoparticles used for drug delivery are elicited as a solid particle with the polymeric matrix. The therapeutic agent of interest is dispersed in this polymeric matrix with a preferable size between one nanometer to a few hundred nanometers. The use of polymeric nanoparticle as drug carriers began in the 1980s. In 1987, Aprahamian reported that polyalkylcyanoacrylate nanocapsules could be used as a drug carrier via transmucosal passage in the small intestine.[21] Since then, various polymeric nanoparticles with different structures, components and functions have been fabricated for drug delivery.[17,22-25] Compared with other drug carriers, polymeric nanoparticles exhibit three major advantages (Figure 1-1).

First, polymeric nanoparticles demonstrate a higher surface area compared with conventional drug carriers, due to their nanoscale size. This high surface area changes particle surface properties and the interactions with disperse phase, especially with respect to the dissolution rate.[26] More than 40 % of therapeutic compounds are poorly water soluble, and their clinical usefulness greatly limited by their bioavailability. Formulating these hydrophobic drugs into a nanoparticle form could efficiently improve their dissolution rate, and eventually improve their performance. In the in vitro drug delivery study, the sub-cellular size of the particle improves its cellular uptake efficiency.[27]

For example, Desai reported that the Caco-2 cell uptake of 100 nm gold nanoparticles was 2.5-fold higher compared to that of 1 μm microspheres and 6-fold higher compared to that of 10 μm microspheres. Some cell lines (e.g. Hepa 1-6, HepG2, and KLN 205) express favored uptake of nanoparticles over microspheres.[28] During in vivo drug delivery, nanoparticles can easily penetrate through fine capillaries into deep tissues, and cross biological barriers. The reason that nanoparticles could penetrate throughout the submucosal layers, whereas the microparticles are localized in the epithelial lining, is mainly due to their size difference. An important research area that holds tremendous promise for treating diseases that affect the brain is using nanoparticles to deliver therapeutic agents across the blood-brain barrier (BBB). The BBB is an endothelial cell monolayer connected by tight junctions in the brain capillaries for the separation of circulating blood and cerebrospinal fluid. This barrier is tremendously challenging for therapeutics to cross. Development of nanoparticulate vectors to provide efficient trans-vascular delivery of a therapeutic drug for difficult-to-treat diseases like brain tumors could provide life-saving drugs and is under intense investigation throughout the world.

Second, sustained release of therapeutic agent could be achieved by encapsulating it within different biopolymers. A variety of functional polymers could be used to encapsulate drug compounds, including naturally occurring (chitosan and serum) and synthetic polymers (polylactic acid (PLA) and polylactic-co-glycolic acid (PLGA)). By selecting different polymers, nanoparticles could gain specific functions, such as sustained or triggered release. Drug molecules are physically dispersed into the polymeric matrix of the nanoparticle, and the release duration of drug molecule from these nanoparticles could either be over a long duration of time with a controlled manner

or triggered by outer environmental stimulus such as pH, temperature, or electric field variance. For sustained release studies, the drug encapsulated within the nanoparticle is released at a sustained rate, controlled by drug molecule diffusion and degradation of the polymer matrix. Therefore, the molecular weight of polymer, the functional groups and kinds of polymer are of great importance in the release duration. The release duration of the drug molecule could vary from days to months.[29] It is preferred that the release of drug molecule in an in vivo environment maintains a constant drug biodistribution together with an extended blood circulation time. Sustained release of drug molecule could also improve the drug performance and avoid repetitive uptake of drug, which would improve the quality of life of the many who take painful invasive treatments, such as needle injection based insulin delivery for diabetics. For particle materials, PLA and PLGA are two common biopolymers widely used for sustained release. Jacobson and co-workers reported that luciferin encapsulated inside the PLA nanoparticles showed an in vivo sustained release time of over 40 days.[29] In triggered release, polymer molecules are responsive to an environmental stimulus, and alter their polymer chain network morphology or structure accordingly, resulting in the drug molecules being released from the nanoparticle. Among many sensitive biopolymers, chitosan is responsive to pH variance; PLGA-PEG-PLGA triblock polymer to temperature variance; and polyperryle (PPy) to electric field variance. Besides the above polymers, more triggered release polymers are being revealed.[30,31]

Third, targeted drug delivery could be achieved by coupling targeting ligands to the drug encapsulated nanoparticle. This coupling allows the specific delivery of therapeutic agents to the tissue of interest bypassing other unrelated tissues. Currently, targeted

delivery is one of the most challenging aspects facing drug delivery, and has tremendous significance for the highly toxic or carcinogenic drug delivery, which is commonly prescribed for the treatment of cancer. The majority of anti-cancer drugs are highly biotoxic to most kinds of cells, both cancerous and healthy. Targeted delivery of these drugs directly to the tumor site helps avoid eliminating normal tissue and thus would minimize the destructive side-effects of chemotherapy. A variety of tumor directed targeting ligands have been developed over the last decade. For instance, chlorotoxin is a short protein extracted from the venom of the deathstalker scorpion and it selectively binds with the conductance chloride ion-channel on the glioma cell membranes.[32,33] Another, cyclic Arginine-Glycine-Aspartic (RGD) peptide is a recognition sequence of αvβ3 integrin associated with tumor angiogenesis.[34,35]

A number of synthetic and naturally occurring polymers have been used in polymeric nanoparticle formulation. For drug delivery purpose, there are generally two requirements for the polymer selection: first, the polymer used for drug delivery is biodegradable; second, it needs to show non-biotoxicity and non-immunogenic response when interacts with cells. In the drug delivery process, the uptaken nanoparticles need to be eventually degraded and eliminated from the cell. Biopolymers are usually degraded by enzymes (e.g. lysozyme) and cleared from the body through the citric acid cycle. On the other hand, non-removable nanoparticle vectors, such as carbon nanotubes and silica nanoparticles, will accumulate inside the patient body, which may cause cell damage and long-term damages to the patient. This accumulation is currently considered as a serious health hazard in drug delivery.[36,37] The design of drug delivery nanoparticles should limit the toxic material in order to reduce the damage to healthy tissues.

Commonly used biopolymers include synthetic polymers such as polylactide polyglycolide copolymers, polyacrylates, polycaprolatones, and naturally occurring polymers such as chitosan, albumin, gelatin, alginate, and collagen.[38-42] Among these different polymers, synthetic constructs normally show a longer sustained release time (several days to weeks) compared to their natural counterparts. But the application of synthetic polymer nanoparticles is usually limited by the harsh synthetic environment required in the particle formation process.

Biodegradable Nanofibers in Tissue Engineering

Tissue Engineering is defined as “an interdisciplinary field that applies the principles of engineering and life sciences toward the development of biological substitutes that restore, maintain, or improve tissue function.” by Langer and Vacanti in 1993.[6] The current application of nanotechnology in tissue engineering is to closely imitate nature. In human and animals, natural tissues can be considered to exist as three components: cells, extracellular matrix (ECM) and signaling system. Majority cells are imbedded in the ECM, and the interaction between these cells and ECM regulates the cell migration, proliferation, differentiation, gene expression, and secretion of various hormones and growth factors. Mimicking the natural ECM is of great importance for tissue engineering. Natural ECM exists as a network of nanofibers containing proteins and glycosaminoglycans, which comprise a three dimensional spatial and temporal environment for cell attachment and growth. ECM also dynamically influences the phenotype by providing indirect or direct informational signaling cues. For example, the type I collagen molecule is essential for osteoblast cell development into the bone marrow as it provides the integrin binding sites in the ECM.[43]

In tissue engineering, tremendous effort has been made to develop nanofibrous scaffold mimicking the natural ECM in chemical composition, morphology and surface functional groups. The existence of these synthetic nanofibrous scaffolds works as a temporary ECM for cells attachment, location and growth. The mixture of cells within the scaffold will be implanted into the target tissue site inside human or animals. Previously formed cell organizations in the scaffold continue growing and eventually merge together with the natural ECM. Thus tissue reparation and regeneration are possible. The synthetic nanofibrous scaffold will be degraded over a period of time. In order to produce an ideal scaffold, there are two requirements: first, similar to the biopolymer used in drug delivery, the polymer used in tissue engineering should be biodegradable; second, polymers used in tissue engineering should also be non-biotoxic and non-immunogenic. After implanting the scaffold in vivo, it must be gradually degraded and replaced by the natural ECM with tissue regeneration. If the scaffold is not biodegradable, it will permanently exist at the implant site and cause an inhomogeneous phase in the newly formed ECM. This phase hinders the biomechanical properties and functions of the new generated tissue especially musculoskeletal tissue.[44] Nanofibrous scaffolds are designed to be implanted in vivo, so biocompatibility is a key factor to evaluate the performance of the scaffold.

Both naturally occurring polymers and synthetic polymers could be used to form a nanofibrous scaffold. In tissue engineering, natural polymers are more extensively used due to their similarity to the natural ECM as well as their in vivo biocompatibility. Popular naturally occurring polymers include collagen, hyaluronic acid, gelatin, silk and chitosan.[45] Among these naturally occurring polymers, collagen is considered the most

promising biopolymer in tissue engineering because it is the primary component in the natural ECM. Collagen is a group of structure proteins which feature a unique triple-helix composed of three polypeptide subunits. In the natural ECM, there are more than 20 types of collagen. The natural isotypes of collagen differ from each other with respect to their non-helical components and the length of the triple-helix. Among the 20 types of collagen, type I collagen is the most abundant and predominant collagen in the natural ECM; usually found in bone and tendon, skin and other connective tissues. The type I collagen molecule is a triple-helical protein, 300 nm in length and 1.5 nm in diameter. Its triple-helix consists two identical α1 (I) chains and one α2 (I) chain. Under certain conditions, such as pH, temperature, or ionic strength variance, type I collagen could self-assemble into a macromolecular structure. Initially, type I collagen molecules will self-assemble into fibrils with a mean diameter of 36 nm. If these conditions persist, type I collagen fibrils will eventually form fibers and fiber bundles.[46-48]

Collagen nanofibrous scaffolds have been advantageous in mimicking the chemical and biological function of the natural ECM. For example, utilizing electrospinning, Rho reported that aortic smooth muscle cells could proliferate and infiltrate into the collagen nanofibrous scaffold a with fiber diameter of 100 nm (Type I collagen) and 250 nm (Type III collagen).[49] Both of the resulting type I and type III collagen nanofibers display a characteristic 67 nm banding structure. Venugopal reported a poly(ε-caprolactone) (PCL) coated collagen scaffold with similar mechanical properties to that of skin and showed that human dermal fibroblasts could proliferate on this scaffold for dermal tissue reparation.[50]

On the other hand, organic/inorganic hybrid nanofibrous scaffolds (e.g., nanohydroxyapatite/collagen) are very popular for hard tissue engineering, especially in bone or dental tissue reparation and regeneration. These hybrid nanofibrous scaffolds show a higher mechanical strength compared to the scaffold composed of only biopolymers. Calcium phosphate and calcium carbonate are widely used in the formation of hybrid nanofibers because they exist as the major inorganic materials found in the nature tissues. In addition, carbon nanotubes have also been studied to incorporate into the polymeric scaffold to construct functional scaffold due in large part to their mechanical strength as well as electrical conductivity.[51]

Methods for Producing Biodegradable Nanoparticles and Nanofibers

In the last three decades, extensive effort has been devoted to fabricating biodegradable nanostructure. A considerable number of nanofabrication methods have been developed to formulate polymeric nanoparticles for drug delivery and nanofibrous scaffolding for tissue engineering. In this section, we present a overview of these conventional nanofabrication methods, paying close attention to the advantages and disadvantages in order to provide an unbiased evaluation of our nanopore-injection technique.

Nanoparticle Formation Method

Nanoprecipitation

The nanoprecipitation method (or solvent displacement method) was first introduced by Fessi and co-workers in 1989.[52] This one-step preparation method immediately attracted wide attention due to its simplicity, speed, and economic feasibility. Nanoprecipitation allows the preparation of nanoparticles from preformed polymer such as PLA, PLGA, and PMMA, instead of the respective monomer or oligomer.

Nanoprecipitation systems encompass three parts: polymer; polymer solvent; and non-solvent of the polymer. The polymer is initially dissolved in the polymer solvent, and then the mixture solution is added into the non-solvent (usually aqueous solution) with magnetic stirring. Nanoparticles are formed by precipitation simultaneously with the polymer diffused into the non-solvent. The resulting nanoparticle usually has a mean size of around 200 nm.

In the nanoprecipitation process, the selection of solvent and non-solvent has a crucial impact on nanoparticle formation. The solvent should have a high solubility of the polymer of interest; be miscible in the non-solvent; and be facile to removable from the product following precipitation. Acetone and ethanol are two frequently used organic solvents in the nanoprecipitation process. If the polymer is not very soluble in organic solvents, multiple solvent blend could be used to improve the polymer solubility.

Surfactant is often used in nanoprecipitation to stabilize the formed nanoparticles in the aqueous environment. Surfactants used in nanoprecipitation are usually low molecule weight amphiphilic polymers (a molecule with a hydrophilic group on one end, and a hydrophilic group on the other end), which will spontaneously coated on the surface of the polymeric nanoparticles with the hydrophobic end toward polymer surface and the hydrophilic end toward aqueous solution. Surfactants improve nanoparticle dispersion in the aqueous phase, prevent particle aggregation and minimize surface charge. Common surfactants used in nanoprecipitation include Pluronic F68, Dextran, Poly (vinyl alcohol) (PVA) and Tween® 20 or Tween® 80.

A variety of biomaterials, including peptides and drugs, have been formulated into nanoparticles by nanoprecipitation. For example, Govender prepared PLA and PLGA

nanoparticles by nanoprecipitation and loaded the water-soluble drug procaine hydrochloride into these nanoparticles.[53] Memisoglu reported amphiphilic beta-cyclodextrin nanoparticles which encapsulated the antifungal drugs bifonazole and clotrimazole.[54] Duclairoir and co-workers reported the preparation of gliadin nanoparticles by nanoprecipitation.[55]

The major weakness of nanoprecipitation is its dependence on materials that need to be hydrophobic to dissolve in the polymer solvent. Clearly, this requirement limits the application of this method in formulating water soluble polymers and drugs. The existence of the organic solvent can cause the active therapeutic compounds such as peptides and nucleic acids to deactivate. Producing hydrophilic polymers or drug nanoparticles by nanoprecipitation has been extensively probed. One promising solution, reported by Govender and co-workers, is to control the pH of the solvent in order to minimize the ionization of the hydrophilic polymers or drugs in the nanoprecipitation process.[53]

Nano-Emulsion

In contrast to the nanoprecipitation method, the emulsion based nanofabrication method involves two steps for particle formation (Figure 1-3). The first step is the preparation of emulsified system and the second is the solidification of nanoparticles. The solidification of nanodroplets occurs by either precipitating the polymer (solvent evaporation, self-assembly of a macromolecule, and polymerization of monomers) or spray drying.

In the first step, the emulsion system is usually formed by emulsifying two immiscible phases (such as water and oil); the resulting emulsion droplets are stabilized by the surfactants. Several methods have been proposed that decrease the size of the emulsion droplet from micro- to nanoscale. One common method for decreasing the size

is via a high energy (mechanical) process that forms the nano-emulsion.[56,57] High energy devices, such as rotor/stator devices, ultrasound generators,[58] and high-pressure homogenizers,[57] are introduced into the emulsion process to create higher interfacial areas resulting in nanoscale emulsion droplets. Another popular strategy to reach the nano-level is a low energy method which generates nanoscale emulsion droplets by varying the intrinsic physicochemical properties of the surfactants and co-surfactants (which stabilize the emulsion droplets). For example, when polyethoxylated surfactants are used in the emulsion process, their partitioning coefficient is a function of the environmental temperature. By controlling the temperature, the emulsion system will express a phase inversion and the bicontinuous system broken up into smaller droplets.[59]

The second step in nano-emulsion is solidifying the emulsion droplets into nanoparticles. There are several methods for accomplish this process: polymerization, solvent removal, or solvent evaporation. If the particle material is monomer, polymerization is the method most commonly utilized. In this polymerization process, monomer droplets are first stabilized by adsorbed surfactants in the nano-emulsion, then initiator molecules are introduced into the monomer matrix by premixing or just following nanodroplet formation. Subsequently, the radical polymerization reaction occurs within the monomer droplets by triggering initiator molecules with a specific stimulus, such as temperature, pH, UV, ultrasound, or enzyme.[60-63] If the particle material is a preformed polymer it is precipitated out by extracting the organic solvent from the nano-emulsion system. Several solvent extraction methods exist including solvent evaporation, fast diffusion after dilution and salting out.[64-67]

Ionic Gelation

Ionic gelation is a simple and mild method to prepare polymeric nanoparticles via complexation between oppositely charged macromolecules. In ionic gelation, charged polymers are first dispersed in the aqueous solution and small ions with opposite charges are added into the same solution (Figure 1-4). Then the ionic nanogels are obtained from an aqueous solution by taking advantage of the electrostatic interaction between charged polymers and opposite charged ions. Ionic gelation is an organic solvent free synthesis method, as the entire formation process happens inside the aqueous phase, in contrast to that with the nanoprecipitation and nano-emulsion methods. In ionic gelation, polymeric nanoparticles are solidified and stabilized by electrostatic interactions instead of chemical crosslink, which avoids the potential toxicity and other side effects from crosslinkers.

A widely used gelling polymer in ionic gelation is chitosan, a cationic polysaccharide. Chitosan is positively charged in slightly acidic aqueous solutions due to the basic amine group. Chitosan nanogels are usually formed by addition of a polyanion, such as tripolyphosphate (TPP), into the chitosan solution. TPP provides electrostatic interactions with the positively charged polysaccharide and forms a spherical complexation particle. The size of the complexation particle shows a strong dependence on the concentration of the corresponding cationic solution. Tokumitosu and co-workers reported the formation of chitosan-gadopentetic acid complex nanoparticles and explored their application in cancer therapy.[68] Polk successfully encapsulated albumin into chitosan-alginate complex microcapsules by ionic gelation.[69] Drug encapsulated chitosan nanoparticles prepared by ionic gelation have demonstrated a unique advantage—namely triggered release responding to either a pH variance or an ionic stimulus. This triggered release is attributed to the physicochemical property of chitosan. The amine groups on chitosan are

deprotonated by raising the pH and neutralizing the solution. As a result, the electrostatic interactions between the oppositely charged chitosan and TPP become weaken. In addition, the nanostructure of the chitosan nanoparticle starts dissociating and swelling, causing the release of therapeutic agents trapped within the polymeric matrix. This triggered drug release of these chitosan nanoparticle shows promise for the functional delivery of therapeutic agents.

Nanofiber Formation Method

Extensive research has been focused on developing three dimensional artificial scaffolds at the nanoscale level for tissue engineering. Nanofibrous scaffolds are very popular due to its high similarity to the natural ECM. There three major nanofabrication methods for preparing nanofibers scaffold: electrospinning, self-assembly, and phase separation. Among these three methods, electrospinning is commonly used to prepare aligned polymer nanofibers; self-assembly can provide insight into the nanofiber formation conditions and can produce very thin nanofiber; phase separation generates mesh nanofibrous scaffolds with a controllable pore size.

Electrospinning

Electrospinning was first patented in 1902 by Morton.[70] However, it was not until the 1980s that electrospinning became a popular nanofabrication technique, due in large part to the rapid development of nanoscience and nanotechnology. Electrospinning is the most often employed method to formulate nanofibers from biomaterials. A general electrospinning setup is composed of three major components (Figure 1-5): a high voltage power supply, a capillary tube with a pipette or needle of small diameter, and a conductive receiver plate. In most electrospinning cases, hypodermic needles are used as spinnerets, and aluminum foil as the receiver plate. The principle of electrospinning is

based on the electrostatic interaction between polymeric molecules. Electrospinning uses the electrostatic field to create and accelerate the liquid jet from a tip of the capillary and obtains nanofibers via post-solidification. In the electrospinning process, the polymer is first dissolved in order to form a polymeric solution. This polymeric solution is filled in a capillary tube. Then a high voltage is applied between the tip of capillary tube and the receiver plate. Charged polymer molecules produce a repulsion force against each other in a direction opposite to the surface tension. When the applied voltage increases to the critical intensity, the repulsive force will overcome the surface tension and generate a polymer jet ejected from the tip of capillary tube. The solvent in the polymer jet is evaporated in the air and eventually forms randomly oriented nanofibers. The resulting nanofibers are collected by a grounded receiver plate.

The fiber diameter is mainly controlled by the jet size and the polymer contents within the jet. In most of the electrospinning experiments, a single jet is formed between the capillary and receiver plate[71-73] and the diameter of the nanofiber is related to the polymer concentration. Normally nanofibers with smaller diameter could be formed by using a low concentration polymer solution.[74] In addition, during jet transfers from the capillary to the receiver plate, one jet may be split into multiple sub-jets which reduce the diameter of the nanofibers.[74-76]

Various polymers, both naturally occurring and synthetic, have been successfully electro-spun into nanofibers: Schreuder-Gibson and co-workers reported the formation of polycarbonate nanofibers by electrospinning;[77] Wang and Santiago-Aviles successfully synthesized the polyacrylonitrile (PAN) nanofibers by electrospinning;[78] Ding and co-workers obtained polyvinyl alcohol (PVA) nanofibers by electrospinning;[79] Zong

reported the successful preparation of the naturally occurring polymer polylactic acid (PLA) nanofibers by electrospinning.[80]

Although most of the polymers are dissolved in appropriate solvents before electrospinning, there are some melted and electrospun into nanofibers, instead of in a solution. These polymers include polyethylene (PE), polypropylene (PP) and polyethylene teraphthalate (PET). Electrospinning nanofibers can create complex and interesting structures, such as beaded, ribbon, porous, and core-shell fibers.[81-83]

Electrospinning has many shortcomings. One major problem is the “sharkskin effect”.[84] It is a phenomenon whereby the polymer jet is extruded during the spinning process, instead of into uniform thin nanofibers, into spherical or spindle-like bead chains. In the electrospinning process, surface tension plays an important role in the bead chain formation. When the polymer jet is extruded to form very thin fibers, the surface tension of the liquid jet tends to form spherical droplets in order to minimize its surface energy. This “sharkskin effect” has proved to be the most difficult obstacle to overcome in electrospinning.

Phase Separation

Phase separation was first reported by Ma and Zhang in 1999 (termed thermally induced liquid-liquid phase separation) for the formation of nanofibrous foam materials.[85] A typical phase separation process includes the following steps: first dissolve polymer in appropriate solvent and make a homogeneous polymer solution with magnetic stirring; second the polymer solution is rapidly transferred into a refrigerator or freezer set at a certain temperature. Then phase separation and gelation would happen in the polymer solution. After the polymer solution gels completely, the polymer gel would be immersed into deionized water for solvent exchange, and water would replace the polymer solvent

within the gel. The solvent exchange process usually takes more than two days. After that, the polymer gel would be lyophilized, and eventually a nanofibrous polymer matrix would be obtained. In this nanofibrous matrix, the resulting nanofibers are similar to the natural protein nanofibers in the ECM (50-500 nm).

In phase separation, several parameters may affect the final nanofiber formation. Gelation is the most important factor in controlling the porosity of the nanofibrous scaffold. Gelation temperature normally affects the diameter of nanofibers. A mild gelation temperature (e.g. 22 °C or room temperature) led to fine nanoscale fibers. However, high gelation temperatures cause a platelet-like micron-sized gel due to polymer chain nucleation and crystal size growth. Polymer concentration also has a significant influence on the nanofibers mechanical properties. Increasing polymer concentration can improve the nanofiber mechanical property but will also decrease the porosity of the scaffold. Other factors that affect morphology need to be taken into account; these factors include polymer type, solvent type, and thermal treatment. [86]

The phase separation method can fabricate three dimensional porous nanofibrous scaffolds which have potential applications in the tissue engineering. Ma and co-workers revealed that a nanofibrous scaffold formed by phase separation could process porosity as high as 98%.[85] In the three dimensional tissue scaffold, macroporosity is an important structural parameter that allows cells to localize and proliferate within the matrix and form more organized tissue, instead of growing only on scaffold surface. Macroporosity with pore size between 50–100 μm is preferred in the three dimensional tissue scaffold. Macroporosity could be introduced by incorporating porogens such as sugar or salt micron crystals in the polymer solution during the phase separation. Several studies have

shown that these macroporous scaffolds could enhance cell attachment and distribution.[85-87]

Compared with electrospinning, phase separation requires minimal experimental instrumentation. It could also simultaneously preserve nano- and macro-sized structures within the scaffold greatly benefiting the development of novel three dimensional tissue scaffolds. The disadvantage of phase separation is its long process duration. It usually takes more than two days to finish one experiment and thus increasing the efficiency of phase separation is important.

Self-Assembly

Molecular self assembly is another important pathway for polymeric nanofiber formation. Molecules spontaneously organize into stable and ordered nanofibers via non-covalent bands, such as hydrogen bonds, electrostatic interactions, and/or van der Waals forces.[88] Although these non-covalent bonds are relatively weak compared with covalent bonds, the combination of several non-covalent bonds provides a stable structure with fine mechanic strength.

Among the various polymers, biological molecules, especially peptides and proteins, are of particular interest as the new building blocks in tissue engineering. This technique imitates the natural structural proteins self-assemble into the natural ECM under in vivo environment. Phospholipids are amphiphilic compounds, composed of a cell membrane with other proteins via self-assembly. A number of naturally occurring or synthetic polymers have been formulated into nanofibers via self-assembly. For example, Malkar and colleagues successfully synthesized the triple-helix structure from a peptide amphiphile, which shares many features with the natural ECM.[89] Stupp and co-workers reported peptide nanofibers self-assembled from engineered peptide amphiphile under

pH variance.[90] Aggeli demonstrated that beta sheet peptides could be transformed into a nanofiber structure via self-assembly.[91]

In the self-assembly process, chirality of the peptides plays an important role in the nanofiber formation. For example, a right handed twist of a peptide chain in the beta stranded conformation usually leads to a left handed helical ribbon structure. The detailed mechanisms of these self-assembly nanofibers are still under the investigations.[92] Nanofibers formed by self-assembly also show low polydispersity and good yield, however, self-assembly is a time consuming process.

In summary, biocompatible and biodegradable nanostructured materials are widely expected to play an important role in the future of medicine and the biological sciences. Nano-sized drug vehicles could improve drug delivery specificity/activity with much reduced side toxicity. For tissue engineering, the development of novel three dimensional artificial nanofibrous scaffolds becomes feasible due to the many new nanofabrication technologies.

Professor Charles Martin at University of Florida pioneered a template fabrication technique for preparing nanostructures. A variety of different nanostructures have been successfully prepared by utilizing nanoporous membranes.[93-117] We try to develop, using chemical intuition, a simple and efficient fabrication technique for synthesizing biodegradable nanoparticles and nanofibers. Along the way, we will explore the biomedical applications of the obtained nanostructured materials, paying close attention to drug delivery and tissue engineering.

Dissertation Overview

The goal of this thesis is to develop a simple and scalable method to produce nanostructured biomaterials for drug delivery or tissue engineering applications. We

present here a novel strategy, termed nanopore-injection (N-I) method, based on the use of a nanoporous membrane that separates the feed and receiver solutions. By pumping one solution into the other, through the membrane, we can generate nanostructured materials at the exits of the membrane nanopores.

In Chapter 2, we successfully prepared hydrophobic drug nanoparticles using the N-I method. The resulting nanoparticles were compared to nanoparticles produced via solution enhanced dispersion and supercritical fluids system. The influence of flow rate on particle size was studied. The dissolution profile of hydrophobic drug nanoparticles was tested and compared with the untreated drug powder.

In Chapter 3, ultrafine organic nanoparticles (size < 30 nm) were prepared using the N-I method. Low molecular weight biopolymer chitosan was selected as the particle material. We also investigated the influence of flow rate and viscosity on size control of the particle formation. The fluorescent dye rhodamine 6G was encapsulated in the chitosan nanoparticle and the encapsulation rate was determined by fluorescent spectra measurements.

Chapter 4 described the fabrication of biodegradable polymeric, PLGA-PEG/MCHB and chitosan/luciferin, nanoparticles (~100 nm) using the N-I method and applications of these polymeric nanoparticles in drug delivery in vitro and in vivo. The capability of sustained release was investigated by fluorescent spectra measurements. In vitro cytotoxicity of PLGA-PEG/MCHB nanoparticles was tested in the PC-3 cell line by a clonogenic assay. Bioluminescence imaging was performed on mice to evaluate the in vivo cytotoxicity of chitosan/luciferin nanoparticles.

In Chapter 5, the N-I method was modified to produce biodegradable nanofibers. Type I collagen, a natural structure protein, was selected as the fiber material. The influence of nanopore size on fiber diameter was investigated using a PCTE membrane with different nanopore sizes. A scaffold comprised of collagen nanofibers was prepared for a tissue engineering study. Biomechanical strength of the obtained scaffold was characterized by rheology. Growth and proliferation of cardiac stem cells was investigated on a collagen nanofibrous scaffold.

In Chapter 6, organic/inorganic hybrid nanofibers were prepared using the N-I method for hard tissue engineering. Calcium phosphate doped collagen nanofibers were successfully produced with the characteristic banding structure found in the natural bone matrix. Synthetic polymer poly(acrylic acid) was also used to form hybrid nanofibers with calcium phosphate and calcium carbonate. Human adipose tissue derived stem cells were tested to proliferate and differentiate the obtained nanofibrous scaffold.

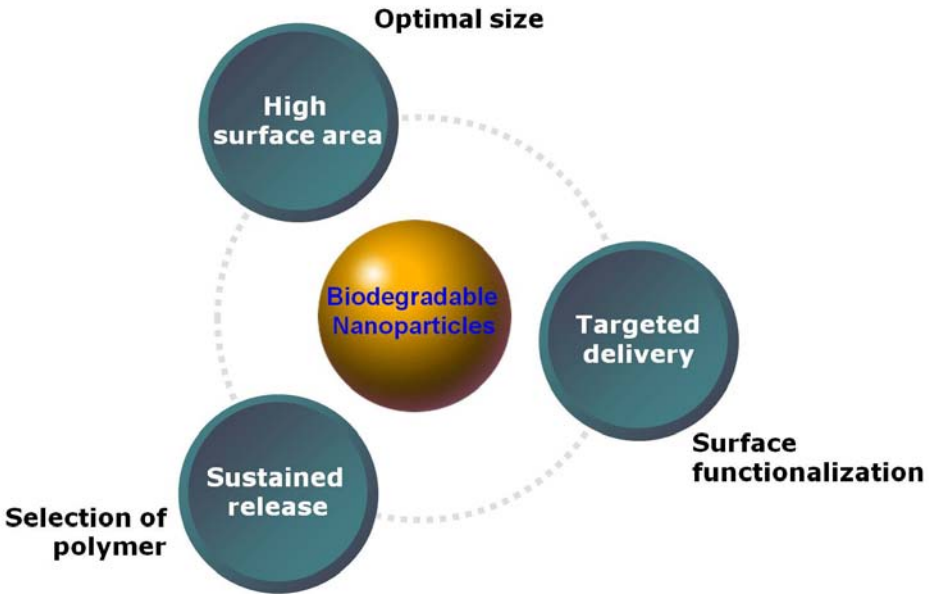

Figure 1-1. Advantages of biodegradable nanoparticles for drug delivery.

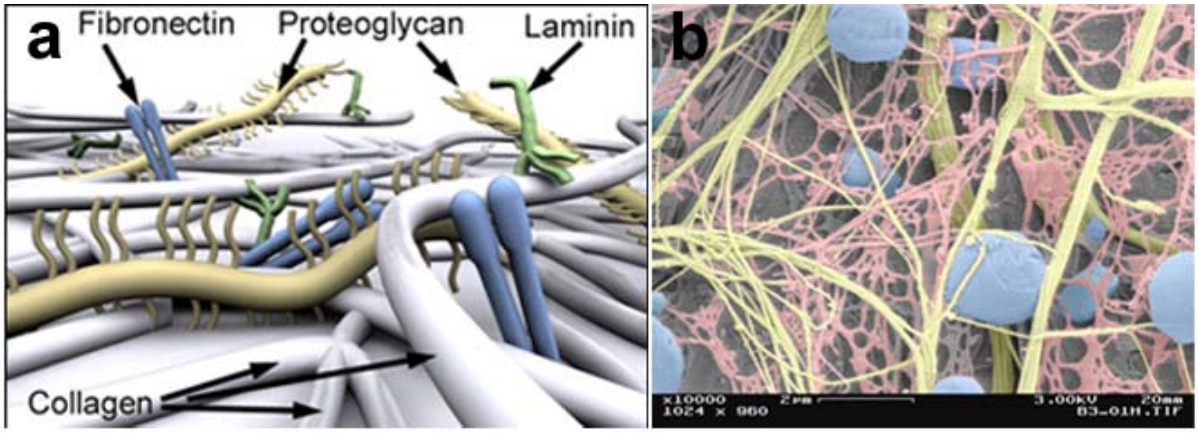

Figure 1-2. (a) Scheme of nanofiber network of natural ECM.[118] (b) A typical SEM image of neural interconnect and ECM.[119] Nerves and nerve bundles (yellow), ECM (red), and ganglion cells (blue).

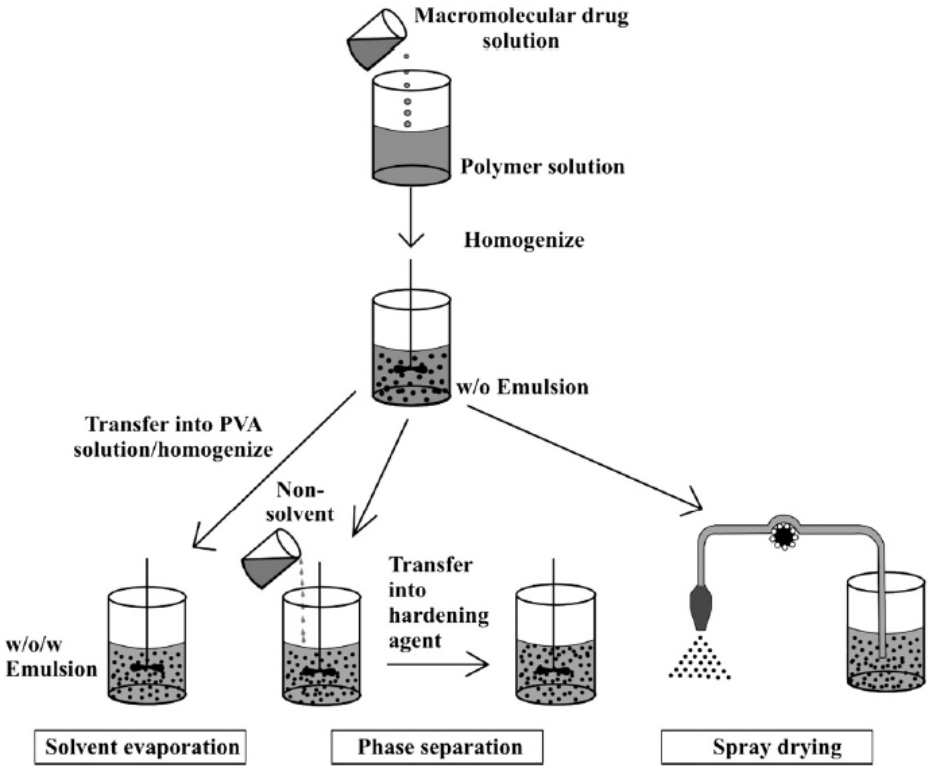

Figure 1-3. Illustration of fabricating biodegradable nanoparticles through nano-emulsion method.[120] (Reprinted with permission from Ref [120]; Copyright 2008 Elsevier.)

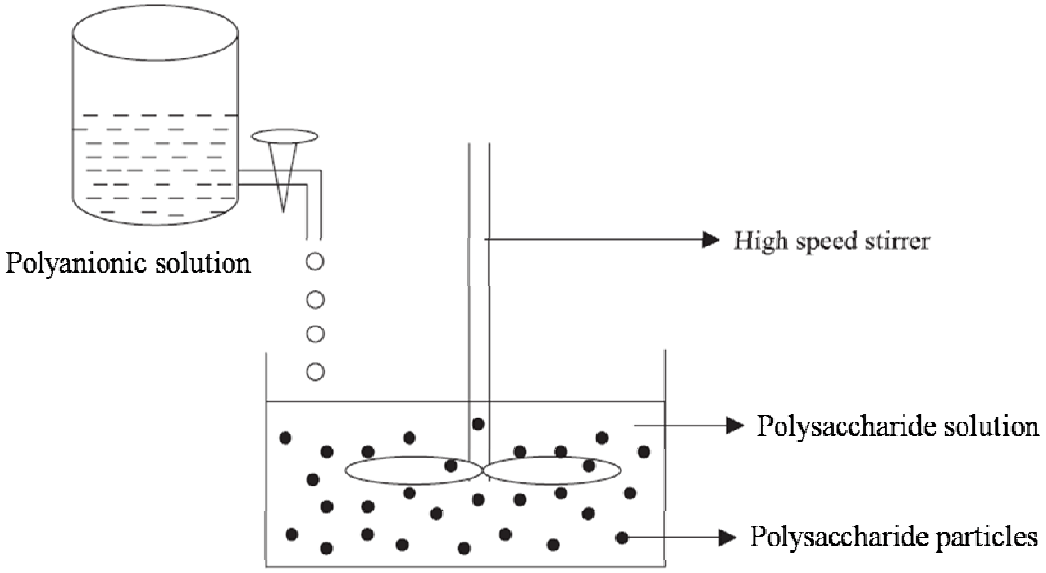

Figure 1-4. Illustration of fabricating biodegradable nanoparticles through ionic gelation method.[121] (Reprinted with permission from Ref [121]; Copyright 2004 Elsevier.)

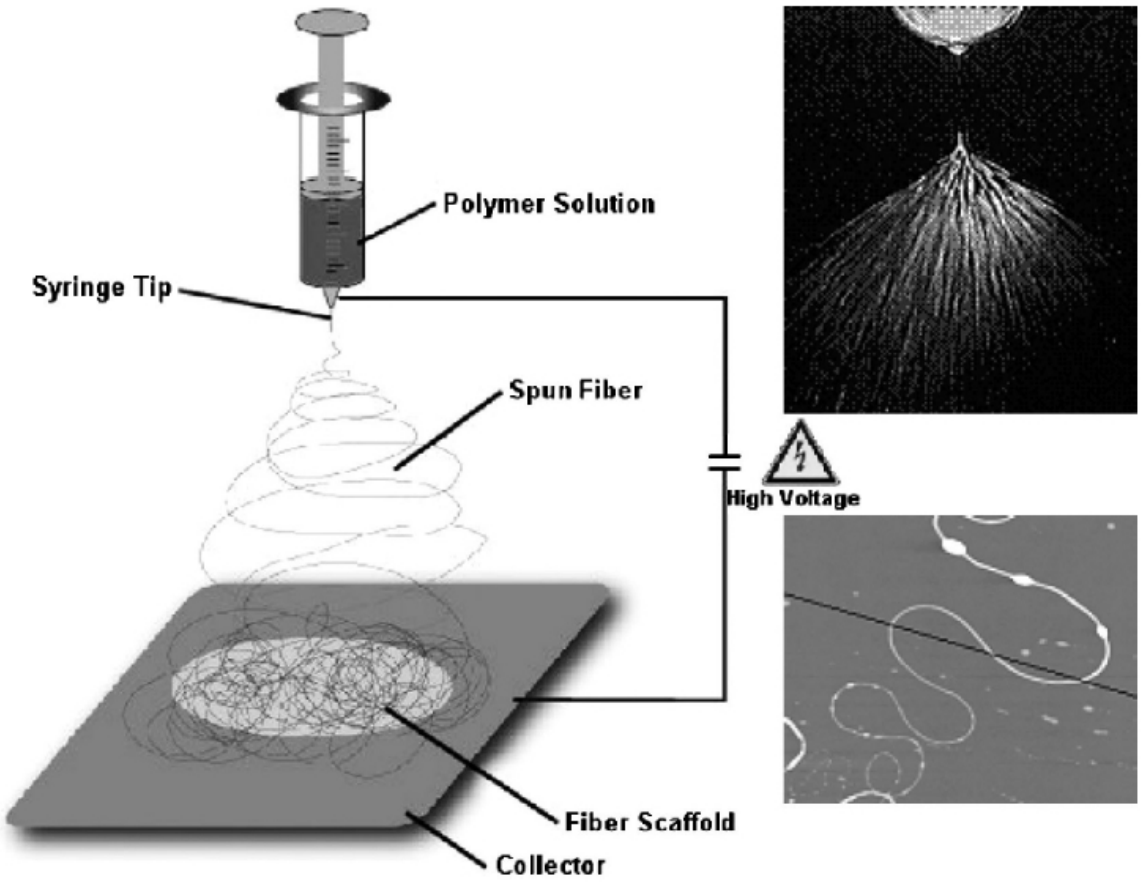

Figure 1-5. Illustration of fabricating biodegradable nanofibers through electrospinning method.[122] (Reprinted with permission from Ref [122]; Copyright 2008 Brill.)

CHAPTER 2
FORMULATING HYDROPHOBIC DRUG NANOPARTICLES

Aim

The clinic applications of hydrophobic compounds are greatly limited by their low bioavailability, as more than 40% of therapeutic compounds are poorly water soluble.[123,124] Considerable effort has been made to improve these hydrophobic drug performance. Among those researches, formulating hydrophobic drugs into nanoparticle form is an efficient strategy to improve the hydrophobic drug delivery, because drug nanoparticles feature a high surface area and sub-cellular size compared with conventional micro-sized drug powder. It has also been proved that dissolution rate of hydrophobic drugs increased when they were formulated into nanoparticulate form, due to the increased contact area between drug and solvent.[125,126] Meanwhile, other studies suggest that the sub-cellular size of nanoparticle leads to a better cell uptake at both in vivo and in vitro system.[127,128] Researchers studied the use of nanoparticle in hydrophobic drug delivery as early as 1970s.[129] Tremendous progress has been made in the last decades during the surging of nanoscience and nanotechnology.[130-133] Several methods have been developed to generate hydrophobic drug nanoparticles, such as nanoprecipitation,[134] nano-emulsion,[135] and ionic gelation.[136] However, drug nanoparticles with uniform small size (<100 nm) and well dispersibility have not yet been produced in a scalable manner.

Herein, we developed a simple and efficient technique for producing hydrophobic drug nanoparticles (NPs) via nanopore-injection (N-I) method (as shown in Figure 2-1). Our strategy is pumping the feed solution dissolved drugs pass through the nanoporous membrane into the receiver solution (in which drugs are insoluble), resulted in

hydrophobic drug nanoparticles formed at the exit of nanopores. Three common hydrophobic therapeutic compounds: silymarin (SM), beta-carotene (BC) and butylated hydroxytoluene (BHT) were selected as model drugs for the demonstration of nanoparticle formation (Figure 2-2). Silymarin is a mixture of flavonolignans exacted from milk thistle, in which silybin is its major chemical constituent with hepatoprotective and anti-cancer clinical effect.[137] Beta-carotene, a terpenoid compound, serves as a precursor to vitamin A in human and animal metabolism.[138,139] Butylated hydroxytoluene is an antioxidant widely used as food addictive.[140] All of three molecules are poorly soluble in water. Meanwhile, according to literature, these molecules show non-toxicity to human body, and are considered safe to be operated in the chemistry laboratory.[137-140]

In order to better evaluate our nanopore injection (N-I) method, we introduced a solution-enhanced dispersion by supercritical fluids system (SEDS), a major commercial formulation method currently used by the pharmaceutics industry, as a comparison method.[141-143] Both of the hydrodynamic drug nanoparticles prepared by N-I method and SEDS method were compared in their diameters, size distributions, and zeta potentials. The particle sizes prepared by N-I method are relatively small with a narrow size distribution. And the producing rate could be as high as 2 mg/min. Compared to other nanofabrication techniques, N-I method provides a simpler and more cost-effective mean to produce hydrodynamic drug nanoparticles. We believe that these small, uniform, and well dispersed drug nanoparticles could exhibit promising applications in the biomedical fields.

Experimental

Materials

Silymarin (SM) and beta-carotene (BC) were purchased from MP Biomedicals, LLC (Solon, OH), and butylated hydroxytoluene (BHT) was purchased from Acros Organics (Geel, Belgium). Anodized aluminum oxide (AAO) membrane (20 nm in diameter) was obtained from Whatman, INC (Piscataway, NJ). All other chemicals were purchased from Sigma-Aldrich (St. Louis, MO) in reagent grade and used as received.

Formation of Hydrophobic Drug Nanoparticles

In N-I experiment, the experimental setup consists of two half U-tubes and a nanoporous membrane which is sandwiched between the two halves (see Figure 2-3). Commercially available anodized aluminum oxide membrane (AAO, Whatman Inc.) was selected as the nanoporous separate with pore diameter of 20 nm (Figure 2-4). The area of AAO membrane exposed to these solutions was about 2 cm^2. The feed solution contained 25 mg of hydrophobic compound in 10 mL organic solvent (SM and BHT was dissolved in acetone, and BC was dissolved in an acetone/tetrahydrofuran (50/50, v/v) blended solution). The receiver solution was 10 mL phosphate buffered saline (PBS, pH 7.4) solution with 0.5 wt% Pluronic F68. One half of the U-tube was filled with 10 mL of feed solution, the other half was filled with 10 mL receiver solution. Gauge pressure was created by connecting a compressed air outlet with a pressure reduction valve to the feed solution side of the U-tube. Usually 2 psi air pressure was applied in a general nanoparticle formation. In this way, the feed solution is pumped into the receiver solution according to the applied pressure. Vigorous magnetic stirring was used in the receiver solution side to help formed nanoparticle disperse in the aqueous solution. Obtained

nanoparticles were collected from the receiver solution by filtration, rinsed three times with deionized water, and dried in the air at room temperature.

In SEDS experiment, the experimental process followed the protocol described in the literature.[141] Briefly, the hydrophobic drug compound solution (2.5 mg/mL SM, BC, BHT in DMSO) was injected (1 mL/min) through a nozzle with 250 mm internal diameter into a supercritical carbon dioxide (SC-CO2) in a speed of 150 g/min at 40 °C and 100 bar. The drug compounds precipitated in the SC-CO2 as an anti-solvent to form nanoparticles.

Analysis of Nanoparticles by Electron Microscope

The morphologies of the obtained hydrophobic drug nanoparticles and untreated drug powder were characterized by a FEI XL30 Sirion SEM. Dry samples on carbon sticky tape were sputter-coated for 90 s at 15 mA with Pd/Au. Average nanoparticle diameters of SM, BC and BHT were determined by measuring 50 random nanoparticles in each SEM image.

Dynamic Light Scattering (DLS) Measurement

Zetasizer Nano ZS (Malvern Instruments, Malvern, PA) was used to measure the hydrodynamic size, polydispersity index (PDI), and zeta potential of the hydrophobic drug nanoparticles. In DLS measurement, obtained nanoparticles were dispersed in the PBS (pH 7.4) with 0.5 wt% Pluronic F68 at a concentration of 100 μg/mL.

X-Ray Diffraction (XRD) Analysis

Powder XRD data were recorded on a PANalytical X'Pert PRO X-Ray Diffractionmeter using filtered Cu Kα radiation (λ=1.5406 Å) at 45 kV and 20 mA. Data were recorded by step scan with a step size of 0.040 ° and a step time of 1.0 s.

Dissolution Rate Measurement

In dissolution profile experiment, 2 mg SM NPs and untreated silymarin powders were weighed accurately, and immersed in the 30 mL PBS at pH 7.4, respectively. The resulting solutions were rotated at 100 rpm, and the temperature of the PBS (pH 7.4) was maintained at 37 ± 0.5 °C. 2 mL of each sample was withdrawn and centrifuged at 10,000 rpm for 5 min. The centrifuge supernatant solution was collected for the ultraviolet (UV) absorbance detection. The UV absorbance intensity was performed at a wavelength of 325 nm using an Agilent 8453 UV-Visible Spectrophotometer. A series of samples were measured at 15 min time interval for 4 h.

Results and Discussion

As shown in Figure 2-3, an experimental setup comprised a nanoporous membrane and two halves of U-tube containing feed solution and receiver solution separately. 2 psi pressured flow was achieved via the connected compressed air on the feed solution, which pumped the feed solution flowing into the receiver solution through the AAO membrane. The AAO membrane is 60 μm thick and contains 20 nm cylindrical pores at the face of the membrane in contact with the feed solution (Figure 2-4). These pores run parallel to one another for approximately 2 μm and then feed much larger (200 nm in diameter) pores that run parallel to one another through the remaining thickness of the membrane. The pore density of the AAO membrane at the entrance, (i.e., in contact with the feed solution) is around $6\times10^{14}/cm^2$.[144] The receiver solution became turbid immediately after the pressure was applied, which indicated the formation of nanodroplets. These nanodroplets formed at the outlet of the 20 nm nanopores, and were detached from the membrane by the transmembrane flow and the continuous stirring flow.

The dispersed nanodroplets were transformed to nanoparticles immediately due to the dissolution of the feed solvent in aqueous solution. No instances of clogging or sticking were found after the experiment. Under a constant air pressure of 2 psi, 40 mg of SM NPs could be obtained within about 20 min (as shown in Figure 2-5).

The obtained hydrophobic drug NPs were imaged using a FEI XL30 Sirion scanning electron microscope (SEM), as well as the untreated drug powder. Figures 2-6 a, d and g show the typical SEM images of the SM, BC and BHT NPs obtained via N-I method. These NPs are spherical in diameter of 80-100 nm with narrow distribution. Figures 2-6 b, e and h show the SEM images of SM, BC, and BHT NPs prepared by SEDS method. Those NPs were in irregular shapes with different sizes. SM, BHT NPs by SEDS have a small diameter at around 20-40 nm, and BC NPs by SEDS has a large diameter at around 200-500 nm. As a comparison, Figure 2-6 c, f, and i show the morphology of untreated SM, BC, BHT, which were all in the form of irregular micro-sized powder.

Hydrodynamic diameters of drug NP was also characterized by dynamic light scattering (DLS) measurement. The obtained DLS data were summarized in Table 2-1. The hydrodynamic diameters of the SM, BC and BHT NPs obtained by N-I method were 83, 105, and 132 nm, with a polydispersity index (PDI) of 0.180, 0.238, and 0.234, respectively (Figure 2-7). As a comparison, the hydrodynamic diameters of SEDS NPs were 496, 546, and 288 nm with a PDI of 0.387, 0.512, and 0.474, respectively (data not shown). All hydrodynamic sizes of the N-I NPs are smaller than those of the SEDS NPs, and their size distributions are narrower. The reason could be attributed to the aggregation of the SEDS NPs, which resulted in the poor dispersibility in aqueous solution. In contrast, N-I NPs have uniform shape and size, and were well dispersed in the

aqueous solution. The hydrodynamic diameters are slightly larger than the sizes obtained by SEM, which might caused by the interaction between the particles and surrounding solvent. It is necessary to point out that the hydrodynamic diameter plays an important role in the drug delivery, especially in the in vivo systems. Nanoparticles with hydrodynamic size range of 10-200 nm are generally considered to be optimal for intravenous injection. Previous studies in other particle systems has proved that bio-distribution of NPs is strongly dependent on the NP hydrodynamic diameter.[127,128,145,146]

The influence of flow rate of feed solution on the particle formation process was investigated (shown in Figure 2-8). SM NPs was selected as the model NPs in this study, and the hydrodynamic sizes of SM NPs were measured by DLS. From the parallel experiments, it could be found that the flow rate of feed solution has an impact on the obtained SM NPs size. While the flow rate of feed solution was varied from 0.03 $mL \cdot min^{-1} \cdot cm^{-2}$ to 2 $mL \cdot min^{-1} \cdot cm^{-2}$ by adjusting the pressure from the compressed air, the hydrodynamic size of SM NPs decreased from 150 to 83 nm. Considering the overlapped size from their error bar, we do not recognize it as a significant size decrease. It was also found that the smallest particle size (83 nm) was obtained at a flow rate flow rate of 1.5 $mL \cdot min^{-1} \cdot cm^{-2}$. These data might not exhibit a clear and significant size decrease with the increase of feed solution flow rate. We can still estimate a slow decreased trend on the increased flow rate from the mean diameter of the N-I nanoparticles.

A crystalline structure change in SM NPs was observed before and after treated with N-I method. The crystalline structure of SMNPs was examined using powder XRD (Figure 2-9). Before N-I process, the untreated silymarin powder was a semi-crystalline

material, exhibiting some peaks of medium intensity together with a strong underneath scattering phenomenon. As for the crystalline portion, five characteristic peaks show up at 14.6°, 16.5°, 19.5°, 22.3° and 24.5° of 2θ, which is also found in other studies.[147-149] After N-I process, SM NP shows no crystalline peaks in the XRD spectra. This is because the resulting SM NPs were transferred into the amorphous phase during the N-I process. Our hypothesis is that the total time for silymarin precipitating into nanoparticle is too short to form ordered crystalline structure during the N-I experiment. A calculated flow rate inside the nanopore is over hundreds micrometers per second. Such a high flow rate resulted in great number of nanodroplets formed at the exit of nanopore, which were detached due to the wall shear force by the transmembrane flow and the continuous stirring flow, and subsequently transformed into nanoparticles rapidly.

As dissolution rate is a crucial factor in hydrophobic drug delivery, we studied the dissolution rate of the N-I NPs. Silymarin NPs was selected as a model compound in this study, and the resulting dissolution profile is compared with that of untreated SM powder. All the dissolution profiles are characterized using UV adsorption spectrometer. Test conditions, including rotation rate, temperature of the medium, and method used to obtain samples, were the same for both samples. Figure 2-10 shows the dissolution profile of SM NPs and untreated silymarin powder. The dissolution rate of SM NPs is significantly greater than that of untreated silymarin powder. At 30 min, the dissolve percentage of SM NPs reached more than 80% compared with that of untreated silymarin powder (~15%). As amorphous nanoparticles normally exhibit a faster dissolution, the enhancement of the dissolution profile is believed to be attributed to the amorphous nature of SM NPs, as well as the increased surface area after N-I process.

Perspective

With the proper design and system control, we fabricate uniform hydrophobic nanoparticles (SM, BC and BHT NPs) with <100 nm size through nanopore-injection (N-I) method. The obtained nanoparticles exhibit smaller hydrodynamic diameter and better dispersibility in aqueous solution, compared with those made through SEDS method. Due to the rapid precipitation, the obtained N-I NPs were amorphous, which resulted in the faster dissolution rate in PBS. This is crucial in drug delivery to enhance the efficiency of the desired pharmaceutical compound. The nanopore-injection (N-I) method can be used to fabricate more poorly water-soluble drugs and enhance they drug performance than those described here. Moreover, because it is intrinsically a low cost direct technology, N-I method can be used for scalable production when such fabrication become difficult or expensive with traditional nanofabrication methods.

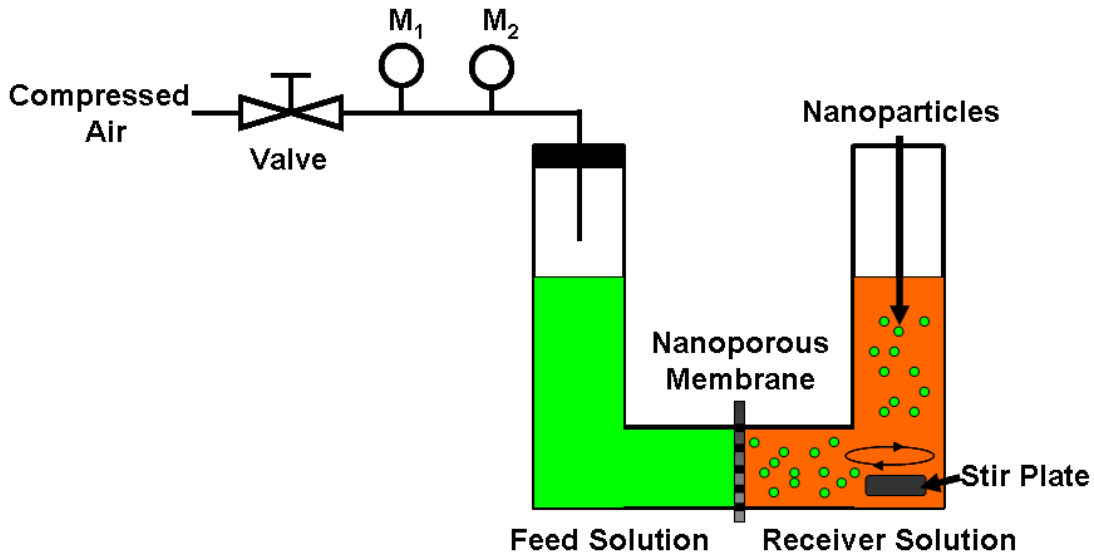

Figure 2-1. Experimental set-up for the hydrophobic drug nanoparticle preparation using nanoporous membrane. M1 Pressure meter. M2 Flow meter.

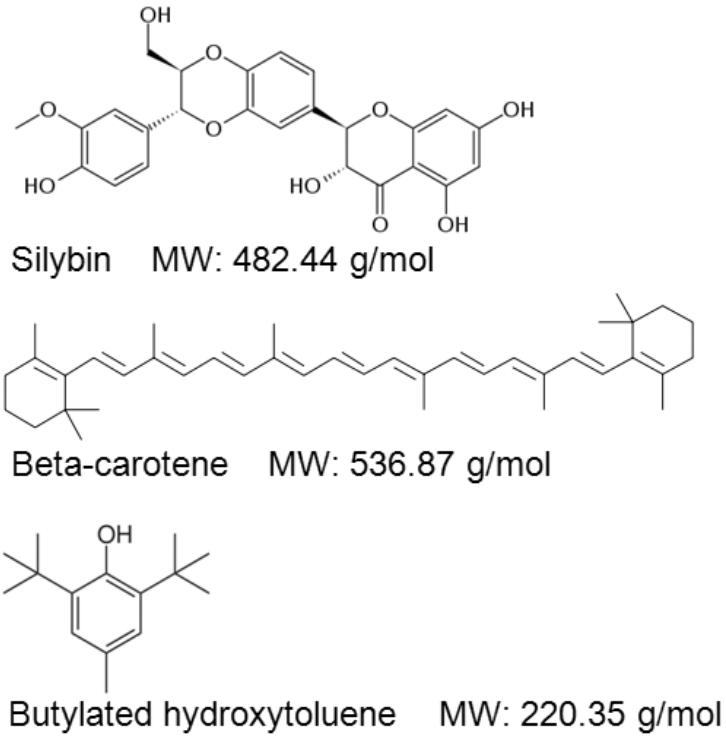

Figure 2-2. Chemical structures of three hydrophobic compounds: silybin, beta-carotene, and butylated hydroxytoluene.

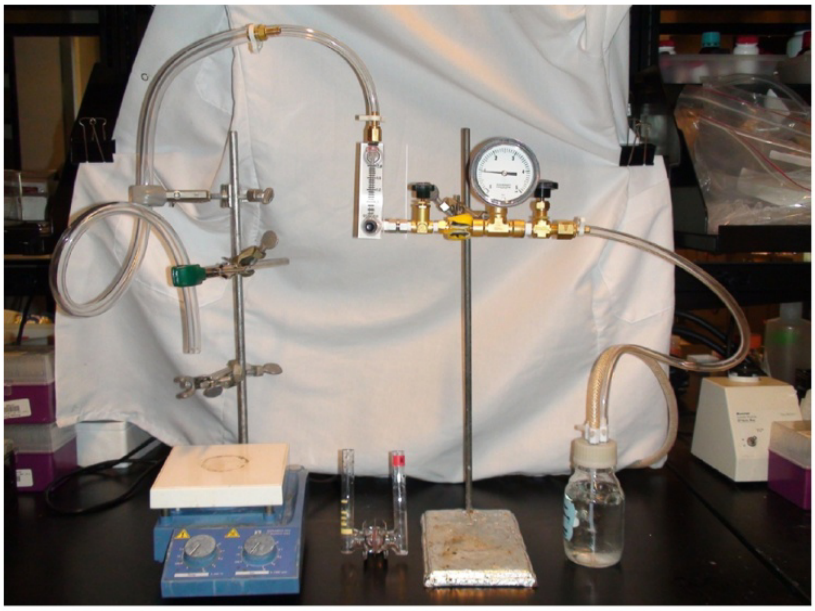

Figure 2-3. Photograph of a typical experimental setup.

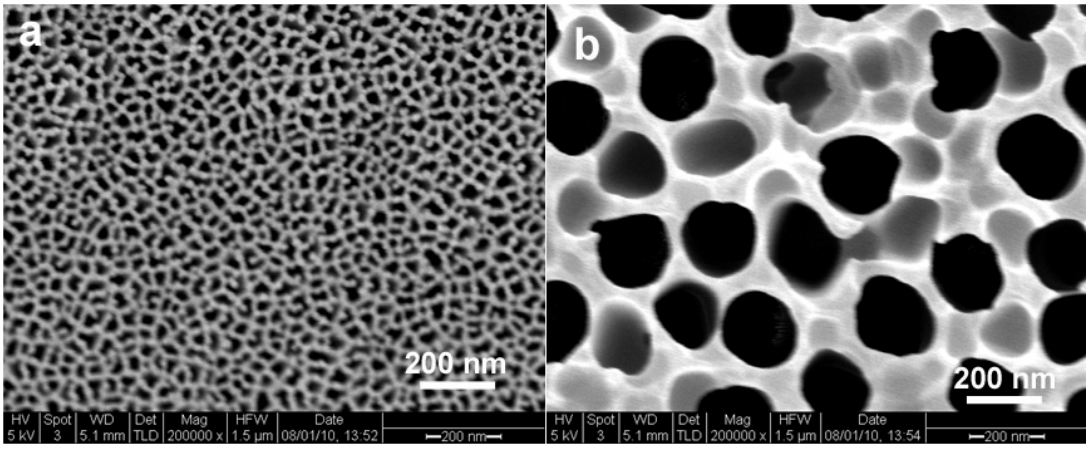

Figure 2-4. SEM images of nanoporous membranes: anodized aluminum oxide (AAO) membrane with (a) 20 nm inlet and (b) 200 nm outlet.

Figure 2-5. Photograph of 40 mg silymarin nanoparticles obtained within 20 min by using AAO nanoporous membrane. A penny serves as a size marker.

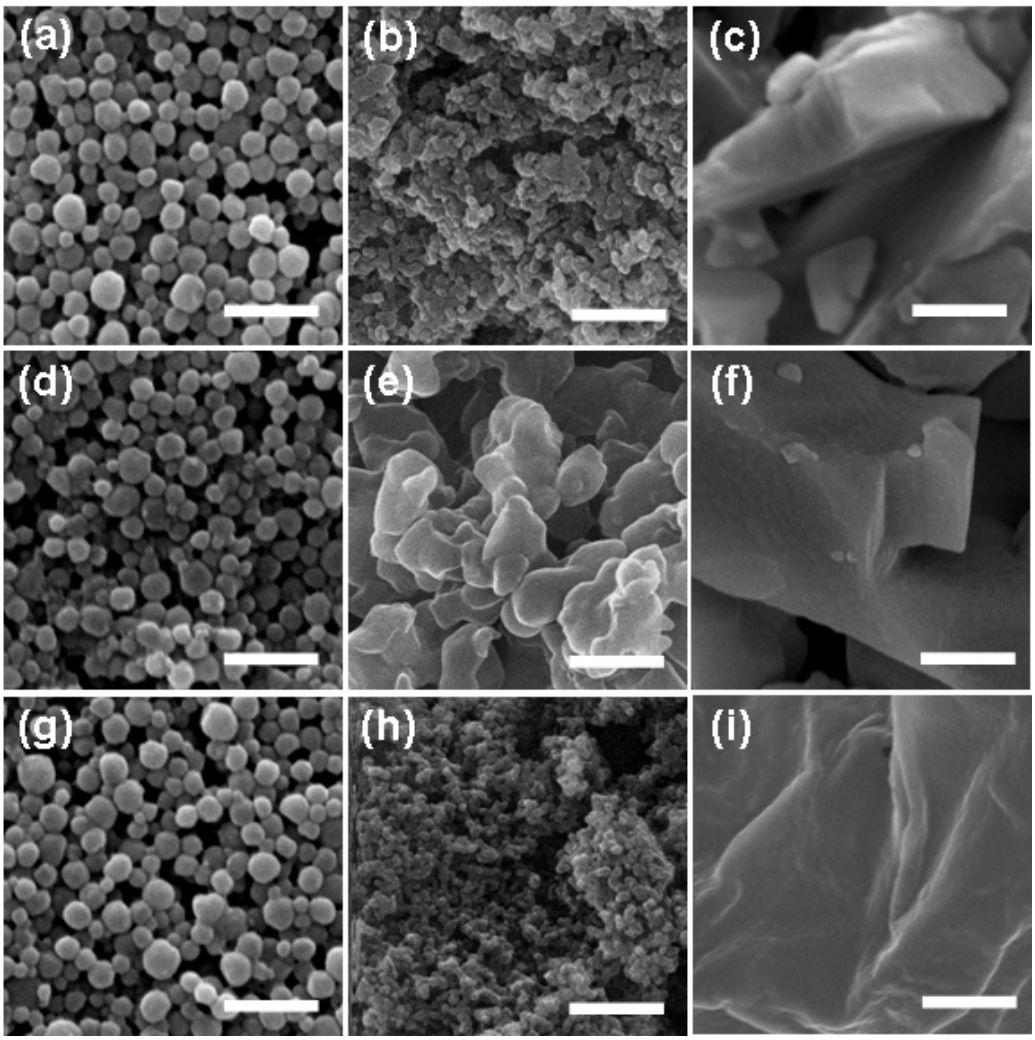

Figure 2-6. SEM images of SM, BC, and BHT drug nanoparticles. a, d, and g are SM, BC, and BHT NPs via N-I method, respectively; b, e, and h are SM, BC, and BHT NPs via SEDS, respectively; c, f, and i are untreated SM, BC, and BHT, respectively. The scale bar is 500 nm in all the figures.

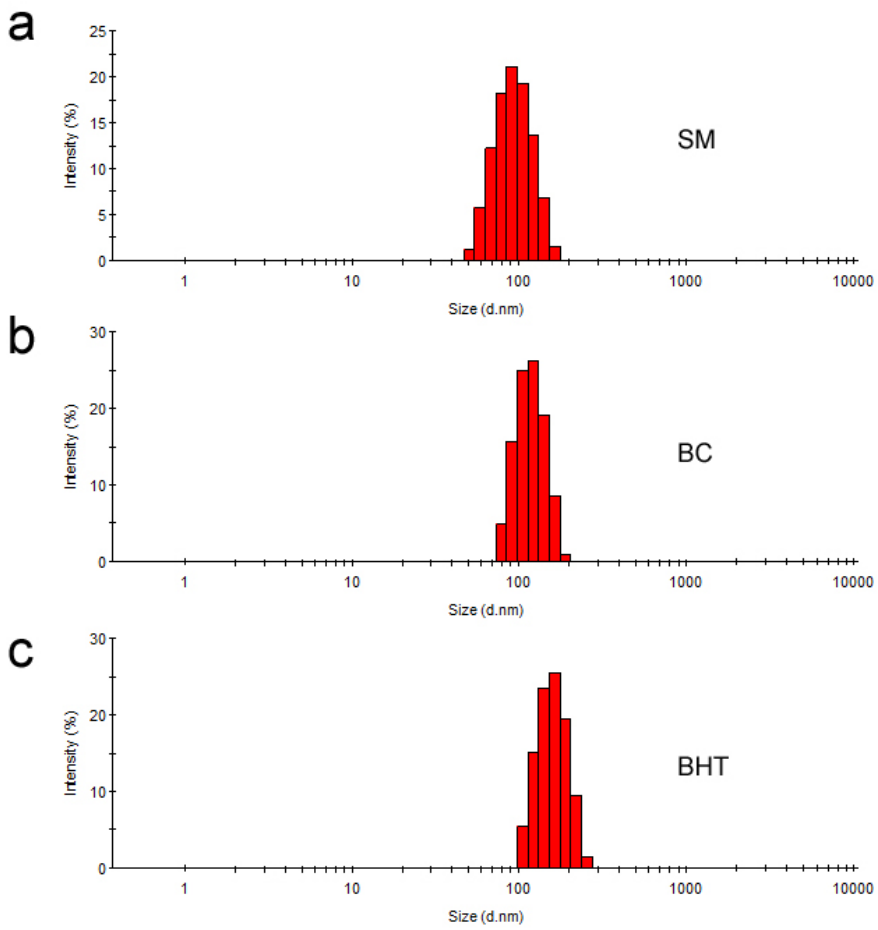

Figure 2-7. Hydrodynamic diameters of (a) SM, (b) BC, and (c) BHT drug nanoparticles determined by DLS.

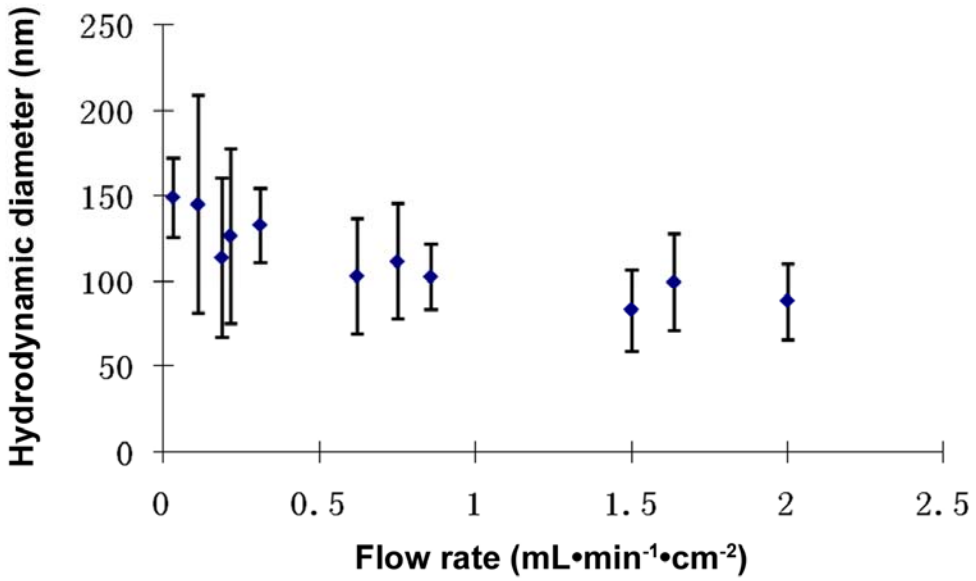

Figure 2-8. Effect of flow rate on diameter of the SM NPs obtained.

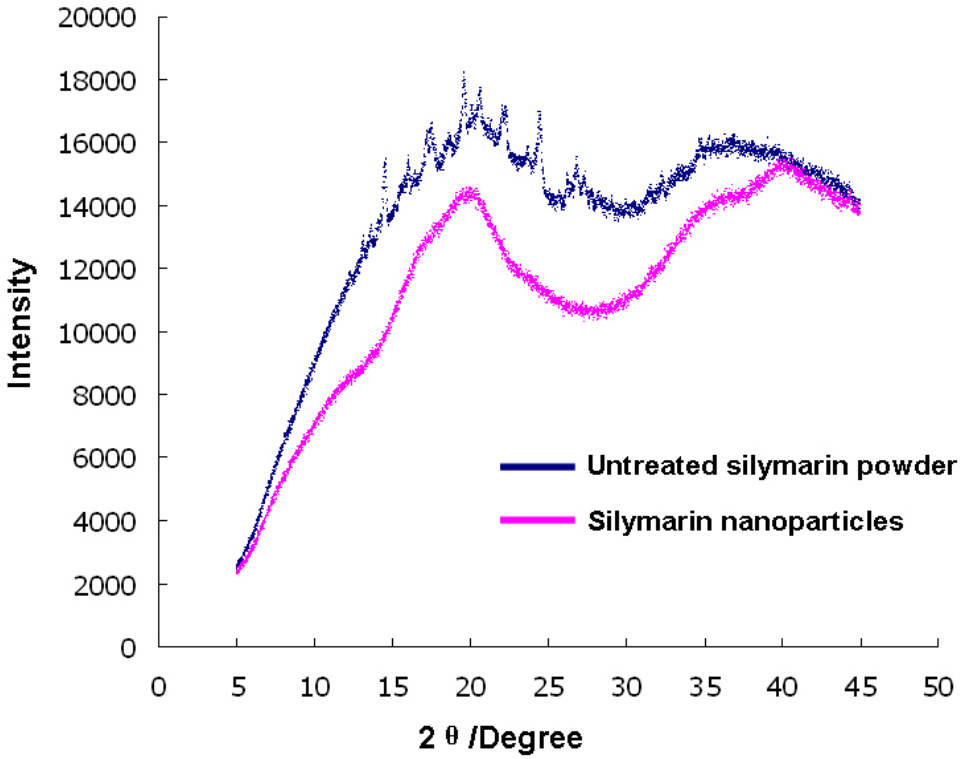

Figure 2-9. XRD pattern of silymarin nanoparticles and untreated silymarin powder.

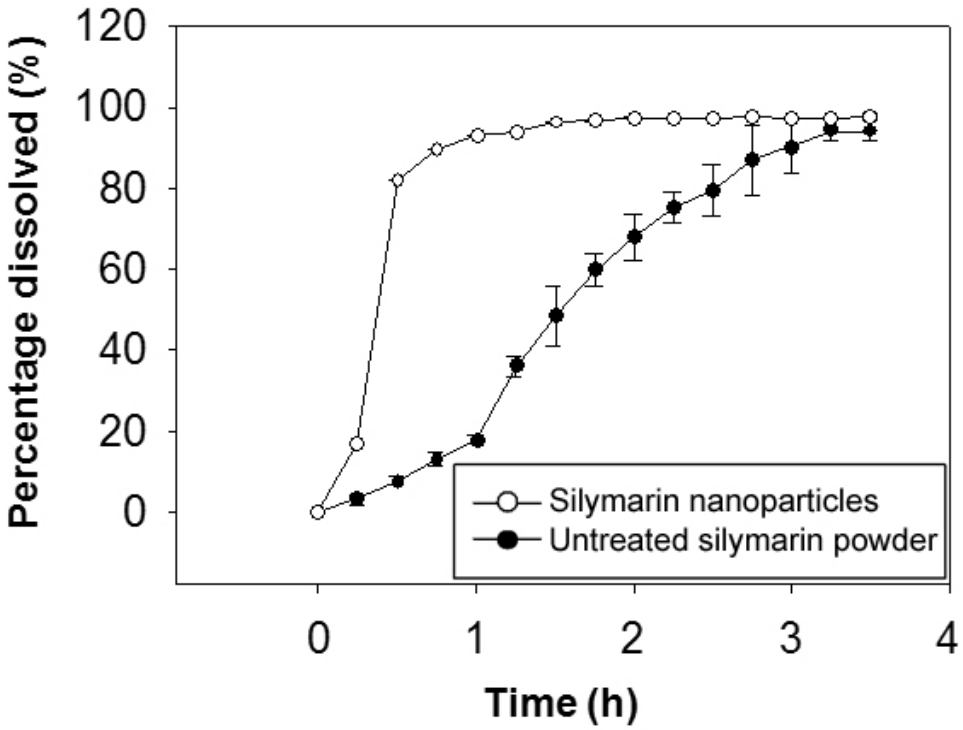

Figure 2-10. Dissolution profiles for silymarin nanoparticles and untreated silymarin powder in PBS (pH 7.4) at 37°C.

Table 2-1. Summary of the DLS analysis of hydrophobic nanoparticles.

Compound	Method	Diameter (nm)	PDI	Zeta-Potential (mV)
SM	N-I	83 ± 18	0.180	-3.3
BC	N-I	105 ± 26	0.238	-7.0
BHT	N-I	132 ± 32	0.234	-7.8
SM	SEDS	496 ± 58	0.387	-10.3
BC	SEDS	546 ± 55	0.512	-11.7
BHT	SEDS	288 ± 16	0.474	-11.8

CHAPTER 3
GENERAL METHOD FOR PRODUCING POLYMERIC NANOPARTICLES USING NANOPOROUS MEMBRANES

Aim

The spatial and temporal control of the release of pharmaceuticals at the site of where they act is a key requirement for the therapeutic use of a drug.[150-152] One method for realizing this objective is to create drug-loaded nanoparticles made out of biodegradable polymers.[141] Previous work in two laboratories, one at Stanford University, the other at the University of Florida, has featured the generation of such nanoparticles.[142,143,153-158] We present here an alternative strategy based on the use of a nanoporous membrane that separates the two liquids. By pumping one liquid into the other, through the membrane, we can generate nanoparticles at or near the exits of the membrane nanopores. We illustrate this technique for the low molecular weight biopolymer chitosan, which is a polysaccharide consisting of 13–17% units of monomeric N-acetyl-glucosamine and 83–87% glucosamine units.[159]

Low molecular weight chitosan (average MW 20,000 Daltons) is used as a model polymer in our work because it is a naturally biodegradable and biocompatible polysaccharide, which has broad applications in pharmaceutical and biomedical fields.[160-162] Chitosan is also known as a pH-response polymer, because at low pH, chitosan's amines are protonated and positively charged causing chitosan to be a water-soluble cationic polyelectrolyte. At high pH, these amines become deprotonated, and the polymer loses its charge and becomes insoluble.[163,164] Chitosan serves as a representative material for our process which can be adopted for other the production of other organic nanoparticles.

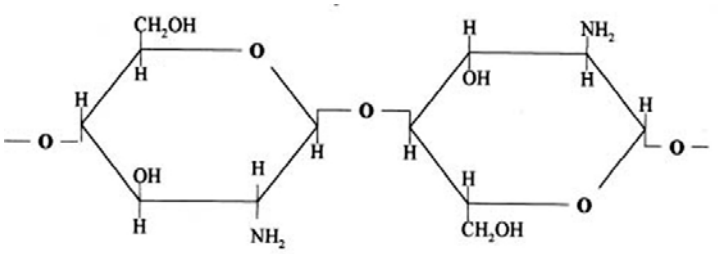

Structure of Chitosan

Experimental

Materials

Track-etched polycarbonate (PCTE, 10 nm in diameter, 6 μm in thickness) was purchased from Osmonic Inc (Minnetonka, MN). Anodized aluminum oxide (AAO, 20 nm in diameter, 60 μm in thickness) was purchased from Whatman Inc (Piscataway, NJ). Low molecular weight chitosan (CS, Mw 20,000) was obtained from Sigma-Aldrich (St Louis, MO). Rhodamine 6G (R6G) was purchased from Fisher Scientific Inc (Worcester, MA). All other chemicals were reagent grade and used as received. Purified water, obtained by passing house-distilled water through a Barnstead, E-pure water purification system, was used to prepare all solutions.

Formation of Ultrafine Chitosan Nanoparticles

The U-tube setup consists of two half U-tubes and a nanoporous membrane which is sandwiched between the two halves (see Figure 3-1). PCTE membrane with pore diameter of 10 nm, and AAO membrane with pore diameter of 20 nm are used in our experiments. The feed solution contained 25 mg of chitosan in 20 mL of 10^{-3} M HCl (pH=3.0). The receiver solution was 10 mL of 10^{-3} M NaOH (pH=11). One half of the U-tube was filled with 20 mL of feed solution, the other half was filled with 10 mL receiver solution. In some experiments 250 mbar gauge pressure was created by connecting a compressed air outlet with a pressure reduction valve to the feed solution side of the

U-tube. In this way, the feed solution is pumped into the receiver solution according to the applied pressure. Nanoparticles formed are collected by filtration through PCTE membranes and dried at room temperature. The filter membranes also serve as the substrate for scanning electron microscopy (SEM).

Characterization of Chitosan Nanoparticles

The size and morphology of formed nanoparticles are observed by scanning electron microscope (SEM) and transmission electron microscope (TEM). SEM images were acquired using an FEI XL30 Sirion SEM. Dry samples on carbon sticky tape were sputter-coated for 120 s at 15 mA with Pd/Au. Transmission electron microscopy (TEM) was carried out using a FEI Tecnai G2 F20 X-TWIN. Samples were deposited on formvar carbon-coated copper grids.

Hydrodynamic size and zeta potential of formed nanoparticles was measured by a Zetasizer Nano ZS (Malvern Instruments, Malvern, PA). Chitosan nanoparticles was dispersed in deionized water at a concentration of 100 μg/mL, pH=7.0.

Encapsulation of Rhodamine 6G in Chitosan Nanoparticles

Rhodamine 6G encapsulated chitosan (CS/R6G) nanoparticles were produced by N-I method. 5.0 wt% R6G is premixed with the feed solution. PCTE and AAO membrane were used to produce CS/R6G NPs. The morphology and size of formed nanoparticles were characterized by TEM and DLS.

The amount of R6G encapsulated in the chitosan particle was determined by a fluorescent intensity method. Dry CS/R6G particles were dissolved in a phosphate/citrate buffer solution at pH=3.0. The fluorescence of dissolved solution was measured. The resulting fluorescence intensity was calculated into a R6G concentration in phosphate/citrate buffer solution using standard concentration curve. The R6G loading

efficiency of CS/R6G was calculated using the amount of R6G encapsulated divided by the amount of R6G premixed in the feed solution.

Results and Discussion

The experimental device (Figure 3-1) is composed of a nanoporous membrane, which separates two solutions. The pH of the feed solution (left in Figure 3-1) is adjusted so that chitosan is soluble in this solution. The feed solution is forced under pressure through the pores of the membrane into the receiver solution (right in Figure 3-1). The pH of the receiver solution is adjusted such that chitosan is insoluble. When nanodroplets of the soluble chitosan are injected through the membrane into the receiver solution nanoparticles of chitosan are formed. For the preparation of nanoparticles with reduced sizes, membranes with uniform and well-defined nanopores are essential.[165-167] In our work, we use commercially available track-etched polycarbonate (PCTE, OSMONIC Inc.) and anodized aluminum oxide (AAO, Whatman Inc.) nanoporous membranes. The PCTE membrane is 6 μm thick and contains track-etched cylindrical pores with a diameter of 10 nm and pore density of $6\times10^{8}/cm^{2}$ (Figure 3-2 a.). The AAO membrane contains is 60 μm thick and contains 20 nm cylindrical pores at the face of the membrane in contact with the feed solution. These pores run parallel to one another for approximately 2 μm and then feed much larger (200 nm in diameter) pores that run parallel to one another through the remaining thickness of the membrane. The pore density of the AAO membrane at the entrance, (i.e., in contact with the feed solution) is around $6\times10^{14}/cm^{2}$ (Figure 3-2 b, c).[144]

The feed solution contained 25 mg of chitosan in 20 mL of 10^{-3} M HCl (pH=3.0). The receiver solution was 10 mL of 10^{-3} M NaOH (pH=11). The area of membrane exposed to these solutions, either PCTE or AAO, was 2 cm^{2}. Gravity flow was achieved via a height

difference between the two solutions, causing the low pH chitosan feed solution to flow into the high pH receiver solution. Nanodroplets are formed at or near the outlet of the PCTE nanoporous membrane in contact with the high pH solution, causing precipitation of the chitosan. In the case of the AAO membrane the precipitation likely occurs at near the exits of the 20 nm nanopores. The chitosan nanoparticles (CSNPs) are carried away from the membrane by the constant gravity flow. No instances of clogging or sticking were found.

Nanoparticles were collected from the receiver solution by filtration, rinsed three times with deionized water, and dried in air at room temperature. We obtained 4.2 μg of nanoparticles per hour by PCTE, and 610 μg of particles per hour by AAO. These differing values are caused by the large pore density difference between the two kinds of nanoporous membranes.

CSNPs were imaged using a TEM-1230 (JEOL) electron microscope, operated at 100 kV. Samples were deposited on carbon-coated copper grids and negatively stained with 1% uranyl acetate. Figure 3-3 a shows a typical TEM image of the CSNP obtained using the PCTE membrane having 10 nm nanopores. The nanoparticles were found to have a mean diameter of 5 nm. Figure 3-3 b shows that CSNPs obtained using the AAO membrane. These nanoparticles have a mean diameter of 21 nm, which suggests that they are formed near at the exit of the smaller nanopores (20 nm) in the AAO membrane.

Dynamic light scattering (DLS), measured with a Zetasizer Nano ZS (Malvern Instruments, Malvern, PA), was used to obtain hydrodynamic particle diameters. The hydrodynamic diameters of the particles obtained using the PCTE and AAO membranes were 9 nm and 26 nm, respectively (Figure 3-4). The particle size from DLS is slightly

larger than the diameter estimated using electron microscopy because DLS measures the diameter of the particles while still in solution, whereas TEM provides the diameter of the particles after thorough drying.[168] That larger particles are obtained using the AAO membranes reflects the fact that the pore diameter in contact with the receiver solution is 20 nm for this membrane vs. 10 nm for the PCTE membrane.

We also investigated the effect of flow rate of chitosan solution on the particle-formation process. CSNPs obtained using the AAO membrane were used in these studies. The flow rate of chitosan solution was varied from 7.2 $\mu L \cdot min^{-1} \cdot cm^{-2}$ to 32 $\mu L \cdot min^{-1} \cdot cm^{-2}$ by adjusting the height difference between the feed and receiver solutions. DLS measurements were used to obtain the particle diameters. Particle diameter was found to increase exponentially with flow rate, over the flow-rate range investigated (Figure 3-5). At higher flow rates nanowires are formed as found from SEM images (not shown). It was also found that the narrowest particle size distribution was obtained at a flow rate flow rate of 7.2 $\mu L \cdot min^{-1} \cdot cm^{-2}$.

The viscosity of the chitosan feed solution also has a profound effect on nanoparticle-formation process. The viscosity of chitosan feed solution was varied by adding glycerol, while maintaining its pH at 3. Particle sizes initially increased with viscosity but leveled at higher viscosities (Figure 3-6). We suggest that this is caused by a change in the diffusion rate, which decreases rapidly as the viscosity increases, causing larger particles to be formed at slower diffusion rates. When the viscosity of chitosan solution achieves a certain point, particle size stops growing, perhaps owing to the gravity-induced detachment of the nanodroplets from the membrane into the sodium hydroxide solution.

For the drug loading and encapsulation study, we use rhodamine 6G (R6G) as a model system to mimic a drug molecule. The organic molecule R6G is one of with most often used fluorescent dyes with excitation and emission wavelengths at 525 nm and 555 nm, respectively.[169-171] Using such a fluorescent model compound provides us with a rapid method to evaluate the encapsulation data, which in turn allows us to optimize the process parameters.

In our experiment, 5.0 wt% R6G is premixed with the chitosan solution. Figure 3-7 shows the TEM images of R6G-loaded chitosan nanoparticles obtained using the PCTE and AAO membranes, respectively, and Figure 3-8 show the corresponding results obtained using dynamic light scattering.

The amount of R6G encapsulated in the chitosan particle was determined by dissolving the dry particles in a phosphate/citrate buffer solution at pH=3 followed by fluorescence measurements of the released R6G. When 5.0 wt% of R6G, referred to the weight of chitosan, was added to the feed solution, and the PCTE membrane was used, the amount of R6G incorporated into the nanoparticles was 2.7 wt% (Table 3-1). The amount incorporated into the particles prepared using the AAO membrane was 3.3 wt%. Table 2-1 summarized these results and includes the polydispersity index (PDI) values.

Perspective

In this chapter, we successfully prepared ultrafine chitosan nanoparticles by N-I strategy. The obtained nanoparticle has a small size (<30 nm) with narrow size distribution. Particle size increases with flow rate and viscosity of feed solution. Fluorescent dye rhodamine 6G was encapsulated into chitosan nanoparticles with a encapsulation ratio of about 3 wt%. It provides a general technique for incorporating guest molecules in the host chitosan nanoparticles. We believe that many other

biodegradable polymer systems can be loaded with different organic compounds, which suggests the practical use of this technique in preparing pharmaceuticals in nanoparticle form for drug delivery.

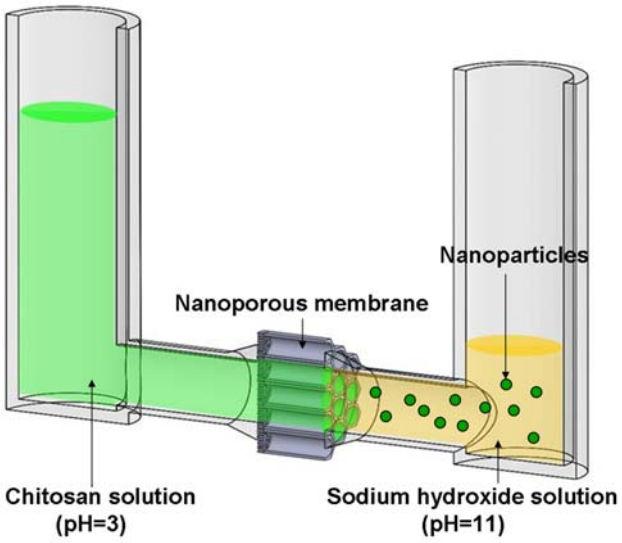

Figure 3-1. Method for producing chitosan nanoparticles by flow though a nanoporous membrane.

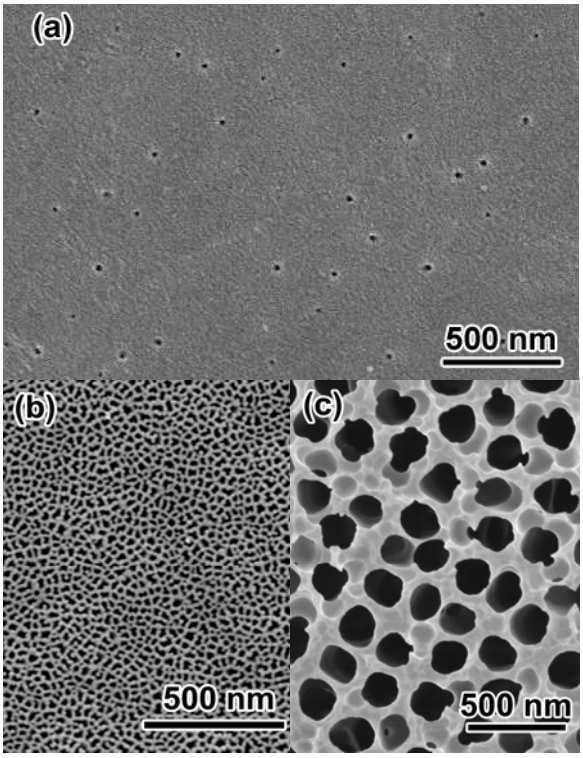

Figure 3-2. SEM images of nanoporous membranes: (a) track-etched polycarbonate (PCTE) membrane with 10 nm pores; and anodized aluminum oxide (AAO) membrane with (a) 20 nm inlet and (c) 200 nm outlet.

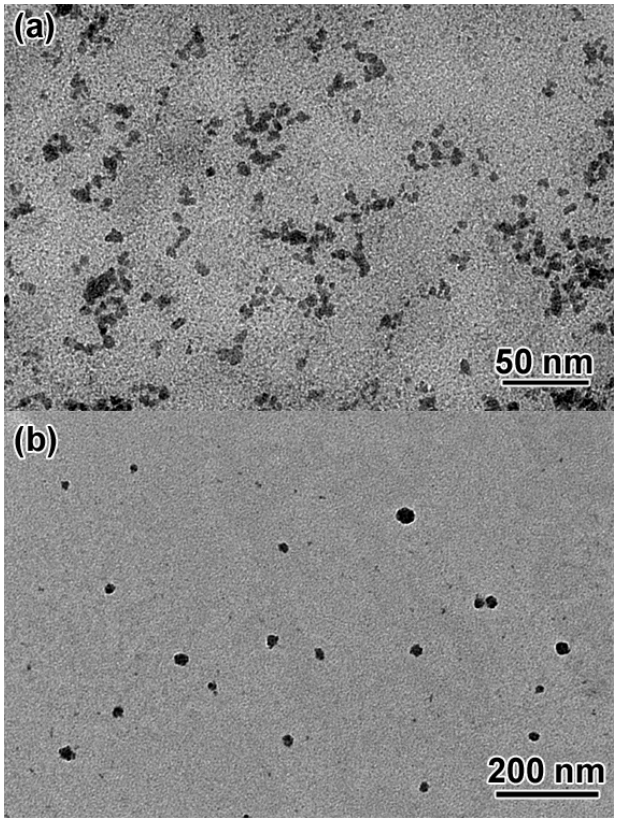

Figure 3-3. Typical TEM images of chitosan nanoparticles (CSNPs) prepared by using (a) the PCTE membrane; and (b) the AAO membrane. In these TEM images, the black area represents the nanoparticle, and the grey area represents the background.

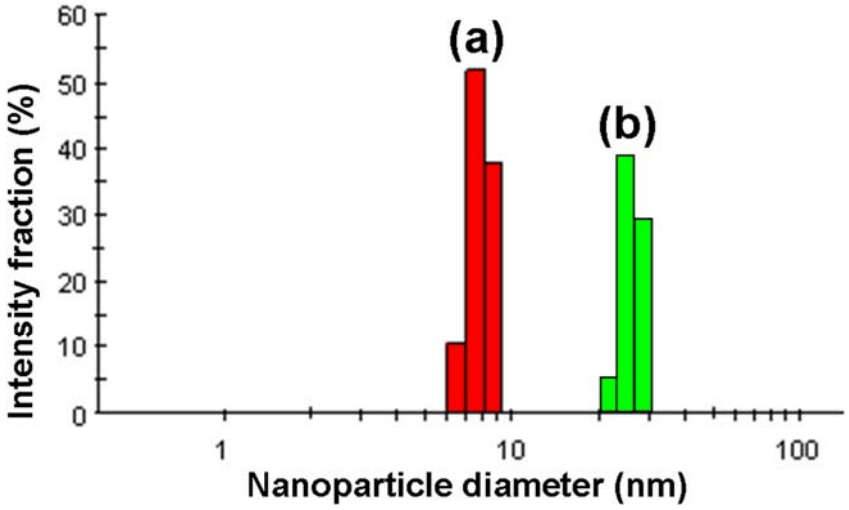

Figure 3-4. Comparison of size distributions of chitosan nanoparticles (CSNPs) prepared by using different nanoporous membranes determined by dynamic light scattering: (a) size of CSNPs obtained by PCTE membrane; and (b) size of CSNPs obtained by AAO membrane.

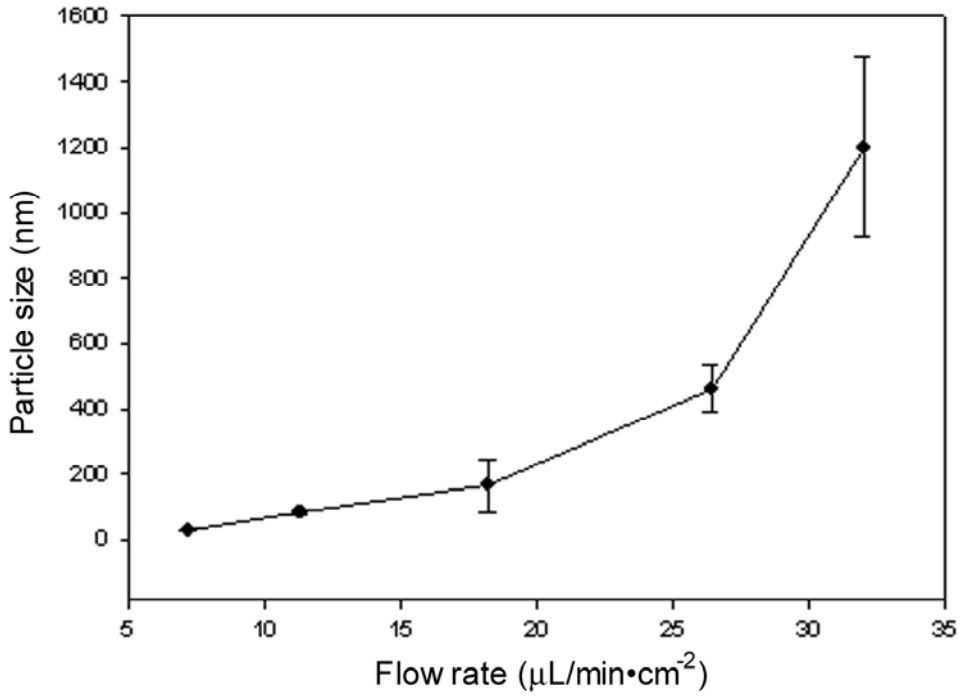

Figure 3-5. Effect of solution flow rate on the diameter of the chitosan nanoparticle obtained.

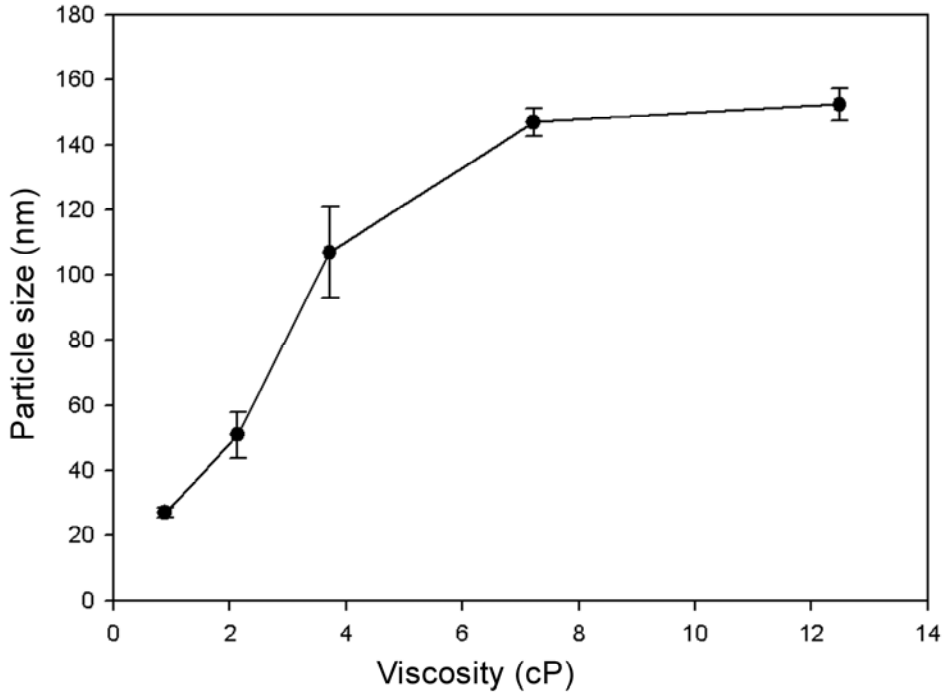

Figure 3-6. Effect of the viscosity of the chitosan feed solution on the diameter of the nanoparticles obtained.

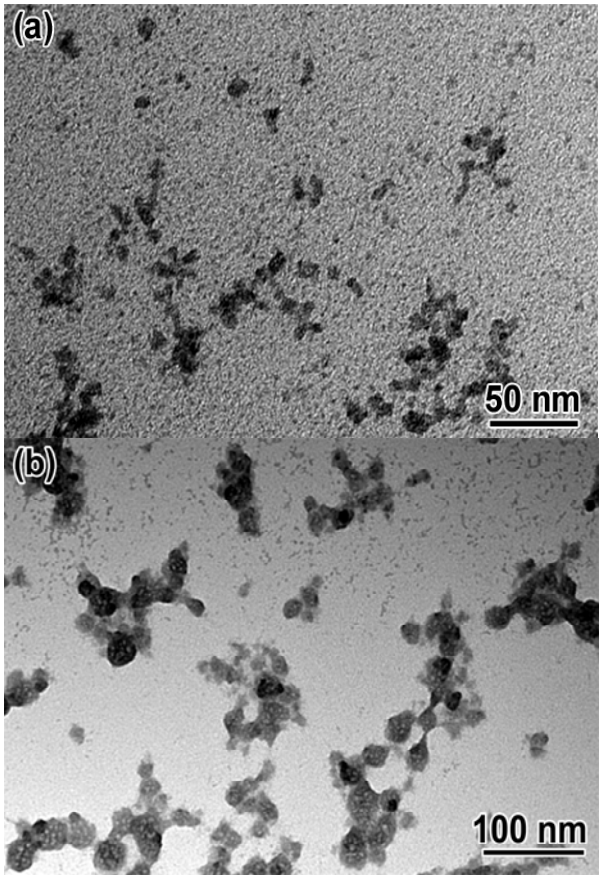

Figure 3-7. Typical TEM images of chitosan-rhodamine 6G nanoparticles prepared by using (a) the PCTE membrane and (b) the AAO membrane. In these TEM images, the black area represents the nanoparticle, and the grey area represents the background.

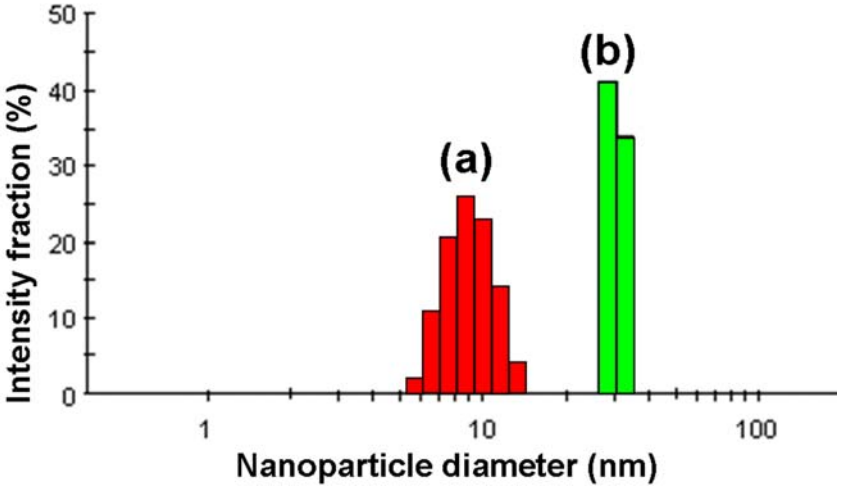

Figure 3-8. Comparison of size distributions of chitosan-rhodamine 6G nanoparticles prepared by using different nanoporous membranes determined by dynamic light scattering: (a) PCTE membrane; and (b) AAO membrane.

Table 3-1. Statistical size and encapsulation efficiency data for rhodamine 6G loaded chitosan nanoparticles.

Membrane	Particle	Diameter TEM (nm)	Diameter DLS (nm)	PDI	Encapsulation Ratio (%)
PCTE	CS NP	5 ± 2	8 ± 1	0.204	
PCTE	CS-R6G NP	5 ± 3	9 ± 2	0.108	2.7
AAO	CS NP	21 ± 5	26 ± 2	0.228	
AAO	CS-R6G NP	30 ± 8	30 ± 4	0.333	3.3

CHAPTER 4
BIODEGRADABLE POLYMERIC NANOPARTICLES AS DRUG DELIVERY VEHICLE

Aim

The applications of nanostructured biomaterials in drug delivery increase the need of developing specific and active drug delivery systems, which should distinctly advantage in improved bioavailability, enhanced drug performances, targeted delivery and sustained release. Biodegradable polymeric nanoparticles have been extensively investigated for sustained release or targeted delivery of various therapeutics, including small molecular drugs and macromolecules. Tailoring of the functional nanocarriers, such as the selection of matrix material and encapsulation efficiency, has a profound influence on release profile, delivery efficacy and drug performance.

In this chapter, we use nanopore-injection (N-I) method for preparing two different biodegradable polymeric nanoparticles: poly(lactide-co-glycolide)-co-poly(ethylene glycol) (PLGA-PEG) and chitosan nanoparticles. PLGA-PEG is a synthetic amphiphilic polymer composed of two biodegradable polymers widely applied in the drug delivery realm, while chitosan is a naturally occurring biopolymer used in many areas such as biomedical, pharmaceutical and biotechnological fields as well as in the food industry. Both PLGA-PEG and chitosan are Food and Drug Administration (FDA) approved safe biopolymer for drug delivery research. Therapeutic agents were physically dispersed in the biodegradable polymer matrix (9-Amino-6-chloro-5H-benzo(a)phenoxazine-5-one (MCHB) in PLGA-PEG NPs; Luciferin in chitosan NPs). MCHB is a toxic drug converted from a novel non-toxic prodrug 6-chloro-9-nitro-5-oxo-5H-benzo(a)phenoxazine (CNOB) using an specific enzyme E. coli nitroreductase, ChrR6 (discovered by Professor A. C. Matin at Department of Microbiology and Immunology in Stanford University). Utilization

of prodrug in drug delivery, instead of directly delivery of toxic drug, could greatly minimize the damage to the normal tissue, thus enhance the effectiveness in treating cancer diseases.

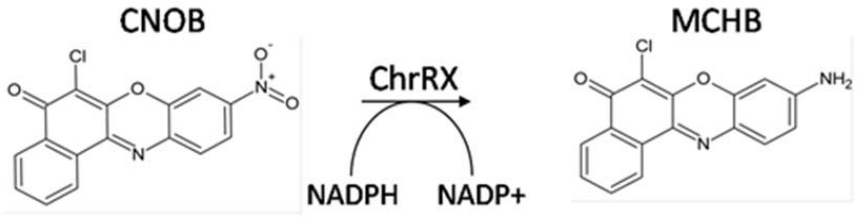

Hydrophilic compound luciferin is selected as another model therapeutic agent. Luciferin is a substrate for the enzyme luciferase that produces a bioluminescent signal at approximately 610 nm at 37 °C which can be measured in vivo. In our experiments, luciferin was encapsulated with chitosan to form chitosan/luciferin (CS/Luc) nanoparticles.

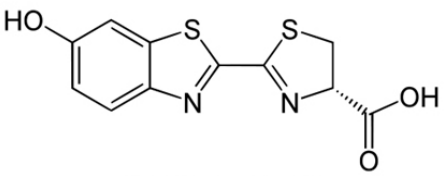

Structure of Luciferin

Our drug encapsulated biodegradable nanoparticles exhibited the capability of sustained release, which is favored in drug delivery. In vitro cytotoxicity of PLGA-PEG/MCHB nanoparticles tested by clonogenic assay revealed an improved drug performance in eliminating PC-3 prostate cancer cells. CS/Luc nanoparticles expressed in vivo biocompatibility demonstrated by bioluminescence imaging. We believe that biodegradable polymeric nanoparticles produced by N-I method have a promising future as novel drug delivery vehicle.

Experimental

Materials

9-Amino-6-chloro-5H-benzo(a)phenoxazine-5-one (MCHB) was provided by Prof. A. C. Matin (Department of Microbiology and Immunology, Stanford University). Luciferin was obtained from Polysciences Inc. (Warrington, PA) and used as received. Heterobifunctional PEG (amine-PEG-carboxylate) (MW =3,400 g/mol) was obtained from Nektar Therapeutics (San Carlos, CA). Poly(D, L-lactide-co-glycolide) (PLGA) was obtained from Lactel Absorbable Polymers (Pelham, AL) with terminal carboxylate groups. All other chemicals were purchased from Sigma-Aldrich (St Louis, MO) and used without further purification.

Synthesis and Characterization of PLGA-PEG Diblock Copolymer

Synthesis of PLGA-PEG diblock copolymer is using the protocol reported by Gu and co-workers,[172] covalent bind PLGA-COOH with NH2-PEG-COOH using EDC/NHS chemistry:

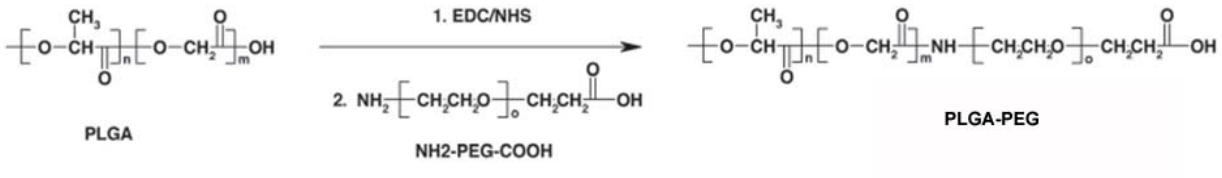

Reactant solutions were prepared as follows: a total of 10 g of PLGA-carboxylate (0.56 mmol) was weighed accurately, and dissolved in 20 mL dichloromethane (DCM); 270 mg N-hydroxysuccinimide (NHS, 2.2 mmol) and 460 mg 1-ethyl-3-(3-dimethylaminopropyl)-carbodiimide (EDC, 2.4 mmol) were weighed accurately, and dissolved in 4 mL DCM separately. EDC/NHS solution was slowly added into the PLGA-carboxylate solution. The resulting PLGA-NHS was precipitated with 20 mL ethyl ether/methanol (50/50, v/v) blended solution. The PLGA-NHS was separated by

centrifugation at 4,000 rpm for 20 min. The precipitation was washed and centrifuged for three times, and dried under vacuum over night. A total of 2 g PLGA-NHS (0.118 mmol) resulting from the last step was weighed accurately and dissolved in 8 mL DCM, then added with 500 mg amine-PEG-carboxylate (0.148 mmol) and 56 mg N,N-Diisopropylethylamine (DIEA, 0.44 mmol), and stirred for 2 h. The resulting PLGA –PEG diblock copolymer was precipitated with ether/methanol (50/50, v/v) blended solution and washed with the same solution for three times, to remove the unreacted PEG. PLGA-PEG diblock copolymer was dried under vacuum over night, and stored in -20 °C for further experiment.

NMR characterization of PLGA-PEG diblock copolymer: the PLGA-PEG diblock copolymer was characterized by a Mercury 400 nuclear magnetic resonance (NMR, 400 MHz ^{1}H). For the preparation of sample solution: 5 mg PLGA-PEG was dissolved in 1 mL of deuterated chloroform ($CDCl_3$).

Formation of Drug Encapsulated Nanoparticles

PLGA-PEG/MCHB NPs Preparation: N-I method was used to prepared the nanoparticles. The detailed process was described as in Chapter 2. Briefly, in a typical U-tube setup, 50 mg PLGA-PEG and 2.5 mg MCHB were completely dissolved in 40 mL acetone as the feed solution, and PBS (pH 7.4) with 0.5 wt% Pluronic F68 was used as the receiver solution. 20 nm AAO membrane was selected as the nanoporous membrane. 2 psi gauge pressure was applied on the feed solution side. Obtained nanoparticles are collected by filtration and rinsed with deionized water for three times, and dried at room temperature.

Chitosan/luciferin NPs Preparation: N-I method was used to prepared the nanoparticles. Feed solution contained 1.25 mg/mL chitosan and 62.5 μg/mL luciferin in

phosphate buffered saline (PBS, pH 3.0). Receiver solution contained PBS (pH 11.0) with 0.5 wt% Pluronic F68. All other parameters remained the same as described in the PLGA-PEG/MCHB NPs Preparation.

Characterization of Drug Encapsulated Nanoparticles

Scanning electron microscope (SEM) images were obtained using a FEI XL30 Sirion SEM. Dry samples on carbon sticky tape were sputter-coated for 90 s at 15 mA with Pd/Au.

Zetasizer Nano ZS (Malvern Instruments, Malvern, PA) was used to measure the hydrodynamic size, polydispersity index (PDI), and zeta potential of the obtained nanoparticles. In DLS measurement, nanoparticles were dispersed in the PBS (pH 7.4) with 0.5 wt% Pluronic F68 at a concentration of 100 μg/mL.

Sustained Release Study of Drug Encapsulated Nanoparticles

A total of 2 mg obtained nanoparticles are accurately weighed and immersed in the 30 mL PBS (pH 7.4). The resulting solution was rotated at 100 rpm, and the temperature of the PBS (pH 7.4) was maintained at 37 ± 0.5 °C. 500 μL of each sample was withdrawn and centrifuged at 10,000 rpm for 5 min in order to remove the nanoparticles from the solution. The centrifuge supernatant solution was collect for the fluorescence absorbance measurement. The fluorescence absorbance intensity was performed using a Spectra Max Gemini EM Fluorescence Microplate Reader. A series of samples were measured within total time duration up to 2 weeks.

Fluorescent Microscopy Imaging

For cell uptake studies, PC-3 prostate cancer cell line was used in this experiment. PC-3 cells were seeded on 35 mm glass-bottomed culture dishes at a density of 8.5×10^4 cells/dish. On day 2 of culture, the cells were rinsed with PBS prior to addition of

PLGA-PEG/MCHB NPs dropwise (200 µL) with incubation at 4 °C for 1 h. Unbound NPs were rinsed off with a gentle PBS wash, the incubation buffer was replaced, and the cells were warmed to 37 °C for various times up to 4 h in the absence or presence of treatments. After incubation, the cells were rinsed four times with PBS and imaged with a Zeiss LSM 510 Meta NLO imaging system equipped with a Coherent Chameleon multiphoton laser mounted on a vibration-free table.

In Vitro Cytotoxicity Study by Clonogenic Assay

In the clonogenic assay, 1000 PC-3 prostate cancer cells were incubated with the following three samples: free MCHB (9.66 µg), PLGA-PEG Null nanoparticles (200 µg), and PLGA-PEG/MCHB nanoparticles (200 µg, MCHB: 9.66 µg) for 1 h at 37 °C, trypsinized and plated for clonogenic assay. The cultures of PC-3 cell lines were incubated at 37 °C in a humidified incubator with 7.5% CO_2. After two weeks, the number of colonies formed in each dish was counted with an Omnicon FAS II counter (Bausch & Lomb, Rochester, NY). Drug effects on the PC-3 cells are assessed as a reduction in PC-3 cell colony growth in the treated cultures compared to the untreated controls. In our experiment, control sample was the untreated PC-3 cells.

In Vivo Cytotoxicity Study by Bioluminescence Imaging

We use transgenic mice that express firefly luciferase (FVB-luc+) to evaluate delivery of luciferin from the chitosan nanoparticles. Four mice were intravenously injected with CS/Luc NPs (two mice) and chitosan null NPs (two mice); two mice were subcutaneously injected with CS/Luc NPs (right area in the mice) and chitosan null NPs (left area in the mice). For all injected nanoparticle solutions, they contain 2.0 mg nanoparticles dispersed in 250 mL of 0.5 wt% Pluronic F68 in PBS. Bioluminescence imaging was performed on a Xenogen IVIS 200 using a cooled charge-coupled device

camera. Data was analyzed with LivingImage software (Xenogen) and expressed in photons per steradian per second for each region of interest such that the data are not dependent on camera settings, chamber geometry, or integration time.

Results and Discussion

PLGA-PEG/MCHB Nanoparticle

In order to synthesize PLGA-PEG copolymer, we covalent bind PLGA-COOH with NH2-PEG-COOH using EDC/NHS chemistry:

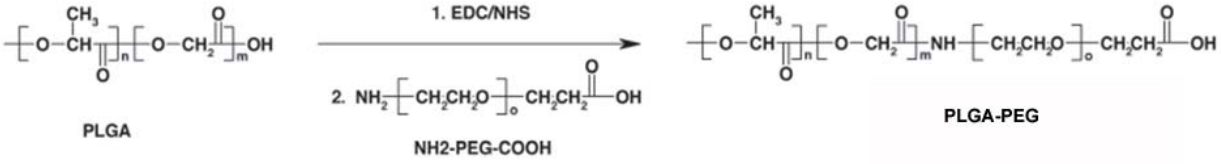

The terminal carboxyl group on the hydrophobic PLGA reacted with the terminal amine group on the hydrophilic PEG, and form an amphiphilic diblock polymer. The 1H NMR characterization of PLGA-PEG is shown in the Figure 4-1. The presence of PEG on the PLGA-PEG was visualized by the characterized peaks between 3.4 and 3.8 ppm, which is in accordance with literature.[172] It confirmed that PEG was covalently bonded with PLGA and formed diblock copolymer.

PLGA-PEG/MCHB NPs were formulated by N-I method, and a typical SEM image is shown in Figure 4-2. From this image, it could be found that PLGA-PEG/MCHB NPs exhibit a smooth spherical morphology with a relatively narrow size distribution. The mean diameter of these NPs is around 90 nm calculated by the size measurement using ImageJ.

Dynamic light scattering (DLS) measurement was performed on a Zetasizer (Nano ZS) to analyze the hydrodynamic diameter and the zeta potential. As shown in Figure 4-3, PLGA-PEG/MCHB NPs show a hydrodynamic diameter of 96 ± 7 nm with a low

polydispersity index (PDI) of 0.143. It revealed that PLGA-PEG/MCHB NPs formed by N-I method have a uniform size with in 100 nm, and could be well dispersed in the aqueous environment without forming aggregations. The zeta potential of these NPs is –3.5 mV in pH=7.4 PBS. The negative charge is from the carboxyl groups at the terminal end of the hydrophilic PEG block. The outer sphere composed of PEG is believed to help nanoparticle escape from reticuloendothelial system elimination, resulted in enhanced biocompatibility and circulation half-life in vivo. It also minimizes electrostatic interactions with opposite charged biomolecules in the in vivo environment, preventing from aggregation. Meanwhile, the functional PEG chains will facilitate surface modification of the nanoparticles, such as antibody conjugation for targeted delivery.

MCHB as a fluorescent model compound (ex: 575 nm, em: 625 nm) allows us to evaluate the encapsulation ratio with a rapid method, i.e. fluorescence spectrum. In our experiment, the amount of MCHB encapsulated in PLGA-PEG particle was determined by dissolving the cleaned dry nanoparticles in acetone followed by fluorescence measurements. When 5.0 wt% of MCHB, referred to the weight of PLGA-PEG, was added to the feed solution, the amount of MCHB incorporated into the nanoparticles was 4.8 wt%. The encapsulation efficiency (EE) of MCHB is calculated to be 97%, using the formula EE = Amount of drug bound/Total amount of drug used for nanoparticle production.

The in vitro sustained release of PLGA-PEG/MCHB NP was studied under the intimating degradation condition in human body, dispersing them in PBS (pH 7.4) at 37 °C and rotated at a low speed. The release profile of PLGA-PEG/MCHB NPs is shown in Figure 4-4. In this figure, the profile demonstrates a rapid increase of cumulative drug

release in the first 12 h, over 50 wt% MCHB was released. It may suggest that the MCHB encapsulated at or near the surface of the particle released much faster than those encapsulated within the center. After that, the release speed of MCHB slowed down, and the nanoparticles gradually released the rest MCHB over a total time of 7 days (approached 95%). Such a controlled release profile facilitates the NPs for the delivery of anticancer therapeutics.

The efficacy of the MCHB encapsulated NPs to defeat cancer cells is reflected by their cytotoxicity for the cancer cells. Then, we tested the in vitro cellular cytotoxicity of the obtained PLGA-PEG/MCHB NPs by clonogenic assay, which is a microbiology technique for studying the effectiveness of specific agents on the survival and proliferation of cells. The in vitro differential cytotoxicity of MCHB free drug, PLGA-PEG null NPs, and PLGA-PEG/MCHB NPs, as well as the blank control, were tested using PC-3 prostate cancer cell line. The total number of colonies in blank control sample was counted and serviced as a background. Figure 4-5 shows the quantitative analysis results. In the free drug samples, around 50 % of PC-3 cells were eliminated. No killing effect was observed in the PLGA-PEG null NPs samples, which suggests that PLGA-PEG nanoparticle, as a drug delivery vector, is non-toxic to PC-3 cells. When PLGA-PEG/MCHB NPs were cultured with PC-3 cells, all the PC-3 cells were eliminated after 1 h incubation. It suggests that PLGA-PEG/MCHB NPs are significantly more cytotoxic than free MCHB. The observed toxicity in the PLGA-PEG/MCHB may due to the cell uptake and subsequent MCHB release. These cell viability data confirmed that using PLGA-PEG NP as a vector improved the MCHB delivery efficiency, and enhanced MCHB in vitro performance.

The fluorescent image of PC-3 cells after cultured with PLGA-PEG/MCHB NPs was shown in Figure 4-6 a. Fluorescence signals were from the internalized PLGA-PEG/MCHB NPs by PC-3 cells. The image is blurred because PC-3 cells were vibrating under the microscope due to the cytotoxicity of MCHB. A much clearer fluorescent image was observed by incubating PC-3 cell with non-toxic PLGA-PEG/CONB NPs, which is shown in Figure 4-6 b.

Chitosan/luciferin Nanoparticles (CS/Luc NPs)

As reported in the Chapter 3, we have successfully prepared ultrafine chitosan nanoparticles (< 30 nm) by N-I method. In this chapter, we prepared chitosan nanoparticles (130 nm in diameter) for drug delivery through the similar procedure. Figure 4-7 shows a typical SEM image of the CS/Luc NPs. The nanoparticles were found to have a mean diameter of about 130 nm. Dynamic light scattering (DLS) was used to determine the hydrodynamic diameter of the CS/Luc NPs (Figure 4-8). The hydrodynamic diameter of the particles obtained using the AAO membranes was 137 ± 13 nm with a PDI of 0.274. The zeta-potential of CS/Luc NP is 7.0 mV in pH=7.4 PBS. This positive surface charge of obtained nanoparticle attributes to free amine groups on chitosan polymer chain. Those free amine groups acquire protons from aqueous solution at near neutral pH and lead to a slightly positive charge existing on the surface of the nanoparticles.

The drug loading and encapsulation of CS/Luc NP was examined following the same method in PLGA-PEG/NPs. Luciferin is natural fluorescent compound with the excitation wavelength at 330 nm and the emission wavelength at 525 nm. When 5.0 wt% of luciferin, referred to the weight of chitosan, was added to the feed solution, and the AAO membrane was used, the amount of luciferin incorporated into the nanoparticles was 1.8 wt%. The encapsulation efficiency (EE) of luciferin is calculated to be 36%. EE of

luciferin in CS NPs (36%) is much lower than that of MCHB in PLGA-PEG NPs (97%) because both NPs were eventually precipitated in the aqueous phase, and luciferin (salt form) is very hydrophilic and difficult to be trapped in the polymer matrix compared with hydrophobic MCHB.

The in vitro sustained release of CS/Luc NPs was shown in Figure 4-9. CS/Luc NPs was dispersed in PBS (pH 7.4) at 37 °C and rotated at a low speed. The release half life of CS/Luc NPs, which means 50 wt% of luciferin encapsulated in the CS NPs is released into the solution, is about 3 days. The total release time of CS/Luc NPs is about 12 days. An early rapid release of luciferin in the release profile was observed, which is similar as the one in PLGA-PEG/MCHB NP release profile.

We also studied the in vivo toxicity of obtained CS/Luc NPs. Xenograft model was used by intravenous and subcutaneous injection of CS/Luc NPs within luciferase transgened mice. All mice used in our experiment were transgene engineered mice expressing luciferases, which could convert existing luciferin in mouse body into bioluminescence signals. The results are shown in Figure 4-10. In Figures 4-10 a and b, two pairs of mice were intravenously injected with CS/Luc NPs and CS Null NPs. The first pair of mice showed whole body fluorescent signals, which suggested CS/Luc NPs distributed over the mice body with blood circulation. No bioluminescence signals were observed in the second pair of mice which were injected with CS Null NPs, confirming that the bioluminescence signals observed in the mice were from the luciferin released from CS/Luc NPs. In Figure 4-10 c, a pair of mice was subcutaneously injected with both CS Null NPs (Left side) and CS/Luc NPs (Right side) at areas of interest. Bioluminescence signals were observed at the injection site of CS/Luc NPs due to the release of luciferin,

whereas non fluorescence in the left area. After injections, all three pairs of mice used in our experiment survived and behaved normal activities. No biotoxic effects were observed with those mice, which suggested that our CS/Luc NPs are biocompatible and safe for further in vivo drug delivery study.

Perspective

We have successfully prepared nanoparticles composed of synthetic or naturally occurring materials by N-I method. Hydrophobic/hydrophilic drugs were encapsulated in the polymeric nanoparticles in high efficiency. These nanoparticles exhibit the ability of sustained release of encapsulated drugs: 7 days for PLGA-PEG/MCHB NPs; 11 days for CS/Luc NPs. In vitro cytotoxicity experiment proved that PLGA-PEG nanoparticle vector could enhance MCHB delivery efficiency. CS/Luc nanoparticles could be successfully detected in the in vivo bioluminescence imaging. Many multifunctional drug delivery nanoparticles could be produced by N-I method in the future, combining sustained release with pathway tracking.

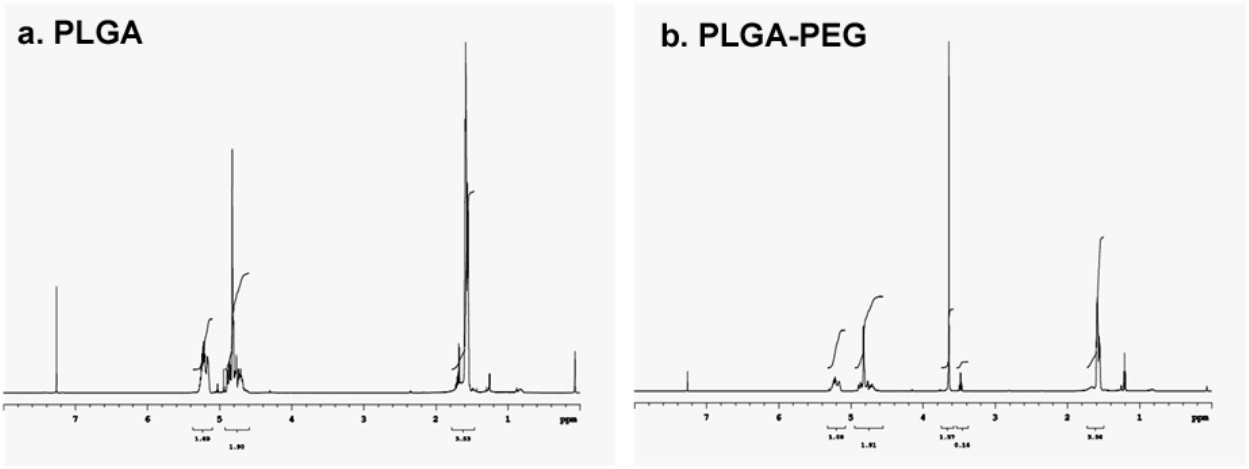

Figure 4-1. NMR characterization of (a) PLGA, (b) PLGA-PEG diblock copolymer.

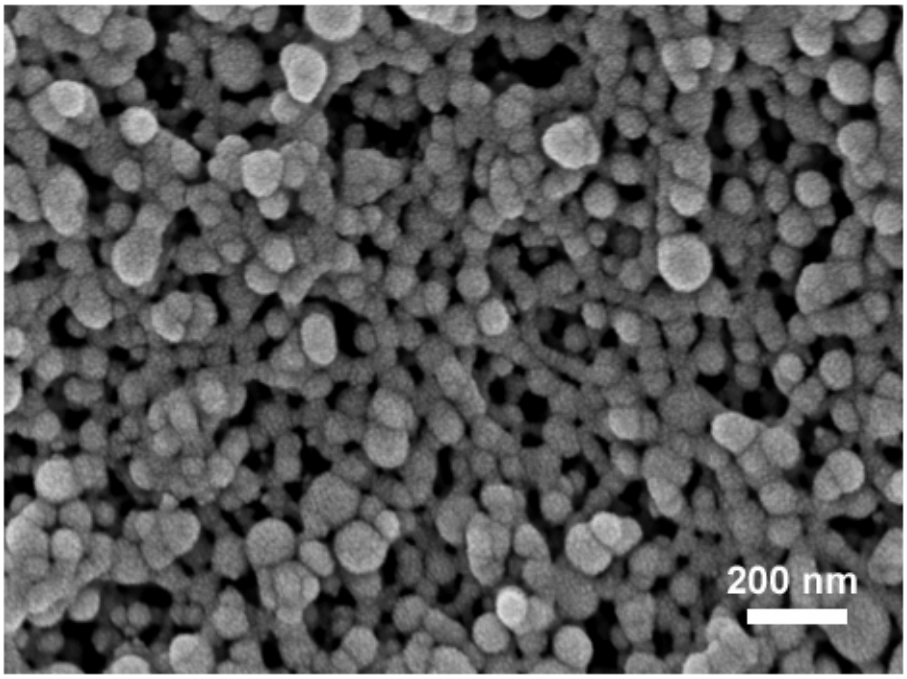

Figure 4-2. Typical SEM image of PLGA-PEG/MCHB nanoparticles.

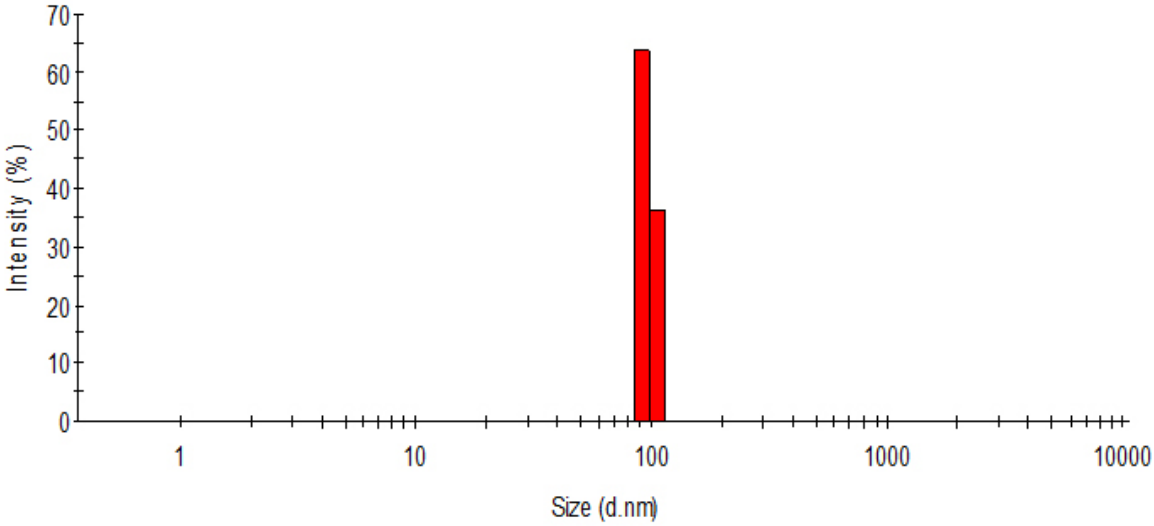

Figure 4-3. Hydrodynamic diameter of PLGA-PEG/MCHB NPs determined by DLS.

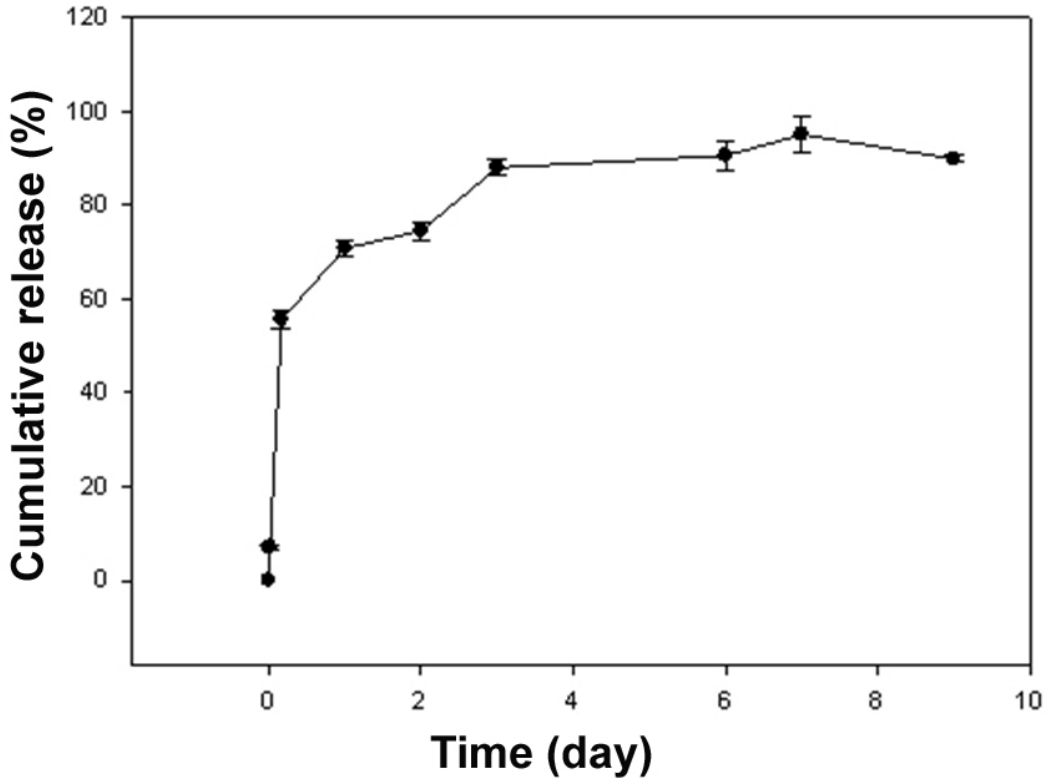

Figure 4-4. In vitro sustained release profile of PLGA-PEG/MCHB NPs.

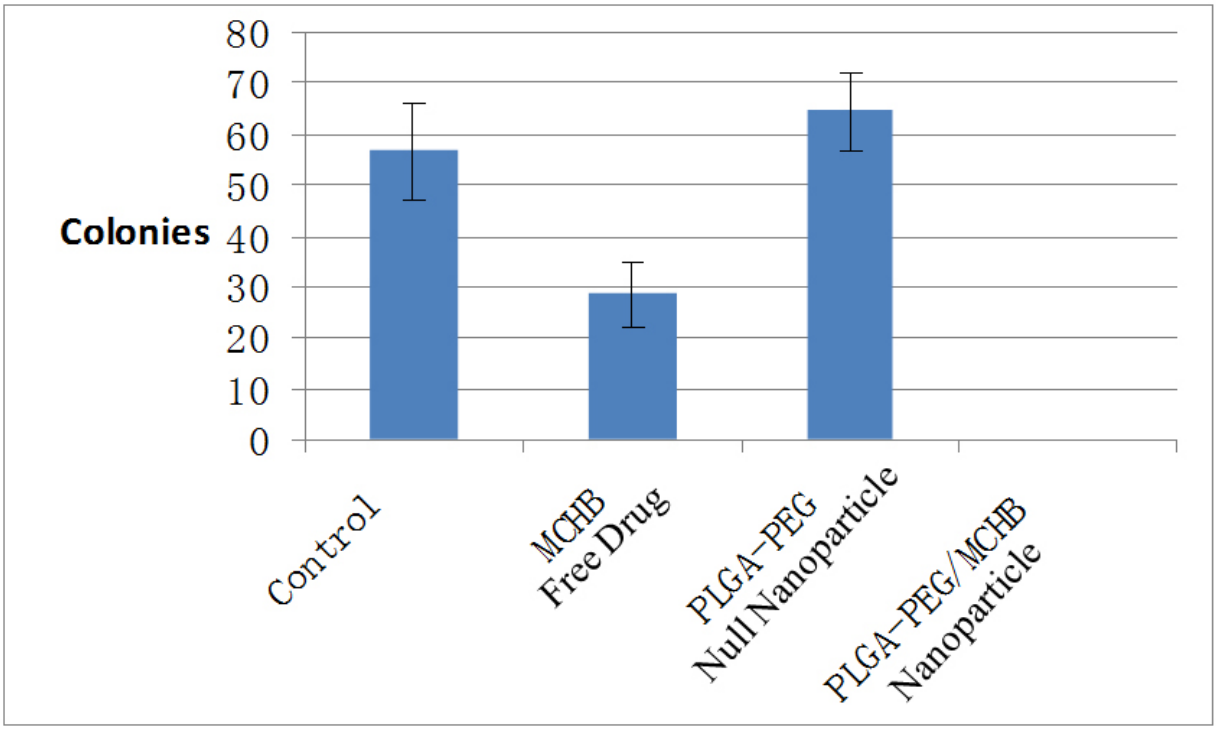

Figure 4-5. In vitro cytotoxicity study of PLGA-PEG/MCHB NPs.

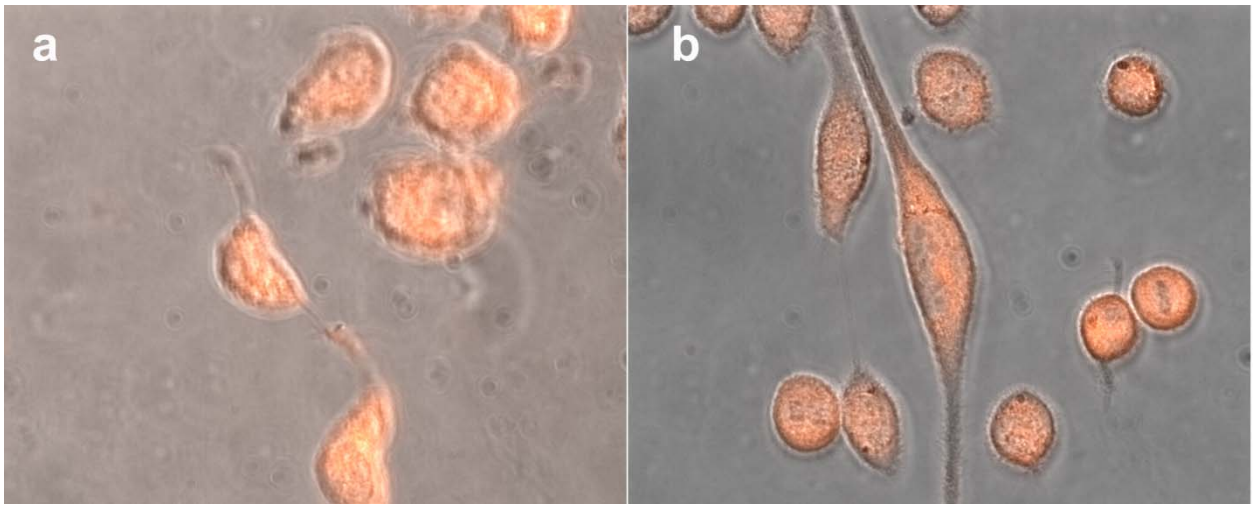

Figure 4-6. Fluorescent image of PC-3 cell incubated with (a) PLGA-PEG/MCHB NPs, and (b) PLGA-PEG/CNOB NPs.

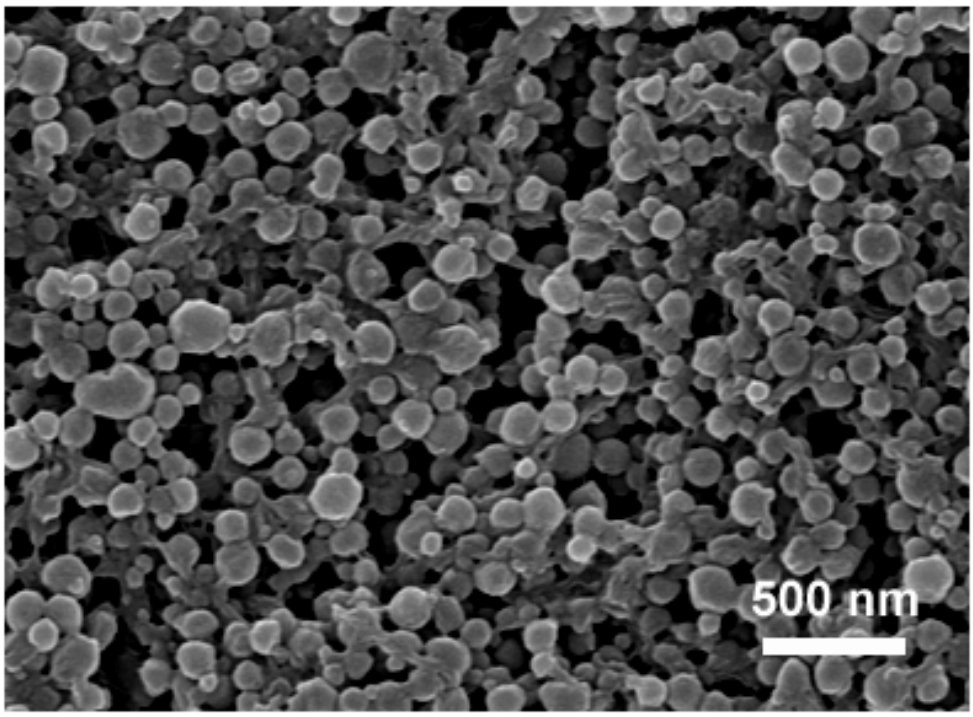

Figure 4-7. Typical SEM image of CS/Luc nanoparticles.

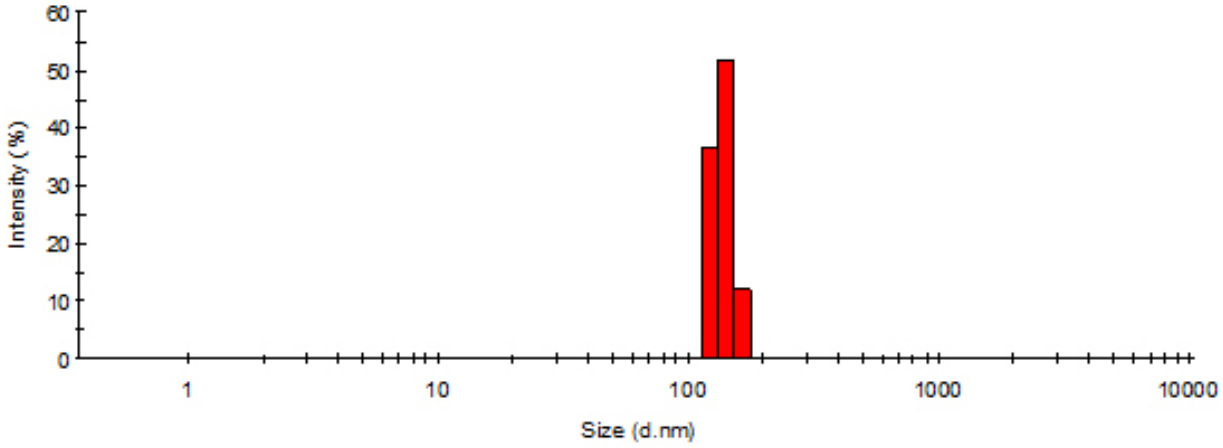

Figure 4-8. Hydrodynamic diameter of CS/Luc NPs determined by DLS.

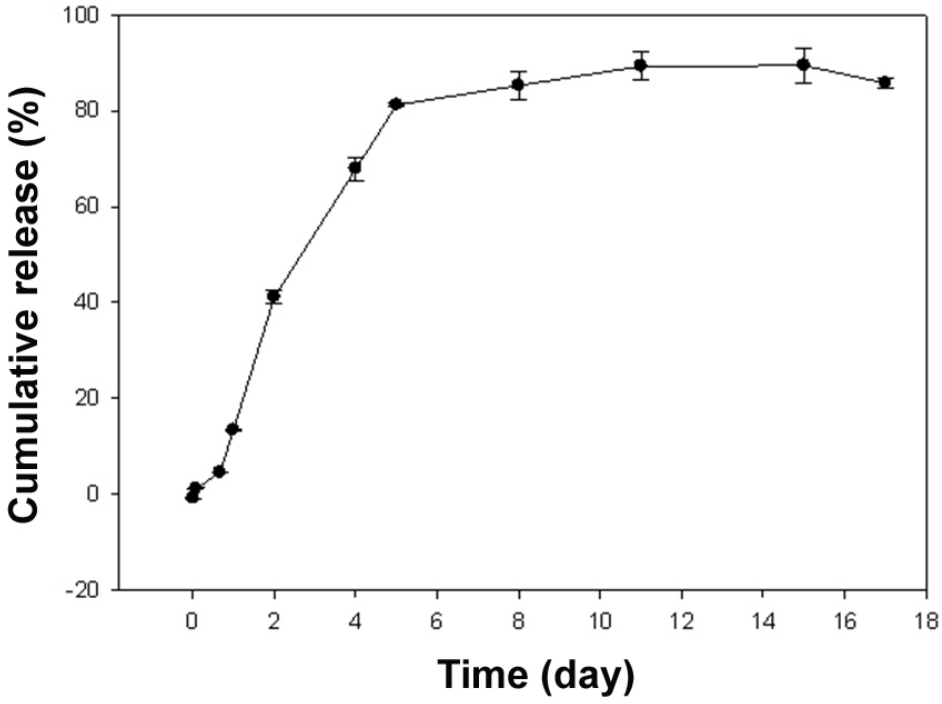

Figure 4-9. In vitro sustained release profile of CS/Luc NPs.

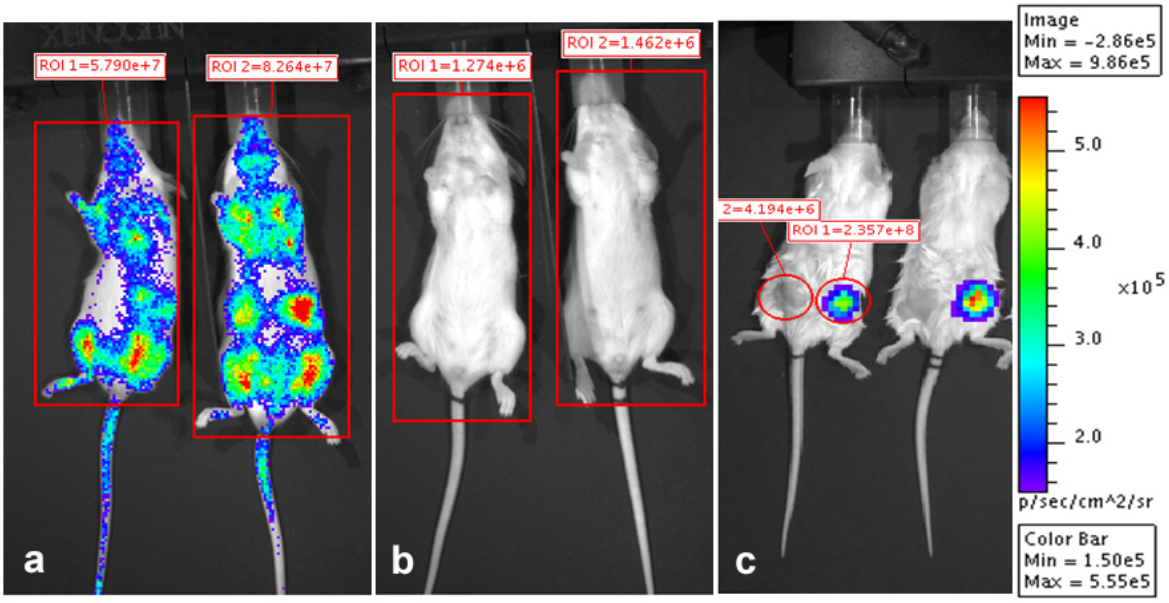

Figure 4-10. In vivo biotoxicity study of CS/Luc NPs by bioluminescence imaging.

Table 4-1. DLS data for PLGA-PEG/MCHB and CS/Luc nanoparticles.

Nanoparticle	Method	Diameter (nm)	PDI	Zeta-Potential (mV)
PLGA-PEG/MCHB	N-I	96 ± 7	0.143	-3.5
CS/Luc	N-I	137 ± 13	0.274	7.0

CHAPTER 5
FORMATION OF BIODEGRADABLE NANOFIBERS BY NANOPOROUS MEMBRANE

Aim

In human and animals, majority cells are imbedded in the natural extracellular matrix (ECM), which is a network of nanofibers containing collagens, glycosaminoglycans, proteoglycans, and glycoproteinsglycosaminoglycans. The interaction between these cells and ECM regulates the cell migration, proliferation, differentiation, gene expression, and secretion of various hormones and growth factors.[43] So mimicking natural ECM is of great importance in the tissue engineering.

Collagen is widely considered as the most promising biopolymer in tissue engineering because it is the primary component in the natural ECM. Collagen is a group of structure proteins featuring a unique triple-helix which is composed of three polypeptide subunits. There are more than 20 types of collagen in human body. The differences between the isotypes of collagen are the nature of the non-helical parts and the length of their triple-helix. Type I collagen is the most abundant and predominant collagen, which is a triple-helical protein with 300 nm in length and 1.5 nm in diameter. Under certain circumstance, such as pH, temperature, or ionic strength variance, type I collagen molecules will self assembly into macromolecular structure (fibrils and bundle of fibrils). Collagen nanofibers are widely used as novel building block in engineered tissue scaffold.[46-48]

In this chapter, we successfully prepared collagen nanofibers by a modified nanopore-injection (N-I) method. The obtained collagen nanofibers exhibit a uniform size distribution with a mean diameter of about 100 nm. Fiber diameter increases with nanopore size of PCTE membrane. Collagen nanofibrous scaffolds were prepared by

filtration of obtained nanofibers, and were used for cardiac stem cells (CSCs) growth and proliferation study. The nanofibrous scaffold prepared by N-I method may provide a solution to the challenge of three dimensional artificial scaffold in tissue engineering.

Experimental

Materials

Type I tropo-collagen extracted via acid-solubilization of rat tail tendon was purchased from BD Biosciences (Bredford, MA). Stock solutions were 3.44 mg/ml in 0.1 M acetic acid. All chemicals were purchased from Sigma Aldrich (St. Louis, MO) and were used without further purification.

Formation of Collagen Nanofibers

The U-tube setup consists of two half U-tubes and a nanoporous membrane which is sandwiched between the two halves (see Figure 5-1). Track etched polycarbonate (PCTE) nanoporous membranes with pore diameters between 50 nm and 1 μm were used in our experiments. One half of the U-tube was filled with 6 mL of feed solution containing 1 mg/mL collagen and 1 mM HCl (pH 3); the other half was filled with 4 mL receiver solution containing 1 mM NaOH (pH 11). A 4 psi gauge pressure was created by connecting a compressed air outlet with a pressure reduction valve to the feed solution side of the U-tube. In this way, the feed solution is pumped into the receiver solution at a constant flowrate according to the applied pressure. Nanofibers formed are collected by filtration through PCTE membranes and dried at room temperature. PCTE filter membranes also serve as the substrate for scanning electron microscopy (SEM). In control experiments, different kinds of membranes (PCTE with different pore sizes) were used in order to investigate the influence of filtration upon artifact formation. The nanofiber always had the same appearance.

Characterization of Collagen Nanofibers

Scanning Electron Microscope (SEM): SEM images were acquired using an FEI XL30 Sirion SEM. Dry samples on carbon sticky tape were sputter-coated for 120 s at 15 mA with Pd/Au. The diameters of the fibers were evaluated with the software ImageJ.

Transmission Electron Microscopy (TEM): TEM analysis was carried out using a FEI Tecnai G2 F20 X-TWIN. For TEM, samples were deposited on formvar carbon-coated copper grids, without prior filtration.

Rheology analysis: The rheological experiments were carried out using a TA AR-G2, equipped with an 8 mm parallel plate geometry. While the plate geometry was oscillated at a frequency, we measured the torque (stress) that was required to arrive at a certain deformation (strain). Frequency sweep tests have been carried out with a strain of $\gamma = 1$ %, strain sweep experiments were held at a constant frequency of $\omega = 1$ rad/s.

The nanofibrous scaffold used in rheology study was prepared by filtration of collagen nanofibers on a PCTE membrane, rinsed with deionized water for three times and dried at room temperature.

Isolation and Culture of Cardiac Stem Cells (CSCs)

Animal protocols were approved by the Stanford University Animal Care and Use Committee. The L2G85 transgenic mice of FVB background with beta-actin promoter driving Fluc-eGFP was used as stem cell donor. CSCs were isolated from 6- to 12-week-old L2G85 mice, The myocardial tissue was cut into a 1 to 2mm pieces, washed with Hanks' balanced salt solution (Invitrogen, Carlsbad, California), and incubated with 0.1% collagenase II for 30 min at 37 °C with frequent shaking. Cells were then filtered through 100 μm mesh. The cells obtained were cultured in Iscove's modified Dulbecco's medium supplemented with 10% fetal bovine serum (FBS) (Hyclone, Logan, Utah), 0.1

mmol/L nonessential amino acids, 100 U/mL penicillin G, 100 µg/mL streptomycin, 2 mmol/L glutamine, and 0.1 mmol/L beta-mercaptoethanol. 2 to 3 weeks post seeding, a population of phase-bright cells appeared over the adhered fibroblast-like cells. These phase-bright cells were collected by 2 washes with phosphate buffered saline (PBS), and 1 wash with cell dissolution buffer (Gibco, Grand Island, New York) at room temperature under microscopic monitoring, and sub-cultured in poly-lysine-coated plates (BD Pharmingen, San Jose, California) with the same medium (Online Videos 1 and 2).

In vitro cell growth and differentiation: an aliquot of CSCs was maintained in culture to monitor cell growth and stability of Luciferase (Luc) expression during the course of the experiment. To determine Luc expression, every 15 days cells were trypsinized, counted and an aliquot containing 2×10^5 cells was re-suspended in reporter lysis buffer (RLB) 1X (Promega) and frozen at −80 °C. At the end of the experiment the collected samples were used to determine Luc activity and DNA concentration

Scaffold Seeding

Small numbers (up to 200,000) of CSCs cells were used to seed the nanofibrous scaffolds. For seeding, each scaffold was immersed in an aliquot (50 µL) of cells in DMEM (containing 10% FBS, Pen/Strep antibiotics. The constructs were maintained under standard cell culture conditions for the rest of the experiment. At that time, 1 mL culture medium was added per construct. After 24 h of incubation, the scaffolds were noninvasively imaged, washed three times with 1 mL of PBS (to eliminate the luciferin), and stored at −20 °C until the in vitro luciferase and fluorescence assays were performed. For comparison purposes, a series of the same number of CSCs cells in suspension in 50 µL PBS were prepared in parallel and treated in the same way as scaffolds seeded with cells.

Microscopy Fluorescent Imaging

CSCs cell seeding and attachment was visualized by phase contrast and fluorescent (excitation filter 470 ± 20 nm, emission filter 525 ± 25 nm, Chroma Technology Corp., Rockingham, VT) microscopy equipment (CK40 microscope, Olympus, Melville, NY) with digital camera (Spot RT color, Diagnostic Instruments Inc., Sterling Heights, MI). For fluorescent imaging, a 530 ± 25 nm wavelength filter (Chroma Technology Corp.) was attached to the CCD camera. Samples were placed in the imaging cabinet and high resolution (1×1 pixel binning) images were acquired at a camera exposure time of 1 s. Fluorescent signal was expressed in cts/pix/s.

Bioluminescence Imaging (BLI)

BLI of cultured CSCs was performed to characterize the cell proliferation condition, when reaching cell confluence. For BLI, medium was removed from the plates, cells were rinsed twice with PBS 1× and 300 µL or 1 mL of luciferin reagent stock (Promega) was added to each well, and imaged immediately. For imaging, a plate was placed in the detection (BLI) was carried out using an IVIS 100 imaging system (Xenogen, Alameda, CA. For in vitro imaging, CSCs cell seeded on 6 well plates or seeded with the collagen nanofiber scaffolds were loaded in individual wells of 24-well plates, immersed with 200 µL of D-luciferin solution (300 µg/mL in PBS), and imaged after 5 min using the medium binning setting of the instrument for 1 min. To monitor cell proliferation on the nanofiber scaffolds in vitro, the cells were imaged on the day of seeding (day 0) as well as days 3, 7, and14 post seeding. Light emission was quantified using Living Image software (version 2.50.2; Xenogen). Each frame depicted the bioluminescent signal in pseudocolor superimposed on the respective gray-scale photographic image. Data from a region of interest surrounding each well were manually selected on the frames and were reported

as the total photon flux defined by the net photon count emitted per second per centimeter squared per steradian (p/s/cm^2/sr).

Statistical Analysis

Each in vitro experiment was performed twice in triplicate. Numerical results were reported as mean ± standard error of the mean.

Results and Discussion

In this chapter, we successfully prepared collagen nanofibers based on the modified nanopore-injection (N-I) setup (as shown in Figure 5-1). Modified N-I method features two major differences in comparison with nanoparticle formation process. First, magnetic stirring is removed from the system because wall shear force created by magnetic stirring may cause obtained nanofibers break into fragments or particles. Second, a higher pressure flow is applied in the N-I experiment (from 2 psi to 4 psi). The resulting high flux of feed solution tends to form fibers instead of particles at the exit of the nanopore.

The morphology of obtained nanofibers was investigated by SEM and TEM. Figures 5-2 a, b show the typical SEM images of collagen nanofibers at low and high magnifications. Collagen nanofibers are in relatively uniform size with smooth surface. The mean diameter of nanofibers measured from the image is 102 ± 13 nm. The length of nanofibers is in the range of few micrometers to hundred micrometers. From Figure 5-2 b, we could see that some collagen nanofibers further self assembly into bundles. Figure 5-3 shows typical TEM images of obtained nanofibers. The average diameter of nanofibers analyzed from TEM image is about 90 nm, which is similar to the result obtained from SEM image. The inset of Figure 5-3 b shows the electron diffraction pattern on a single collagen nanofiber, and it reveals that the collagen nanofibers are in

amorphous phase. A nanofibrous scaffold (~3 mg) could be obtained within 2 h by filtration (as shown in Figure 5-4).

The influence of nanoporous membrane on nanofiber formation was also investigated. A comparative experiment was carried out under other fixed conditions without nanoporous membrane. Resulting products were collected by filtration and characterized by SEM. Compared with the sample produced with N-I method (Figure 5-5 a), no nanofibers were formed in the comparative experiment as shown in Figure 5-5 b. Without nanoporous membrane, feed solution is directly mixed with the receiver solution, and resulted product was a smooth collagen film. It suggested that nanoporous membrane played a crucial role in collagen nanofiber formation. Because the self assembly of collagen molecule is believed happening at the exit of the nanopore. The uniform diameter and spacing between individual nanopores help forming well dispersed nanofibers with a narrow diameter distribution.

Collagen nanofiber formation with four different pore size (50 nm, 200 nm, 400 nm and 1000 nm) PCTEM membrane was investigated (Figure 5-6). In order to reduce the difference in flow speed caused by the difference in flow area, a pressure of 4 psi over atmospheric pressure was applied at the side of the U-tube containing the feed solution. Nanofibers grown in 50 nm pores had a diameter of (50 ± 15) nm, (120 ± 50) nm for 200 nm pores, (270 ± 120) nm for 400 nm pores, and (760 ± 240) nm for 1000 nm pores. Smaller pores prevented the collagen from passing the membrane due to congestion of the pores.

We also studied the biomechanical characteristics of the collagen nanofibrous scaffold measured by rheology measurement. Small-deformation oscillatory

measurements were performed to evaluate the viscoelastic behavior of the nanofibrous scaffold. Figure 5-7 shows the mechanical spectra of the collagen nanofibrous scaffold that was prepared by filtration of collagen nanofibers. In this rheology measurement, the storage modulus (G') and the loss modulus (G") were monitored as a function of different frequency. The value of G' represents energy stored elastically in the system, whereas the value of G" represents energy dissipated through viscous effects. As shown in Figure 5-7, the value of the storage modulus G′ exceeds that of the loss modulus G″ by almost one order of magnitude, indicating that obtained scaffold is a strong and rigid gel.

Collagen nanofibrous scaffold was tested for the ability of supporting cell growth and proliferation using cardiac stem cells (CSCs). CSCs are normally found in heart tissue, capable of differentiating into cardiac cells associated with contracting myocardium and vascular structures. The aim of using nanofibrous scaffold to support CSC growth is eventually replacement of dead tissue in the diseased human heart with new generated tissues seeded in our biodegradable scaffold. In our experiment, collage nanofibrous scaffold and blank control were incubated with CSCs. After 1 week incubation, CSC proliferation was evaluated by fluorescent imaging and bioluminescence imaging, as shown in Figure 5-8. Figure 5-8 a shows fluorescent image of CSCs growth with collagen scaffold, compared with the blank control sample. These fluorescent cell images showed that CSCs on collagen scaffold could grow and proliferate normally as in the control sample. In the high magnification image, it is clearly shown some stretched CSCs, which suggests that scaffold interacts with cells resulting in cell flattening and spreading on the scaffold surface.

Bioluminescence imaging assay was also used to evaluate the activity of CSCs on collagen scaffold. Basically, luciferin was added to the CSCs on scaffold, and expressed as bioluminescence signals through luciferase. Bioluminescence intensity was measured and represented the activity of luciferase in CSCs indicating the viability of CSCs. From Figure 5-8 b, it could be observed that bioluminescence intensity of CSCs on scaffold is similar to that of control sample, which confirmed that CSCs proliferated in a similar way as cell grew in blank sample. It could be drawn that collagen nanofibrous scaffold shows non-biotoxicity, and could be used to support cardiac stem cell proliferation.

Perspective

In conclusion, we present a novel and efficient method for the fabrication of biodegradable type I collagen nanofibers. Uniform collagen nanofibers were produced with PCTE membrane. Furthermore, diameter of collagen nanofiber could be controlled by the pore size of nanoporous membrane. Using the membrane with pore size ranging from 50-1000 nm, nanofibers with diameter ranging from 50-760 nm could be obtained. The nanofibrous scaffold exhibited distinct biomechanical strength. In vitro experiment shows the nanofibrous scaffold supports cardiac stem cell growth and proliferation, as an early indication of scaffold biocompatibility. We believe that many other biopolymers could be formulated into nanofibers by N-I method for tissue engineering purposes.

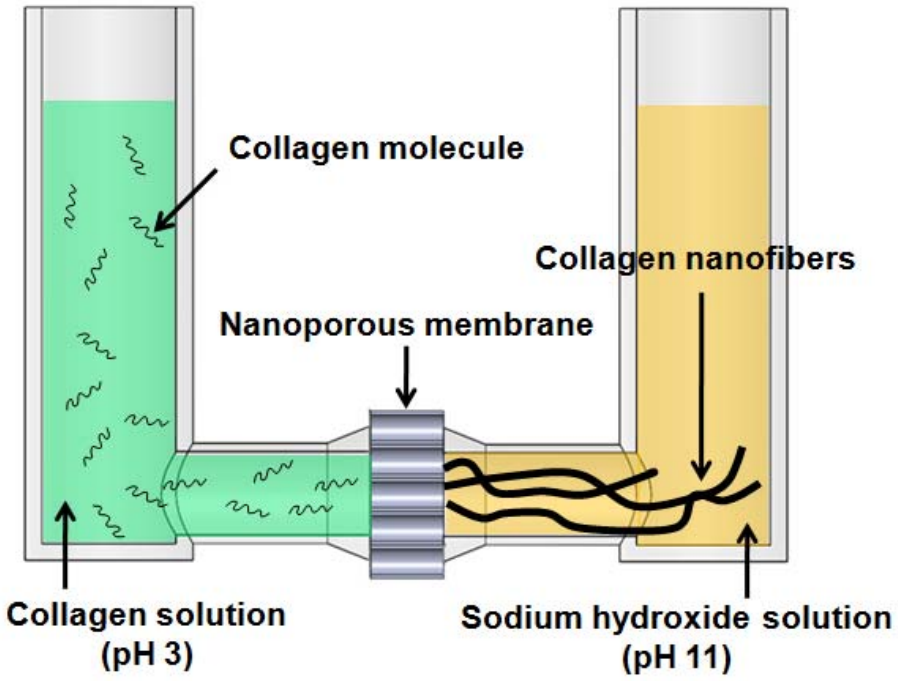

Figure 5-1. Method for producing collagen nanofibers by flowing though a nanoporous membrane.

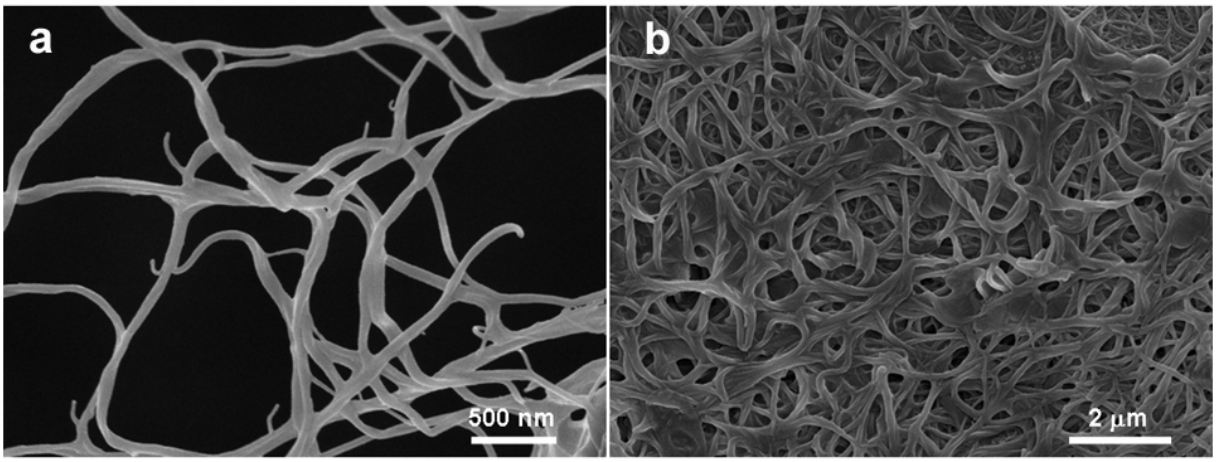

Figure 5-2. Typical SEM images of collagen nanofibers prepared by using the PCTE membrane at (a) high magnification and (b) low magnification.

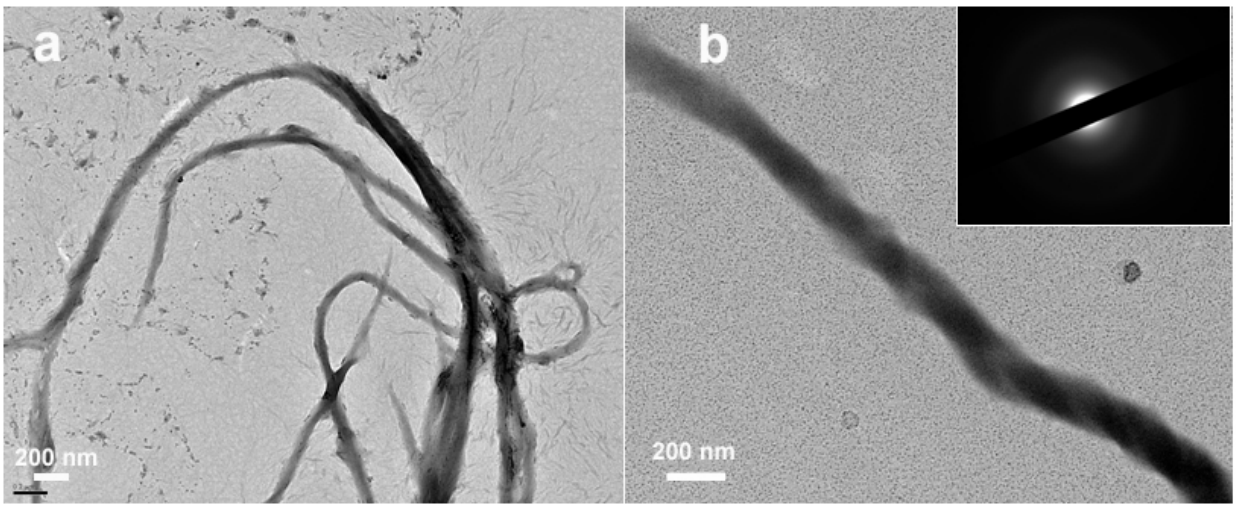

Figure 5-3. Typical TEM images of (a) a bundle of collagen nanofibers (b) a single collagen nanofiber. Inset is the related selected area electron diffraction pattern (SAED pattern).

Figure 5-4. Photograph of collagen nanofibrous scaffold prepared by N-I method in 2 h. A penny is used as a size marker.

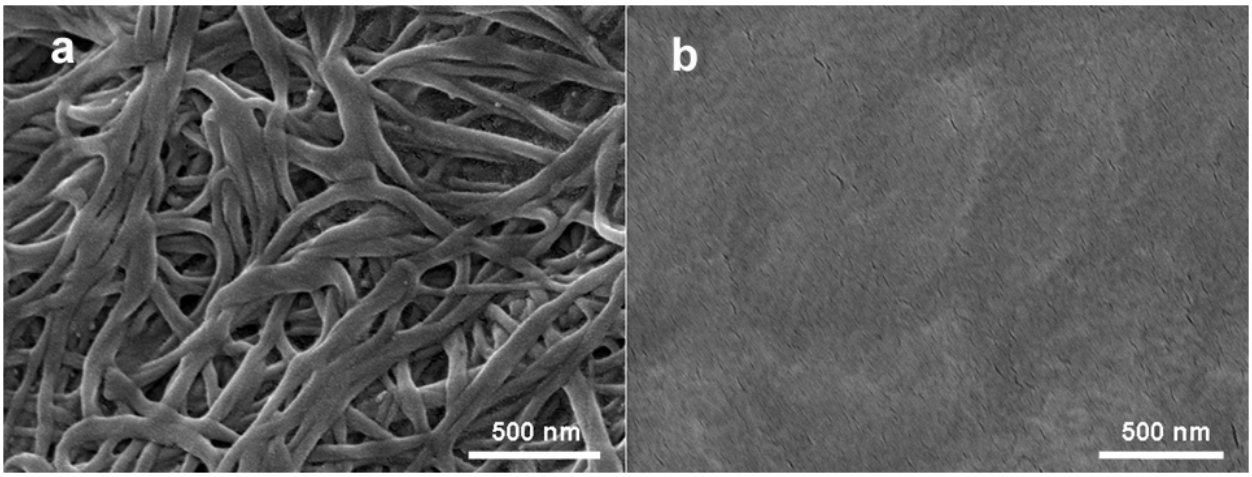

Figure 5-5. SEM images of (a) collagen nanofibers prepared by N-I method (b) collagen film prepared without nanoporous membrane.

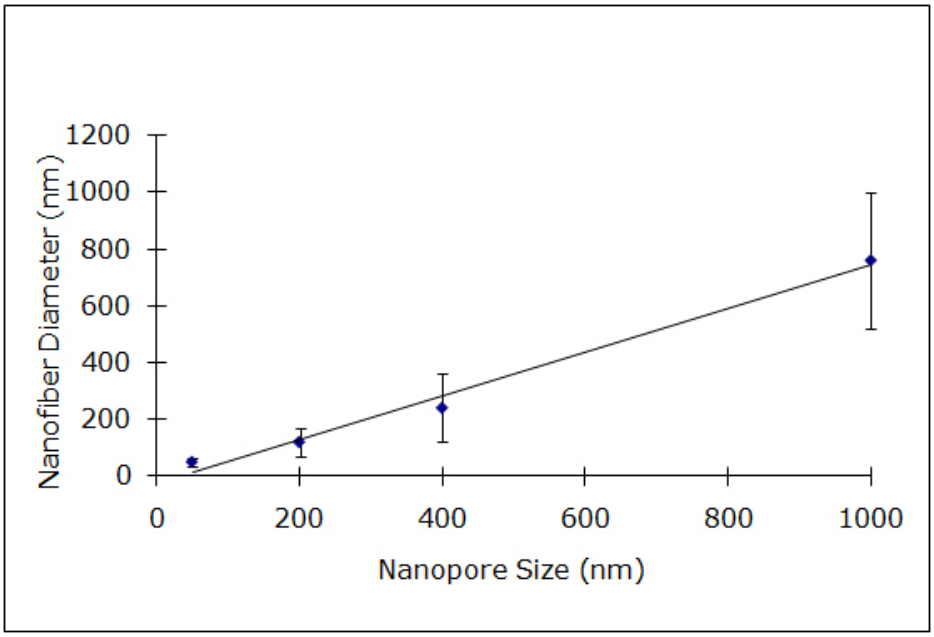

Figure 5-6. Effect of nanopore size on the diameter of the collagen nanofibers.

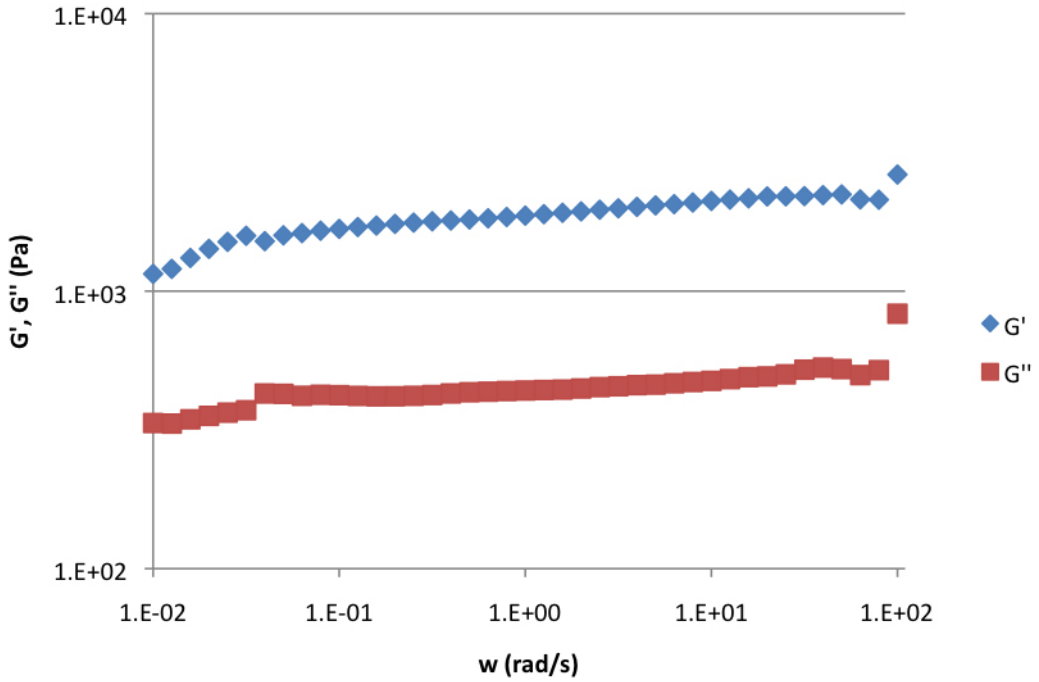

Figure 5-7. Rheology study of collagen nanofibrous scaffold.

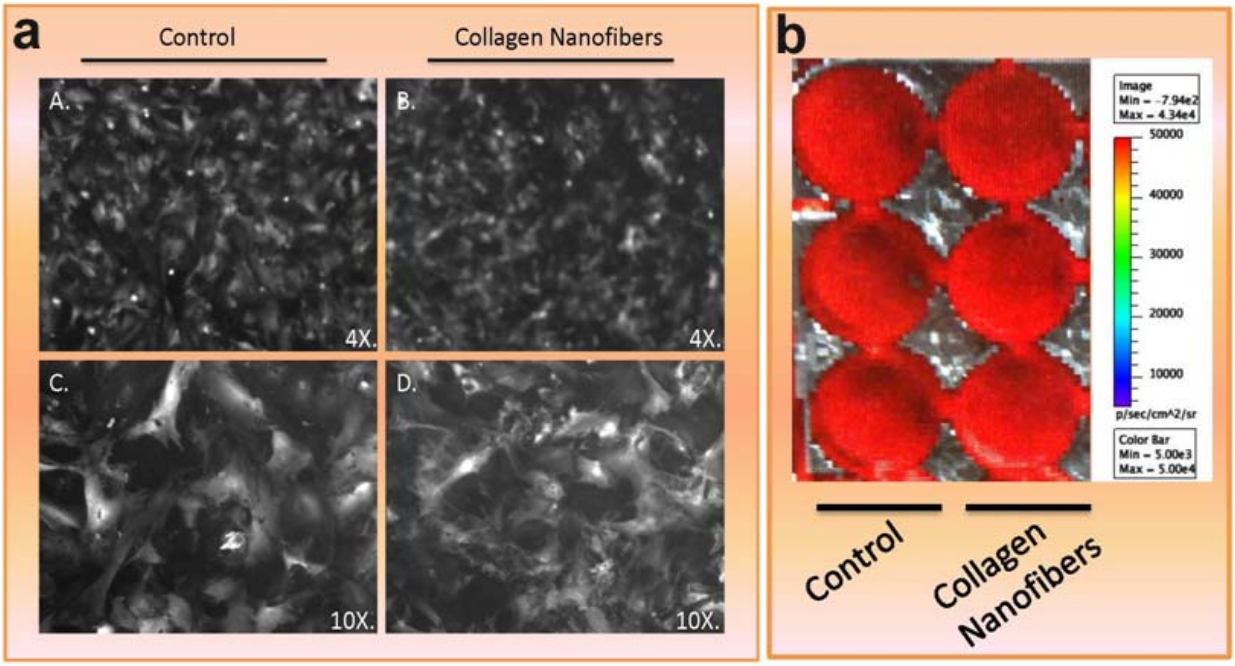

Figure 5-8. (a) Fluorescent microscope imaging of CSCs in (A) and (C) blank control (low and high magnification); (B) and (D) collagen nanofibrous scaffold (low and high magnification). In fluorescent microscope images, bright area represents CSCs, and black area represents background. (b) bioluminescence image of CSCs proliferation on blank control and collagen nanofibrous scaffold.

CHAPTER 6
ORGANIC/INORGANIC HYBRID NANOFIBERS FOR TISSUE ENGINEERING

Aim

Organisms bring forth a wide variety of organic/inorganic hybrid materials, called biominerals. The most common biominerals are the phosphate and carbonate salts of calcium that are used in conjunction with organic polymers such as collagen and chitin to give structural support to bones and shells. Biomineralization has inspired chemists to seek new synthetic strategies for creating inorganic materials with complex forms e.g. by pattern recognition of self-organized organic assemblies.[173,174] Next to the advancement of our understanding of biological processes, the main goal of these studies is to find new materials for bone grafting, tissue engineering, or other medical applications.

One of the most prominent features of biominerals is that they seldom exhibit typical crystalline morphologies, including sharp edges and angled corners. In fact, in many cases biominerals seem to be molded into a specific shape, just like polymeric plastics that are extruded in industrial processes.[175,176] Several non-classical crystallization pathways have been proposed for biomineralization.[177-180] In the last several years, evidence for the importance of an amorphous precursor phase rapidly accumulated and quickly became the dominant view in the field.[176,181,182] In 2003 Gower and co-workers[175,181] proposed the polymer induced liquid precursor (PILP) process for the crystallization of calcium carbonate ($CaCO_3$). Using acidic hydrophilic polymers as additives, they were able to observe a transient phase of liquid calcium carbonate droplets. These droplets can be extruded into constrained volumes where they coalesce and transform into a more stable mineral phase.[183,184] As has been established by several

studies,[185-187] the role of the acidic polymer is twofold: it suppresses bulk crystallization of $CaCO_3$ and stabilizes the amorphous phase.

In this chapter, we present a new approach for preparing nanofibers that was inspired by these biomineralization processes. Our strategy is based on the use of a nanoporous track etched polycarbonate (PCTE) membrane that separates two liquids, a feed solution and a receiver solution. Nanofibers are formed by pumping the feeder solution through the membrane into the receiver solution. In prior chapters, this strategy has been successfully used for the fabrication of biodegradable nanoparticles. The feed solution contains an inorganic cation, such as Ca^{2+}, and a long-chain polymer, such as collagen, which serves as the scaffolding for the nanofiber. The receiver solution contains an anion, such as phosphate or carbonate, which induces precipitation of the respective inorganic salt along the long-chain polymer.

Using this method, for the first time, it was possible to incorporate calcium phosphate into collagen nanofibers without any additional polymers or proteins.[188-190] This was possible due to the simultaneous formation of collagen nanofibers and amorphous calcium phosphate at the exit of the pores of the PCTE membrane. Therefore, we are able to present a bottom-up approach for the artificial formation of the basic building blocks of bones.

In further experiments, our method was also tested with a synthetic polymer/biomineral composite system. The feed solution was an aqueous solution of Ca^{2+} and poly(acrylic acid) (PAA), while the receiver solution was an aqueous solution of carbonate (CO_3^{2-}). By pumping the feed solution through the nanoporous membrane into the receiver solution, we were able to generate nanofibers that consist of amorphous

calcium carbonate and PAA. Similar experiments featuring phosphate anions instead of carbonate, gave rise to nanofibers that consist of a composite of amorphous calcium phosphate and PAA.

In order to demonstrate the clinical usefulness of the fibers generated with this approach in a tissue-engineering context, human adipose derived stem cells (hADSCs) have been grown on the collagen scaffold consisting of aggregates of nanofibers.

Experimental

Materials

All chemicals were purchased from Sigma Aldrich (St. Louis, MO) and were used without further purification. Calcium chloride ($CaCl_2$), sodium bicarbonate (Na_2CO_3) solutions and sodium biphosphate (Na_2HPO_4) were prepared fresh on a daily basis using Millipore water. Poly(acrylic acid) (MW 8,000 g/mol, 45% in water) was added to the $CaCl_2$ prior to the experiments. The PAA concentration in the $CaCl_2$ solution was 150 mg/mL unless otherwise noted. The samples were vortexed for 2 min in order to insure proper dissolving of the polymer. Type I tropo-collagen from rat tails was purchased from BD Biosciences (Bredford, MA). Stock solutions were 3 mg/mL tropo-collagen in 10 mM HCl. 10X PBS buffer was obtained from Invitrogen (Carlsbad, CA).

Formation of Hybrid Nanofibers

The U-tube setup consists of two half U-tubes and a nanoporous membrane which is sandwiched between the two halves (see Figure 6-1). Track etched polycarbonate (PCTE) nanoporous membrane with pore diameter of 200 nm was used in our experiments. One half of the U-tube was filled with 6 mL feed solution containing 1 mg/mL collagen, 1 mM $CaCl_2$ and 1mM HCl (pH 3), the other half was filled with 4 mL receiver solution containing 0.66 mM Na_2HPO_4 and 1 mM NaOH (pH 11). In some experiments 4

psi gauge pressure was created by connecting a compressed air outlet with a pressure reduction valve to the feed solution side of the U-tube. In this way, the feed solution is pumped into the receiver solution according to the applied pressure. Nanofibers formed are collected by filtration through PCTE membranes and dried at room temperature. PCTE filter membranes also serve as the substrate for scanning electron microscopy (SEM). In control experiments, different kinds of membranes (AAO, PCTE with different pore sizes) were used in order to investigate the influence of filtration upon artifact formation. The nanofiber always had the same appearance.

PAA/$CaCO_3$ and PAA/Calcium Phosphate nanofibers were produced in the similar way as described above. For PAA/$CaCO_3$ formation, feed solution contained 20 mM $CaCl_2$ and 150 mg/ml PAA; receiver solution contained 20 mM Na_2CO_3. For PAA/Calcium Phosphate formation, feed solution contained 20 mM $CaCl_2$ and 150 mg/mL PAA; receiver solution contained 15 mM Na_2HPO_4. Other conditions remain the same as in collagen/Calcium Phosphate experiments.

Analysis of Nanofibers by Electron Microscope

SEM images were acquired using an FEI XL30 Sirion SEM. Dry samples on carbon sticky tape were sputter-coated for 120 s at 15 mA with Pd/Au. The diameters of the fibers were evaluated with the software ImageJ.

Transmission electron microscopy (TEM) was carried out using a FEI Tecnai G2 F20 X-TWIN. For TEM, samples were deposited on formvar carbon-coated copper grids, without prior filtration.

Stem Cell Preparation

Human adipose derived stem cells (hADSC's) were isolated from donors and expanded in culture. Cells were cultured in Dulbecos Modified Eagles Medium (DMEM)

supplemented with 10% fetal bovine serum, 1% penicillin/streptomycin and 0.05% fibroblast growth factor. Two-dimensional sheets of nanofibers prepared on PCTE filter membranes were placed at the base of a 96 well plate (n=3). Trypsin was added to the hADSC's to remove them from cell culture flasks and 8x103 cells were seeded per well in 200µl of media further supplemented with β-glycerolphosphate, ascorbic-2-phosphate, dexamethasone and sodium pyrinate. Cells were cultured for 16 days and media was refreshed every second day.

In Vitro Cytotoxicity Study by Cell Titer Assay

Cell Titer 96® (Promega) assay was performed to quantify cell proliferation at days 5, 11 and 16. Cell media was removed and Cell Titer 96® AQueous One Solution was added to the cells. Quantification was performed with a microplate reader according to the manufactures protocol.

Fluorescent Microscopy Imaging

Following cell culture, cells were fixed with 4% paraformaldehyde for 15 minutes and washed extensively with phosphate buffered saline solution (PBS). Fluorescein isothiocyanate (FITC) phalloidin (Santa Cruz Biotechnology) was used to stain the actin filaments and samples were mounted with VECTASHIELD ® HardSet Mounting Media containing DAPI.

Statistical Analysis

Statistics was performed using MiniTab. A Tukeys comparison was used to determine differences between timepoints and groups ($p<0.05$ was considered as statistically different). Data is presented as mean ± standard deviation.

Results and Discussion

Triple-helical single tropo-collagen molecules spontaneously self-assemble into fibers under the right conditions.[191-194] In collagen nanofibers, each triple helix is shifted relative to its molecular neighbor by a multiple of 67 nm in the direction of the helix (See the scheme in Figure 6-1). Laterally, the helices are arranged in a hexagonal pattern in respect to each other within the fiber. This arrangement leads to the characteristic band pattern of collagen fibers. Collagen fibers are most stable at moderately basic pH (9-11) and high ion (especially phosphate) concentrations.

In order to obtain mineralized collagen nanofibers, $CaCl_2$ was added to the feed solution while phosphate was given to the receiver solution. The other experimental conditions for the growth of mineralized collagen fibers were similar to the experiment fabricating collagen nanofibers (Figure 6-1). The formation of mineralized fibers is especially sensitive to the calcium concentration. With lower calcium concentrations (1 mM $CaCl_2$ in the feed solution), only the inside of the fibers was mineralized, as can be clearly seen by the visible enhancement of the band pattern of the collagen fibers (compare Figures 6-2 a and c). With higher calcium concentrations (up to 5 mM $CaCl_2$), the fibers exhibit mineralized shells (Figure 6-2 e, f). The shells appear to be segmented with each segment having a diameter of roughly 67 nm, which equals the distance found in the band pattern of collagen fibers. With $CaCl_2$ concentrations as high as 20 mM, plate-like hydroxyapatite crystals precipitate in large bundles that are interconnected by collagen. Selected area electron diffraction (SAED) and energy dispersive spectroscopy (EDS) were performed for all experimental conditions. While EDS showed amounts of calcium and phosphate that were roughly proportional to the amount of $CaCl_2$ in the feed solution, the mineral phase was always amorphous (see inserts in Figure 6-2).

It is important to note that in these experiments, collagen does not induce the PILP phase.[188] For this mechanism an acidic polymer would be necessary. In our experiments, collagen fibers form at the same time as the amorphous calcium phosphate. The prevalence of the amorphous phase is a result of the rapid flow of the feed solution that results in the creation of a highly supersaturated phase at the exit of the pores. A rough estimation of the flow rate of the feed solution through the membrane gives a flow speed of the order of 100 μm/s. In comparison, derived from the diffusion coefficient of collagen[195] and the resulting diffusion length, collagen molecules in dilute solutions move at a speed of about 5 μm/s. As a result, the nanofiber formation only takes around 2 h. For the formation of a crystalline phase of calcium phosphate, reaction times of at least four days are typical.[188] This fast and coincident formation of nanofibers and particles yields a collagen/calcium phosphate composite material without the addition of acidic polymers or natural non-collageneous proteins.

In a further series of experiments, synthetic polymer, instead of naturally occurring biopolymer, was used in the formation of nanofibers. The advantage of using synthetic polymer is that they are much less expensive than those natural proteins, which allows the scale-up production for tissue engineering applications. Poly(acrylic acid), an acidic and hydrophilic polymer, is selected as the model synthetic polymer in our experiments. Poly(acrylic acid) has been successfully used as a mimic to acidic proteins and polysaccharides for facilitating biomineralization. The formation of nanofibers made of calcium carbonate and PAA was investigated. These nanofibers can be easily observed by scanning electron microscopy (SEM). Nanofibers grown in 200 nm pores had a diameter of 110 ± 60 nm for 200 nm pores. The length is poorly controlled. It is very likely

that the nanofibers break as a result of the filtration process or at an unspecified time during the extrusion. While some nanofibers were as long as 100 µm, the length of most fibers is on the order of 20 µm. The nanofibers are evenly distributed across the filter substrate with the occasional occurrence of bundles (Figure 6-3 a).

The structure of the nanofibers was examined by selected area electron diffraction (SAED), which was coupled to TEM (Figure 6-3 b). The resulting diffractogram shows that the nanofibers were amorphous.

Several control experiments were performed by exchanging one of the reaction components by water to prove that the fibers indeed consist of calcium carbonate and PAA. Without PAA, uncontrolled precipitation of mainly vaterite crystals occurred. Without calcium chloride or without sodium bicarbonate, no nanofiber formation could be observed.

One control experiment was performed by reversing the flow direction of the PAA-rich phase. In this experiment, PAA was dissolved in the sodium bicarbonate solution instead of the calcium chloride solution. No nanofibers were formed in this experiment. Instead, discs around 10 µm in size were deposited on the filter substrate (Figure 6-3 c). Those were most likely PILP droplets that had been flattened as a result of vacuum filtration.

In additional experiments, the Na_2CO_3 receiver solution was exchanged by Na_2HPO_4 of the same concentration. Here, too, the formation of nanofibers could be confirmed (Figure 6-3 d). The nanofibers containing calcium phosphate are shorter and appear to be more rounded and softer than those with calcium carbonate.

As is evident by the above presentation of the results involving PAA as the polymeric component, the synthesis of fibers is governed by the formation of the PILP phase at the exit of the pores.[181] Upon entering the pores, the PAA chains will likely become axially aligned along the pores as a result of the strong elongational velocity gradients in the entry region of the pores. This alignment will persist within the pores because of the presence of shear gradients. The negatively charged carboxylic polymers are surrounded by a cloud of positively charged calcium ions; near the exit of the pores, carbonate ions are added to the diffuse ion cloud around the polymers, giving rise to the PILP phase. While being extruded from the pores, the acidity of the polymer, in concert with the concentrated ions, sustains the metastable state of the amorphous calcium carbonate phase. Unlike the collagen fibers, the nanofibers are a homogeneous phase of an amorphous mineral/polymer composite without a special pattern as it arises in the self assembly process of collagen. In general, the PILP phase will preferentially form in contact with an additional interface, because of the reduction of the nucleation energy threshold at interfaces. In colloid chemical terms, again, the three-phase contact is energetically favorable in the presence of a finite contact angle.

The fibers were tested for their ability to support cell growth in-vitro using human adipose derived stem cells (hADSCs) as a model cell line for tissue engineering. This cell type is found in abundance within our body, capable of differentiating down the mesenchymal linage and an excellent candidate for future tissue engineering applications.

The Cell Titer 96® proliferation assay demonstrated increasing proliferation in all groups at all time points with the exception of collagen nanofibers at day 16 (Figure 6-4).

There is also a trend indicating that the inclusion of calcium phosphate enhances cell proliferation. Interestingly, only the calcium phosphate containing groups exhibited a statistical increase in alkaline phosphatase (ALP) activity which is an early indicator of bone cell differentiation (Figure 6-5). The introduction of calcium phosphate had a profound effect on fiber morphology and mechanical stiffness, which occurs on a scale at which cells can interact. Within our cellular analysis, the increase in $CaCl_2$ concentration increased proliferation and ALP production. Xie et al. have shown that calcium phosphate can induce osteoblasts differentiation[196] while Sere et al. have shown that by combining calcium phosphate with collagen, cells up-regulate matrix production.[197] Cell actin staining indicated intimate contact with the underlying surface and out-stretched cells with connecting filopodia were witnessed (Figure 6-6). Cells rapidly covered the nanofibrous surface and began to grow in multilayers.

Perspective

In conclusion, we present a straightforward method for the fabrication of organic/inorganic hybrid nanofibers that was strongly inspired by processes found in biomineralization. Naturally occurring type I collagen and synthetic PAA were selected as the polymeric component Using PAA as the polymeric component, nanofibers could be produced that consist of an amorphous mixture of calcium phosphate and collagen, or PAA. That this method is generally suited for the fabrication of nanofibers of different compositions has been demonstrated by exchanging the Na_2HPO_4 solution by Na_2CO_3 of the same concentration in the receiver solution with PAA as polymeric component. The collagen nanofibers could be mineralized by the formation of amorphous calcium phosphate simultaneous to fiber formation. It was also shown that the fibers supported stem cell growth and proliferation, as an early indication of scaffold biocompatibility. It

should also be noted that the inclusion of calcium phosphate within the fibers up-regulated stem cell alkaline phosphatase production. Thus, we believe that this new approach holds much promise in future studies about the production of new nano-structured materials as well as advances in the field of biomineralization.

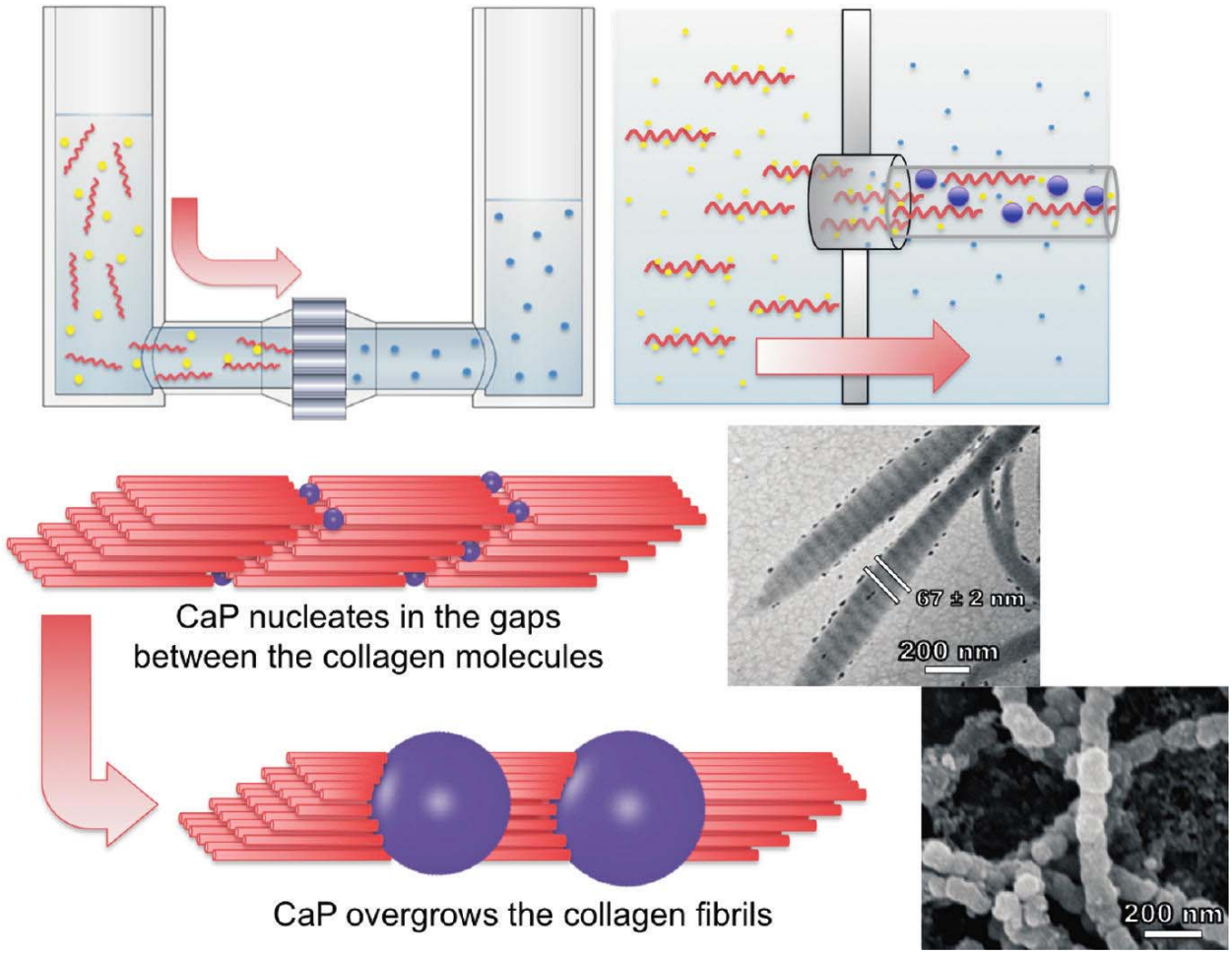

Figure 6-1. Experimental setup and proposed model for the formation of mineralized collagen fibers.

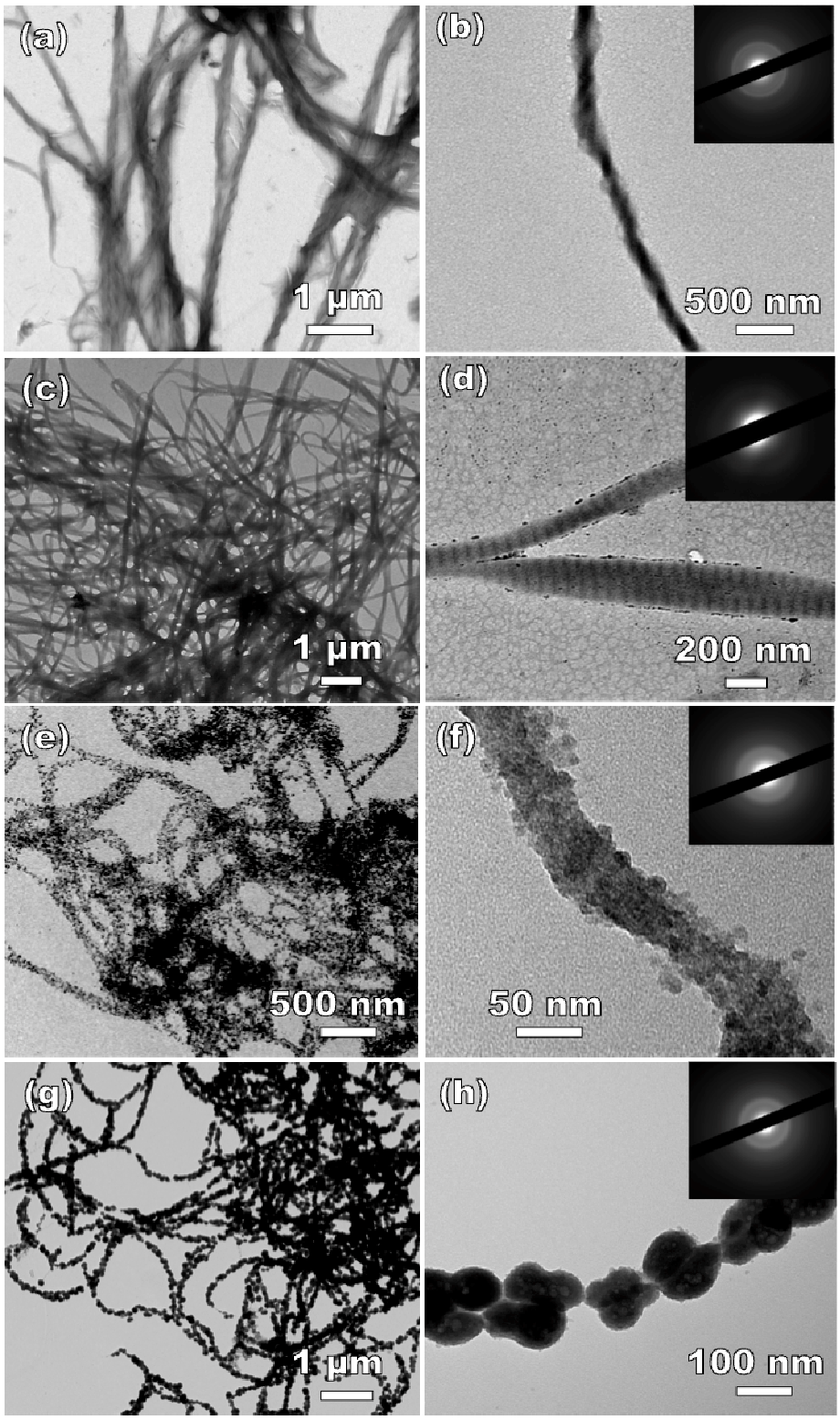

Figure 6-2. (a, b) Unmineralized collagen fibers, (c, d) Mineralized collagen fibers (1 mM $CaCl_2$), (e, f) Mineralized collagen fibers (2.5 mM $CaCl_2$) and (g, h) Mineralized collagen fibers (5 mM $CaCl_2$). Inset images in (b, d, f, h) are SAED patterns.

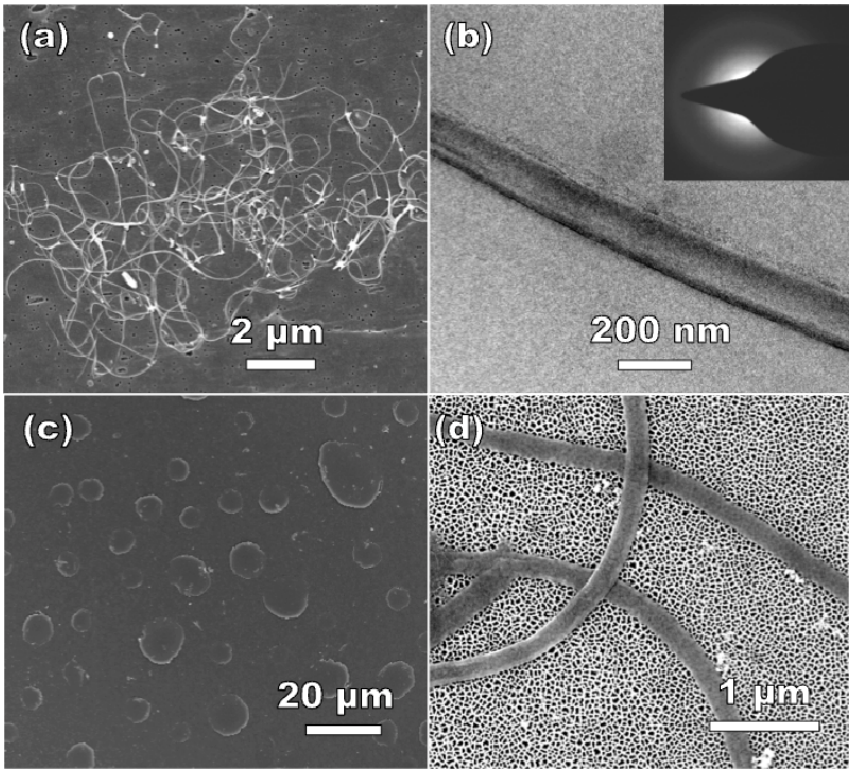

Figure 6-3. (a) Bundle of PAA/$CaCO_3$ nanofibers (b) TEM micrograph and SAED pattern of a PAA/$CaCO_3$ (c) Flattened PILP droplets, (d) PAA/Calcium Phosphate nanofibers.

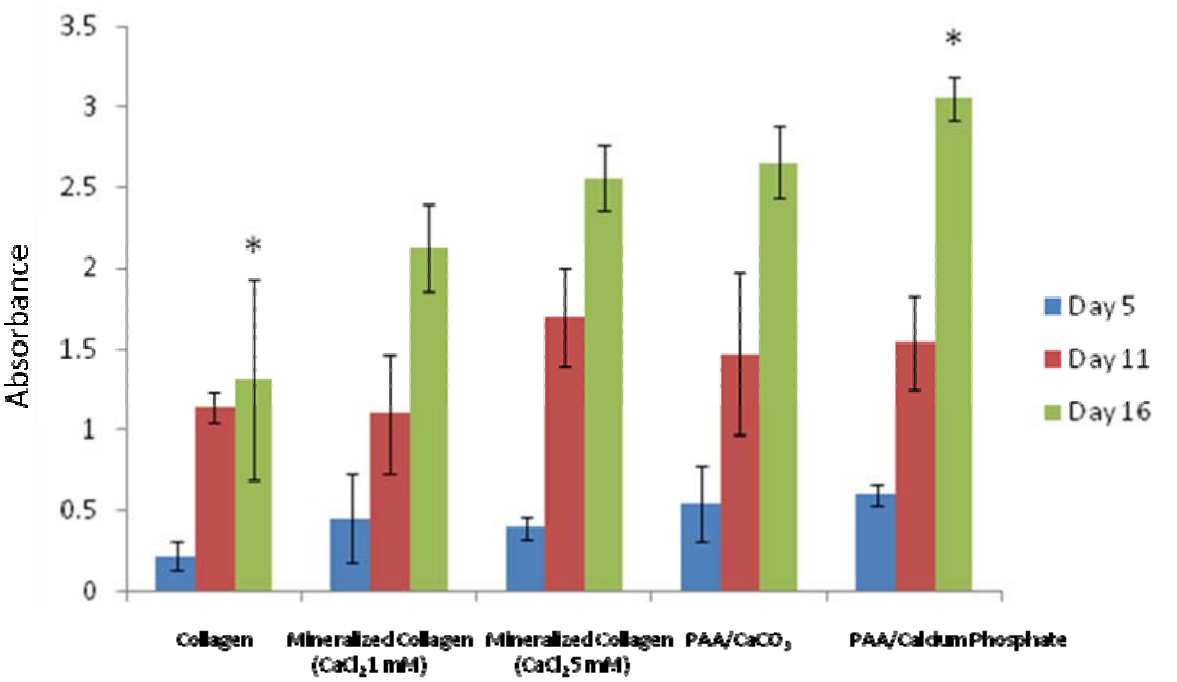

Figure 6-4. Proliferation of hADSC's on nanofibers. * indicate statistical difference between groups at the same timepoint.

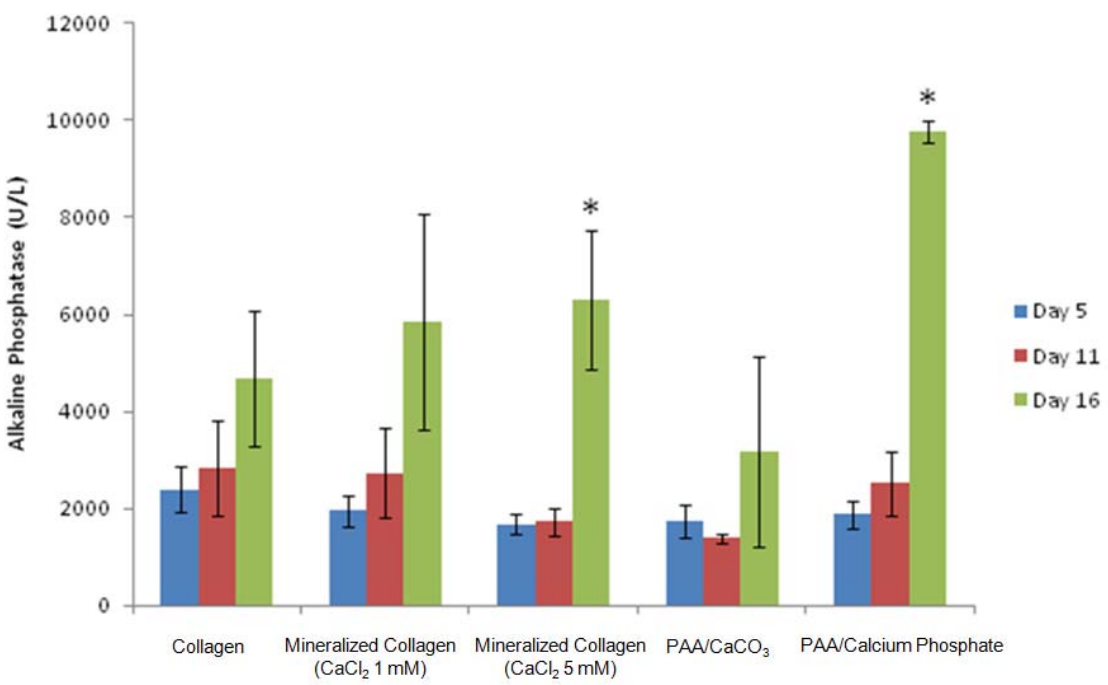

Figure 6-5. Alkaline phosphatase production from hADSC's cultured on nanofibers. * indicates statistical difference at the same timepoint

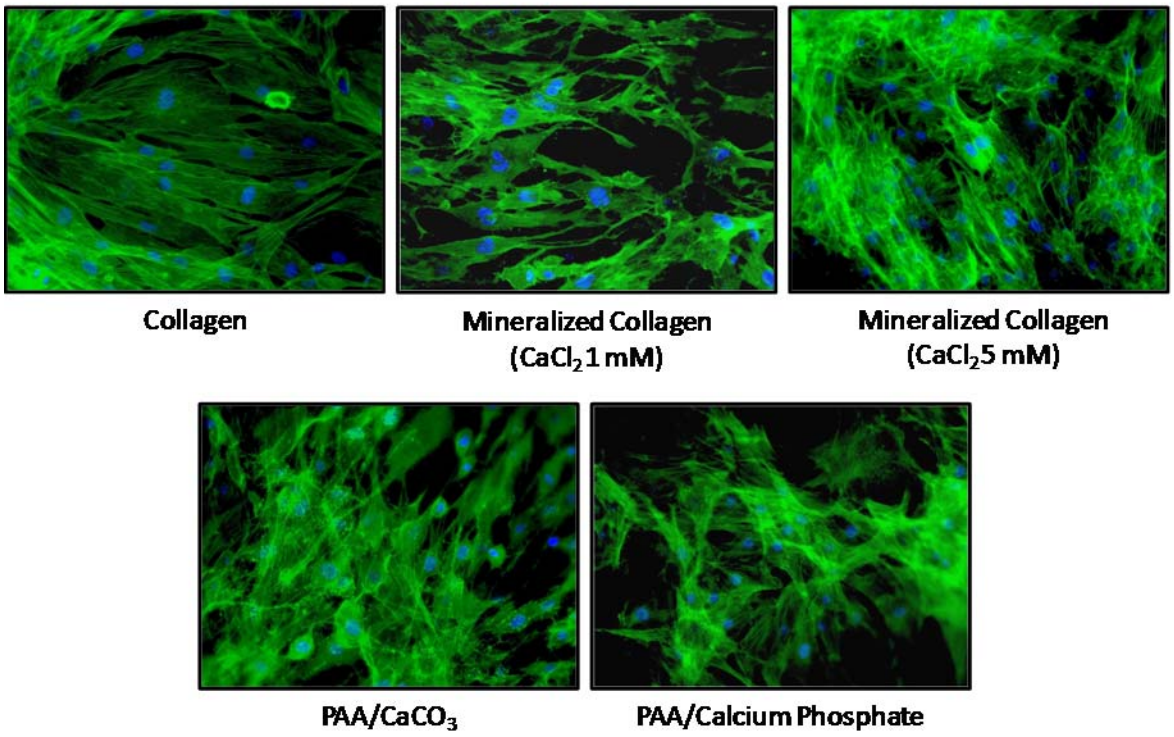

Figure 6-6. Fluorescent images of hADSC's cultured on nanofibers. The green indicates actin filaments while blue indicates cell nuclei.

CHAPTER 7
CONCLUSIONS

We have developed a simple and efficient method to produce biodegradable nanoparticles and nanofibers for drug delivery and tissue engineering applications. This novel nanopore-injection (N-I) method is based on the use of nanoporous membranes.

Chapter 1 introduced and reviewed all relative background information for these studies, including the current progress in nanostructured biomaterials and their applications in drug delivery and tissue engineering, as well as current nanofabrication methods.

In Chapter 2, we fabricated uniform hydrophobic nanoparticles (silymarin, beta-carotene, and butylated hydroxytoluene) with <100 nm size through N-I method. The obtained nanoparticles exhibit smaller hydrodynamic diameter and better dispersibility in aqueous solution, compared with those made through SEDS method. The obtained N-I NPs were amorphous, and showed improved dissolution profile in PBS.

In Chapter 3, we successfully prepared ultrafine chitosan nanoparticles by N-I strategy. The obtained nanoparticle has a small size (<30 nm) with narrow size distribution. Particle size increases with flow rate and viscosity of feed solution. Fluorescent dye rhodamine 6G was encapsulated into chitosan nanoparticles with a encapsulation ratio of about 3 wt%.

In Chapter 4, we have successfully prepared MCHBE encapsulated PLGA-PEG and luciferin encapsulated chitosan nanoparticles by N-I method. These nanoparticles exhibit the ability of sustained release of encapsulated drugs: 7 days for PLGA-PEG/MCHB NPs; 11 days for CS/Luc NPs. In vitro cytotoxicity experiment proved

that PLGA-PEG nanoparticle vector could enhance MCHB delivery efficiency. CS/Luc nanoparticles could be successfully detected in the in vivo bioluminescence imaging.

In Chapter 5, biodegradable collagen nanofibers are prepared by modified N-I method using PCTE membrane. Diameter of collagen nanofiber could be controlled by the pore size of nanoporous membrane. Using the membrane with pore size ranging from 50-1000 nm, nanofibers with diameter ranging from 50-740 nm could be obtained. The nanofibrous scaffold exhibited a strong biomechanical strength. In vitro experiment shows the nanofibrous scaffold supports cardiac stem cell growth and proliferation.

In Chapter 6, organic/inorganic hybrid nanofibers were produced by N-I method, including collagen/calcium phosphate nanofiber, and poly(acrylic acid)/calcium carbonate or calcium phosphate nanofiber. These fibers are amorphous. It was also shown that the fibers supported stem cell growth and proliferation, an early indication of scaffold biocompatibility.

The work presented here has demonstrated that N-I method could be used to produce biodegradable nanoparticles and nanofibers. These obtained nanostructured materials portray a promising future in biomedical applications. Although further studies will be needed to explore the functionalization of those products, the research presented in this dissertation may hopefully provide some insight for related nanomedical studies.

LIST OF REFERENCES

(1) Shi, J.; Votruba, A. R.; Farokhzad, O. C.; Langer, R. *Nano Lett.* **2010**, *10*, 3223-3230.

(2) Wagner, V.; Dullaart, A.; Bock, A.; Zweck, A. *Nat. Biotechnol* **2006**, *24*, 1211-1217.

(3) Zhang, L.; Gu, F. X.; Chan, J. M.; Wang, A. Z.; Langer, R. S.; Farokhzad, O. C. *Clin. Pharmacol. Ther* **2008**, *83*, 761-769.

(4) *The Handbook of Nanomedicine*; Humana Press: Totowa, NJ, **2008**.

(5) Occupational Health & Safety Report: Nanomedicine Market to Surpass $160 Billion by 2015 **2009**.

(6) Langer, R.; Vacanti, J. P. *Science* **1993**, *260*, 920-926.

(7) Khademhosseini, A.; Vacanti, J. P.; Langer, R. *Sci. Am* **2009**, *300*, 64-71.

(8) Goldberg, M.; Langer, R.; Jia, X. *J Biomater Sci Polym Ed* **2007**, *18*, 241-268.

(9) Stevens, M. M.; George, J. H. *Science* **2005**, *310*, 1135-1138.

(10) Taipale, J.; Keski-Oja, J. *FASEB J* **1997**, *11*, 51-59.

(11) Bettinger, C. J.; Langer, R.; Borenstein, J. T. *Angew. Chem. Int. Ed. Engl* **2009**, *48*, 5406-5415.

(12) Huang, J.; Gra ter, S. V.; Corbellini, F.; Rinck, S.; Bock, E.; Kemkemer, R.; Kessler, H.; Ding, J.; Spatz, J. P. *Nano Lett.* **2009**, *9*, 1111-1116.

(13) Park, J.; Bauer, S.; von der Mark, K.; Schmuki, P. *Nano Lett.* **2007**, *7*, 1686-1691.

(14) Norman, J. J.; Desai, T. A. *Ann Biomed Eng* **2006**, *34*, 89-101.

(15) Guo, P.; Martin, C. R.; Zhao, Y.; Ge, J.; Zare, R. N. *Nano Lett* **2010**, *10*, 2202-2206.

(16) Allen, T. M. *Science* **2004**, *303*, 1818-1822.

(17) Vauthier, C.; Bouchemal, K. *Pharm. Res* **2009**, *26*, 1025-1058.

(18) Müller, R. *European Journal of Pharmaceutics and Biopharmaceutics* **2000**, *50*, 161-177.

(19) Benita, S.; Benoit, J. P.; Puisieux, F.; Thies, C. *J. Pharm. Sci.* **1984**, *73*, 1721-1724.

(20) Duncan, R. *Anticancer Drugs* **1992**, *3*, 175-210.

(21) Aprahamian, M.; Michel, C.; Humbert, W.; Devissaguet, J. P.; Damge, C. *Biol. Cell* **1987**, *61*, 69-76.

(22) Allemann, E. *Advanced Drug Delivery Reviews* **1998**, *34*, 171-189.

(23) Couvreur, P.; Vauthier, C. *Pharm Res* **2006**, *23*, 1417-1450.

(24) Juliano, R.; Alam, M. R.; Dixit, V.; Kang, H. *Nucleic Acids Research* **2008**, *36*, 4158-4171.

(25) Soares, A. F.; Carvalho, R. D. A.; Veiga, F. *Nanomedicine* **2007**, *2*, 183-202.

(26) Merisko-Liversidge, E. M.; Liversidge, G. G. *Toxicologic Pathology* **2008**, *36*, 43-48.

(27) Desai, M. P.; Labhasetwar, V.; Amidon, G. L.; Levy, R. J. *Pharm. Res* **1996**, *13*, 1838-1845.

(28) Zauner, W. *Journal of Controlled Release* **2001**, *71*, 39-51.

(29) Jacobson, G.; Shinde, R.; Contag, C.; Zare, R. *Angew. Chem. Int. Ed.* **2008**, *47*, 7880-7882.

(30) Fomina, N.; McFearin, C.; Sermsakdi, M.; Edigin, O.; Almutairi, A. *J. Am. Chem. Soc.* **2010**, *132*, 9540-9542.

(31) Husseini, G. *Journal of Controlled Release* **2000**, *69*, 43-52.

(32) DeBin, J. A.; Strichartz, G. R. *Toxicon* **1991**, *29*, 1403-1408.

(33) Deshane, J.; Garner, C. C.; Sontheimer, H. *J. Biol. Chem* **2003**, *278*, 4135-4144.

(34) Hwang, D. S.; Sim, S. B.; Cha, H. J. *Biomaterials* **2007**, *28*, 4039-4046.

(35) Zerda, A. D. L.; Liu, Z.; Bodapati, S.; Teed, R.; Vaithilingam, S.; Khuri-Yakub, B. T.; Chen, X.; Dai, H.; Gambhir, S. S. *Nano Lett.* **2010**, *10*, 2168-2172.

(36) Porter, A. E.; Gass, M.; Muller, K.; Skepper, J. N.; Midgley, P. A.; Welland, M. *Nat Nanotechnol* **2007**, *2*, 713-717.

(37) *Approaches to Safe Nanotechnology: Managing the Health and Safety Concerns Associated with Engineered Nanomaterials*; National Institute for Occupational Safety and Health. NIOSH (DHHS) Publication: **2009**.

(38) *Biomaterial Handbook-Advanced Applications of Basic Sciences and*

Bioengineering; Marcel Dekker: New York, **2004**.

(39) Okada, M. *Progress in Polymer Science* **2002**, *27*, 87-133.

(40) Qiu, L. Y.; Bae, Y. H. *Pharm. Res* **2006**, *23*, 1-30.

(41) Knowles, K. A. *Hosp. Pract. (Off. Ed.)* **1992**, *27*, 160, 162.

(42) Nair, L.; Laurencin, C. *Progress in Polymer Science* **2007**, *32*, 762-798.

(43) Xiao, G. *Journal of Biological Chemistry* **1998**, *273*, 32988-32994.

(44) Ramay, H. *Biomaterials* **2003**, *24*, 3293-3302.

(45) Bruckmann, P. *Schriftenr Ver Wasser Boden Lufthyg* **1986**, *67*, 199-210.

(46) Chung, H. J.; Steplewski, A.; Chung, K. Y.; Uitto, J.; Fertala, A. *Journal of Biological Chemistry* **2008**, *283*, 25879-25886.

(47) Turakulov, Y. K.; Davlyatov, Y. D. *Zh. Evol. Biokhim. Fiziol* **1975**, *11*, 316-318.

(48) Williams, B. R.; Gelman, R. A.; Poppke, D. C.; Piez, K. A. *J. Biol. Chem* **1978**, *253*, 6578-6585.

(49) Rho, K. S.; Jeong, L.; Lee, G.; Seo, B.; Park, Y. J.; Hong, S.; Roh, S.; Cho, J. J.; Park, W. H.; Min, B. *Biomaterials* **2006**, *27*, 1452-1461.

(50) Zhang, Y. Z.; Venugopal, J.; Huang, Z.; Lim, C. T.; Ramakrishna, S. *Biomacromolecules* **2005**, *6*, 2583-2589.

(51) Harrison, B. S.; Atala, A. *Biomaterials* **2007**, *28*, 344-353.

(52) Fessi, H.; Puisieux, F.; Devissaguet, J.; Ammoury, N.; Benita, S. *International Journal of Pharmaceutics* **1989**, *55*, R1-R4.

(53) Govender, T. *Journal of Controlled Release* **1999**, *57*, 171-185.

(54) Memişoğlu, E.; Bochot, A.; Ozalp, M.; Sen, M.; Duchêne, D.; Hincal, A. A. *Pharm. Res* **2003**, *20*, 117-125.

(55) Duclairoir, C.; Nakache, E.; Marchais, H.; Orecchioni, A. *Colloid & Polymer Science* **1998**, *276*, 321-327.

(56) Landfester, K. *Macromol. Rapid Commun.* **2001**, *22*, 896-936.

(57) Solans, C.; Izquierdo, P.; Nolla, J.; Azemar, N.; Garciacelma, M. *Current Opinion*

in Colloid & Interface Science **2005**, *10*, 102-110.

(58) MacEwen, G. D.; Bunnell, W. P.; Sriram, K. *J Bone Joint Surg Am* **1975**, *57*, 404-408.

(59) Anton, N.; Benoit, J.; Saulnier, P. *Journal of Controlled Release* **2008**, *128*, 185-199.

(60) Craparo, E. F.; Cavallaro, G.; Bondì, M. L.; Mandracchia, D.; Giammona, G. *Biomacromolecules* **2006**, *7*, 3083-3092.

(61) Bradley, M. A.; Prescott, S. W.; Schoonbrood, H. A. S.; Landfester, K.; Grieser, F. *Macromolecules* **2005**, *38*, 6346-6351.

(62) Landfester, K.; Bechthold, N.; Tiarks, F.; Antonietti, M. *Macromolecules* **1999**, *32*, 5222-5228.

(63) Qi, G.; Jones, C. W.; Schork, F. J. *Biomacromolecules* **2006**, *7*, 2927-2930.

(64) Gurny, R.; Peppas, N. A.; Harrington, D. D.; Banker, G. S. *Drug Development and Industrial Pharmacy* **1981**, *7*, 1-25.

(65) Quintanar-Guerrero, D.; Allémann, E.; Doelker, E.; Fessi, H. *Colloid Polym Sci* **1997**, *275*, 640-647.

(66) Quintanar-Guerrero, D. *International Journal of Pharmaceutics* **1996**, *143*, 133-141.

(67) Ibrahim, H.; Bindschaedler, C.; Doelker, E.; Buri, P.; Gurny, R. *International Journal of Pharmaceutics* **1992**, *87*, 239-246.

(68) Tokumitsu, H.; Ichikawa, H.; Fukumori, Y. *Pharm. Res* **1999**, *16*, 1830-1835.

(69) Polk, A.; Amsden, B.; De Yao, K.; Peng, T.; Goosen, M. F. A. *J. Pharm. Sci.* **1994**, *83*, 178-185.

(70) Morton, W. J.; *Method of Dispersing Fluids*, US Patent **1902**, 705,691.

(71) Reneker, D. H.; Yarin, A. L.; Fong, H.; Koombhongse, S. *J. Appl. Phys.* **2000**, *87*, 4531.

(72) Yarin, A. L.; Koombhongse, S.; Reneker, D. H. *J. Appl. Phys.* **2001**, *90*, 4836.

(73) Shin, Y. M.; Hohman, M. M.; Brenner, M. P.; Rutledge, G. C. *Appl. Phys. Lett.* **2001**, *78*, 1149.

(74) Deitzel, J. *Polymer* **2001**, *42*, 261-272.

(75) Tsuda, H.; Yamamoto, K.; Kawabata, M.; Lee, T.; Hidaka, A. *Gynecol. Obstet. Invest* **1997**, *44*, 196-199.

(76) Koombhongse, S.; Liu, W.; Reneker, D. H. *J. Polym. Sci. B Polym. Phys.* **2001**, *39*, 2598-2606.

(77) Seal, D. W.; Bloom, F. R.; Somlai, A. M. *Health Educ Behav* **2000**, *27*, 10-23.

(78) Wang, Y.; Serrano, S.; Santiago-Aviles, J. J. *J. Mater. Sci. Lett.* **2002**, *21*, 1055–1057.

(79) Ding, B.; Kim, H.; Lee, S.; Shao, C.; Lee, D.; Park, S.; Kwag, G.; Choi, K. *J. Polym. Sci. B Polym. Phys.* **2002**, *40*, 1261-1268.

(80) Zong, X. *Polymer* **2002**, *43*, 4403-4412.

(81) Zhang, Y. Z.; Feng, Y.; Huang, Z.; Ramakrishna, S.; Lim, C. T. *Nanotechnology* **2006**, *17*, 901-908.

(82) Sun, Z.; Zussman, E.; Yarin, A.; Wendorff, J.; Greiner, A. *Adv. Mater.* **2003**, *15*, 1929-1932.

(83) Reneker, D. H.; Yarin, A. L. *Polymer* **2008**, *49*, 2387-2425.

(84) Koopmans, R. J.; Molenaar, J. *Polym. Eng. Sci.* **1998**, *38*, 101-107.

(85) Ma, P. X.; Zhang, R. *J. Biomed. Mater. Res* **1999**, *46*, 60-72.

(86) Zhang, R.; Ma, P. X. *J. Biomed. Mater. Res* **2000**, *52*, 430-438.

(87) Woo, K. M.; Chen, V. J.; Ma, P. X. *J. Biomed. Mater. Res.* **2003**, *67A*, 531-537.

(88) Whitesides, G. M. *Proceedings of the National Academy of Sciences* **2002**, *99*, 4769-4774.

(89) Malkar, N. B.; Lauer-Fields, J. L.; Juska, D.; Fields, G. B. *Biomacromolecules* **2003**, *4*, 518-528.

(90) Hartgerink, J. D. *Proceedings of the National Academy of Sciences* **2002**, *99*, 5133-5138.

(91) Caplan, M. R.; Moore, P. N.; Zhang, S.; Kamm, R. D.; Lauffenburger, D. A. *Biomacromolecules* **2000**, *1*, 627-631.

(92) Shamovsky, I. L.; Ross, G. M.; Riopelle, R. J. *J. Phys. Chem. B* **2000**, *104*, 11296-11307.

(93) Buyukserin, F.; Martin, C. R. *Applied Surface Science* **2010**, *256*, 7700-7705.

(94) Mukaibo, H.; Horne, L. P.; Park, D.; Martin, C. R. *Small* **2009**, *5*, 2474-2479.

(95) Buyukserin, F.; Medley, C. D.; Mota, M. O.; Kececi, K.; Rogers, R. R.; Tan, W.; Martin, C. R. *Nanomedicine* **2008**, *3*, 283-292.

(96) Xu, F.; Wharton, J.; Martin, C. *Small* **2007**, *3*, 1718-1722.

(97) Hillebrenner, H.; Buyukserin, F.; Stewart, J. D.; Martin, C. R. *J. Nanosci. Nanotech.* **2007**, *7*, 2211-2221.

(98) Buyukserin, F.; Kang, M.; Martin, C. *Small* **2007**, *3*, 106-110.

(99) Hillebrenner, H.; Buyukserin, F.; Stewart, J. D.; Martin, C. R. *Nanomedicine* **2006**, *1*, 39-50.

(100) Hillebrenner, H.; Buyukserin, F.; Kang, M.; Mota, M. O.; Stewart, J. D.; Martin, C. R. *J. Am. Chem. Soc.* **2006**, *128*, 4236-4237.

(101) Hou, S.; Wang, J.; Martin, C. R. *J. Am. Chem. Soc.* **2005**, *127*, 8586-8587.

(102) Hou, S.; Wang, J.; Martin, C. R. *Nano Lett.* **2005**, *5*, 231-234.

(103) Li, N.; Mitchell, D. T.; Lee, K.; Martin, C. R. *J. Electrochem. Soc.* **2003**, *150*, A979.

(104) Gasparac, R.; Kohli, P.; Mota, M. O.; Trofin, L.; Martin, C. R. *Nano Lett.* **2004**, *4*, 513-516.

(105) Kohli, P.; Wharton, J. E.; Braide, O.; Martin, C. R. *J. Nanosci. Nanotech.* **2004**, *4*, 605-610.

(106) Yu, S.; Li, N.; Wharton, J.; Martin, C. R. *Nano Lett.* **2003**, *3*, 815-818.

(107) Hou, S.; Harrell, C. C.; Trofin, L.; Kohli, P.; Martin, C. R. *J. Am. Chem. Soc.* **2004**, *126*, 5674-5675.

(108) Kang, M.; Yu, S.; Li, N.; Martin, C. *Small* **2004**, *1*, 69-72.

(109) Sides, C. R.; Martin, C. R. *Adv. Mater.* **2005**, *17*, 125-128.

(110) Wirtz, M.; Parker, M.; Kobayashi, Y.; Martin, C. R. *Chem. Eur. J.* **2002**, *8*, 3572.

(111) Wirtz, M.; Yu, S.; Martin, C. R. *Analyst* **2002**, *127*, 871-879.

(112) Miller, S. A.; Young, V. Y.; Martin, C. R. *J. Am. Chem. Soc.* **2001**, *123*, 12335-12342.

(113) Miller, S. *Journal of Electroanalytical Chemistry* **2002**, *522*, 66-69.

(114) Kang, M.; Martin, C. R. *Langmuir* **2001**, *17*, 2753-2759.

(115) Patrissi, C. J.; Martin, C. R. *J. Electrochem. Soc.* **2001**, *148*, A1247.

(116) Li, N.; Martin, C. R. *J. Electrochem. Soc.* **2001**, *148*, A164.

(117) Li, N. *Journal of Power Sources* **2001**, *97-98*, 240-243.

(118) http://www.reading.ac.uk/cellmigration/matrix.htm

(119) http://www.optics.rochester.edu/workgroups/cml/opt307/spr06/joe/

(120) Mundargi, R.; Babu, V.; Rangaswamy, V.; Patel, P.; Aminabhavi, T. *Journal of Controlled Release* **2008**, *125*, 193-209.

(121) Agnihotri, S.; Mallikarjuna, N.; Aminabhavi, T. *Journal of Controlled Release* **2004**, *100*, 5-28.

(122) Moroni, L.; de Wijn, J. R.; van Blitterswijk, C. A. *j biomater sci polym ed* **2008**, *19*, 543-572.

(123) Merisko-Liversidge, E. M.; Liversidge, G. G. *Toxicologic Pathology* **2008**, *36*, 43-48.

(124) Lipinski, C. *Journal of Pharmacological and Toxicological Methods* **2000**, *44*, 235-249.

(125) Liversidge, G. *International Journal of Pharmaceutics* **1995**, *125*, 91-97.

(126) Müller, R. *International Journal of Pharmaceutics* **1998**, *160*, 229-237.

(127) Panyam, J. *Advanced Drug Delivery Reviews* **2003**, *55*, 329-347.

(128) Farokhzad, O. C. *Proceedings of the National Academy of Sciences* **2006**, *103*, 6315-6320.

(129) Poste, G.; Papahadjopoulos, D.; Vail, W. J. *Methods Cell Biol* **1976**, *14*, 33-71.

(130) Roy, I.; Ohulchanskyy, T. Y.; Pudavar, H. E.; Bergey, E. J.; Oseroff, A. R.; Morgan, J.; Dougherty, T. J.; Prasad, P. N. *J. Am. Chem. Soc.* **2003**, *125*, 7860-7865.

(131) Jung, T. *European Journal of Pharmaceutics and Biopharmaceutics* **2000**, *50*, 147-160.

(132) Chawla, J. *International Journal of Pharmaceutics* **2002**, *249*, 127-138.

(133) Sakuma, S.; Hayashi, M.; Akashi, M. *Adv. Drug Deliv. Rev* **2001**, *47*, 21-37.

(134) Legrand, P.; Lesieur, S.; Bochot, A.; Gref, R.; Raatjes, W.; Barratt, G.; Vauthier, C. *Int J Pharm* **2007**, *344*, 33-43.

(135) Antonietti, M. *Progress in Polymer Science* **2002**, *27*, 689-757.

(136) Tokumitsu, H.; Ichikawa, H.; Fukumori, Y. *Pharm. Res* **1999**, *16*, 1830-1835.

(137) Ferenci, P.; Dragosics, B.; Dittrich, H.; Frank, H.; Benda, L.; Lochs, H.; Meryn, S.; Base, W.; Schneider, B. *Journal of Hepatology* **1989**, *9*, 105-113.

(138) Omenn, G. S.; Goodman, G. E.; Thornquist, M. D.; Balmes, J.; Cullen, M. R.; Glass, A.; Keogh, J. P.; Meyskens, F. L.; Valanis, B.; Williams, J. H.; Barnhart, S.; Hammar, S. *N. Engl. J. Med* **1996**, *334*, 1150-1155.

(139) Burton, G.; Ingold, K. *Science* **1984**, *224*, 569-573.

(140) Branen, A. L. *J Am Oil Chem Soc* **1975**, *52*, 59-63.

(141) Jacobson, G.; Shinde, R.; Contag, C.; Zare, R. *Angew. Chem. Int. Ed.* **2008**, *47*, 7880-7882.

(142) Jacobson, G. B.; Gonzalez-Gonzalez, E.; Spitler, R.; Shinde, R.; Leake, D.; Kaspar, R. L.; Contag, C. H.; Zare, R. N. *J Pharm Sci* **2010**, *99*, 4261-4266.

(143) Jacobson, G. B.; Shinde, R.; McCullough, R. L.; Cheng, N. J.; Creasman, A.; Beyene, A.; Hickerson, R. P.; Quan, C.; Turner, C.; Kaspar, R. L.; Contag, C. H.; Zare, R. N. *J. Pharm. Sci.* **2009**, 2750-2755.

(144) Hulteen, J. C.; Martin, C. R. *J. Mater. Chem.* **1997**, *7*, 1075-1087.

(145) Yinwin, K.; Feng, S. *Biomaterials* **2005**, *26*, 2713-2722.

(146) Chithrani, B. D.; Ghazani, A. A.; Chan, W. C. W. *Nano Lett.* **2006**, *6*, 662-668.

(147) Sun, N.; Zhang, X.; Lu, Y.; Wu, W. *Planta Med* **2008**, *74*, 126-132.

(148) Han, W.; Bai, T.; Zhu, J. *J. Chem. Eng. Data* **2009**, *54*, 1889-1893.

(149) Wang, Y.; Zhang, D.; Liu, Z.; Liu, G.; Duan, C.; Jia, L.; Feng, F.; Zhang, X.; Shi, Y.; Zhang, Q. *Nanotechnology* **2010**, *21*, 155104.

(150) Kost, J.; Langer, R. *Adv. Drug Deliv. Rev* **2001**, *46*, 125-148.

(151) Farokhzad, O. C.; Langer, R. *ACS Nano* **2009**, *3*, 16-20.

(152) Nel, A. E.; Mädler, L.; Velegol, D.; Xia, T.; Hoek, E. M. V.; Somasundaran, P.; Klaessig, F.; Castranova, V.; Thompson, M. *Nat Mater* **2009**, *8*, 543-557.

(153) Guo, P.; Martin, C. R.; Zhao, Y.; Ge, J.; Zare, R. N. *Nano Lett.* **2010**, *10*, 2202-2206.

(154) Ge, J.; Jacobson, G. B.; Lobovkina, T.; Holmberg, K.; Zare, R. N. *Chem. Comm.* **2010**, in press.

(155) Buyukserin, F.; Medley, C. D.; Mota, M. O.; Kececi, K.; Rogers, R. R.; Tan, W.; Martin, C. R. *Nanomedicine (Lond)* **2008**, *3*, 283-292.

(156) Buyukserin, F.; Kang, M.; Martin, C. *Small* **2007**, *3*, 106-110.

(157) Hillebrenner, H.; Buyukserin, F.; Stewart, J. D.; Martin, C. R. *Nanomedicine* **2006**, *1*, 39-50.

(158) Hillebrenner, H.; Buyukserin, F.; Kang, M.; Mota, M. O.; Stewart, J. D.; Martin, C. R. *J. Am. Chem. Soc.* **2006**, *128*, 4236-4237.

(159) *Chitosan, a mediator for fiber-water interactions in paper*; University of Washington Press: Seattle, WA, **1977**.

(160) Agnihotri, S. A.; Mallikarjuna, N. N.; Aminabhavi, T. M. *J Control Release* **2004**, *100*, 5-28.

(161) Senel, S.; McClure, S. J. *Adv. Drug Deliv. Rev* **2004**, *56*, 1467-1480.

(162) Berger, J.; Reist, M.; Mayer, J. M.; Felt, O.; Peppas, N. A.; Gurny, R. *Eur J Pharm Biopharm* **2004**, *57*, 19-34.

(163) Yi, H.; Wu, L.; Bentley, W. E.; Ghodssi, R.; Rubloff, G. W.; Culver, J. N.; Payne, G. F. *Biomacromolecules* **2005**, *6*, 2881-2894.

(164) Vårum, K. *Carbohydrate Polymers* **1994**, *25*, 65-70.

(165) Anna, S. L.; Bontoux, N.; Stone, H. A. *Appl. Phys. Lett.* **2003**, *82*, 364.

(166) Xu, S.; Nie, Z.; Seo, M.; Lewis, P.; Kumacheva, E.; Stone, H. A.; Garstecki, P.; Weibel, D. B.; Gitlin, I.; Whitesides, G. M. *Angew. Chem. Int. Ed. Engl* **2005**, *44*, 724-728.

(167) Powell, M. R.; Sullivan, M.; Vlassiouk, I.; Constantin, D.; Sudre, O.; Martens, C. C.; Eisenberg, R. S.; Siwy, Z. S. *Nature Nanotech* **2007**, *3*, 51-57.

(168) Mitchell, D. T.; Lee, S. B.; Trofin, L.; Li, N.; Nevanen, T. K.; Söderlund, H.; Martin, C. R. *J. Am. Chem. Soc* **2002**, *124*, 11864-11865.

(169) Gasparac, R.; Kohli, P.; Mota, M. O.; Trofin, L.; Martin, C. R. *Nano Lett.* **2004**, *4*, 513-516.

(170) Srivastava, D.; Lee, I. *Adv. Mater.* **2006**, *18*, 2471-2475.

(171) Cumberland, S. A.; Lead, J. R. *J Chromatogr A* **2009**, *1216*, 9099-9105.

(172) Gu, F.; Langer, R.; Farokhzad, O. C. *Methods Mol. Biol* **2009**, *544*, 589-598.

(173) Mann, S.; Ozin, G. A. *Nature* **1996**, *382*, 313–318.

(174) Estroff, L. A.; Hamilton, A. D. *Chemistry of Materials* **2001**, *13*, 3227-3235.

(175) Cheng, X.; Gower, L. B. *Biotechnology Progress* **2006**, *22*, 141-149.

(176) Matthew J. Olszta; Damian J. Odom; Elliot P. Douglas; Laurie B. Gower *Connective Tissue Research* **2003**, *44*, 326-334.

(177) Cölfen, H. *Current Opinion in Colloid & Interface Science* **2003**, *8*, 23-31.

(178) Tao, J.; Pan, H.; Zeng, Y.; Xu, X.; Tang, R. *The Journal of Physical Chemistry B* **2007**, *111*, 13410-13418.

(179) Fricke, M.; Volkmer, D. In *Biomineralization I*; 2007; pp. 1-41.

(180) Cölfen, H. In *Biomineralization II*; 2007; pp. 1-77.

(181) Gower, L. B. *Chemical Reviews* **2008**, *108*, 4551-4627.

(182) Weiner, S.; Mahamid, J.; Politi, Y.; Ma, Y.; Addadi, L. *Frontiers of Materials Science in China* **2009**, *3*, 104-108.

(183) Loste, E.; Meldrum, F. C. *Chemical Communications* **2001**, *2001*, 901–902.

(184) Loste, E.; Park, R. J.; Warren, J.; Meldrum, F. C. *Advanced Functional Materials*

2004, *14*, 1211–1220.

(185) DiMasi, E.; Olszta, M. J.; Patel, V. M.; Gower, L. B. *CrystEngComm* **2003**, *5*, 346-350.

(186) Kato, K.; Eika, Y.; Ikada, Y. *Journal of Materials Science* **1997**, *32*, 5533-5543.

(187) Kato, T.; Suzuki, T.; Amamiya, T.; Irie, T.; Komiyama, M.; Yui, H. *Supramolecular Science* **1998**, *5*, 411-415.

(188) Olszta, M. J.; Cheng, X.; Jee, S. S.; Kumar, R.; Kim, Y.; Kaufman, M. J.; Douglas, E. P.; Gower, L. B. *Materials Science and Engineering: R: Reports* **2007**, *58*, 77-116.

(189) Bradt, J.; Mertig, M.; Teresiak, A.; Pompe, W. *Chemistry of Materials* **1999**, *11*, 2694-2701.

(190) Zhang, W.; Liao, S. S.; Cui, F. Z. *Chemistry of Materials* **2003**, *15*, 3221-3226.

(191) Gobeaux, F.; Mosser, G.; Anglo, A.; Panine, P.; Davidson, P.; Giraud-Guille, M.; Belamie, E. *Journal of Molecular Biology* **2008**, *376*, 1509-1522.

(192) Orgel, J. P. R. O.; Irving, T. C.; Miller, A.; Wess, T. J. *Proceedings of the National Academy of Sciences* **2006**, *103*, 9001 -9005.

(193) Eglin, D.; Mosser, G.; Giraud-Guille, M.; Livage, J.; Coradin, T. *Soft Matter* **2005**, *1*, 129.

(194) Kadler, K. E.; Holmes, D. F.; Trotter, J. A.; Chapman, J. A. *Biochem J* **1996**, *316*, 1-11.

(195) Fletcher, G. C. *Biopolymers* **1976**, *15*, 2201-2217.

(196) Xie, J.; Baumann, M. J.; McCabe, L. R. *J. Biomed. Mater. Res.* **2004**, *71A*, 108-117.

(197) Serre, C.; Papillard, M.; Chavassieux, P.; Boivin, G. *Biomaterials* **1993**, *14*, 97-106.

BIOGRAPHICAL SKETCH

Peng Guo was born in Liaoyuan, China in 1983. He entered Jilin University at Changchun, China in 2001 as undergraduate student majoring in chemistry. He obtained a Bachelor of Science degree in July 2005. In August 2006, Peng Guo joined Dr. Charles R. Martin's research group in the Department of Chemistry at University of Florida. He started his research in the fields of biomedical nanomaterials, especially on the fabrication of biodegradable nanostructure for drug delivery and tissue engineering. He completed his research in May 2011, obtaining a Doctor of Philosophy degree in chemistry.